

World Journal of *Radiology*

World J Radiol 2023 June 28; 15(6): 157-215



MINIREVIEWS

- 157 Acute pancreatitis: Structured report template of magnetic resonance imaging
Song LJ, Xiao B
- 170 Radiological parameters to predict pancreatic texture: Current evidence and future perspectives
Kalayarasan R, Himaja M, Ramesh A, Kokila K

ORIGINAL ARTICLE**Retrospective Study**

- 182 Computed tomography angiographic study of surgical anatomy of thyroid arteries: Clinical implications in neck dissection
Bhardwaj Y, Singh B, Bhadoria P, Malhotra R, Tarafdar S, Bisht K

Observational Study

- 191 Role of contrast-enhanced serial/spot abdominal X-rays in perioperative follow-up of patients undergoing abdominal surgery: An observational clinical study
Dilek ON, Atay A, Gunes O, Karahan F, Karasu S

Prospective Study

- 201 Interobserver reliability of computed tomography angiography in the assessment of ruptured intracranial aneurysm and impact on patient management
Elmokadem AH, Elged BA, Abdel Razek A, El-Serougy LG, Kasem MA, EL-Adalany MA

ABOUT COVER

Editorial Board Member of *World Journal of Radiology*, Linda Agolli, MD, Doctor, Research Scientist, Department of Radiation Oncology, Faculty of Medicine, University Hospital Carl Gustav Carus, Dresden 01307, Germany. linda.agolli@gmail.com

AIMS AND SCOPE

The primary aim of *World Journal of Radiology (WJR, World J Radiol)* is to provide scholars and readers from various fields of radiology with a platform to publish high-quality basic and clinical research articles and communicate their research findings online.

WJR mainly publishes articles reporting research results and findings obtained in the field of radiology and covering a wide range of topics including state of the art information on cardiopulmonary imaging, gastrointestinal imaging, genitourinary imaging, musculoskeletal imaging, neuroradiology/head and neck imaging, nuclear medicine and molecular imaging, pediatric imaging, vascular and interventional radiology, and women's imaging.

INDEXING/ABSTRACTING

The *WJR* is now abstracted and indexed in PubMed, PubMed Central, Emerging Sources Citation Index (Web of Science), Reference Citation Analysis, China National Knowledge Infrastructure, China Science and Technology Journal Database, and Superstar Journals Database. The 2022 edition of Journal Citation Reports® cites the 2021 Journal Citation Indicator (JCI) for *WJR* as 0.48.

RESPONSIBLE EDITORS FOR THIS ISSUE

Production Editor: *Si Zhao*; Production Department Director: *Xu Guo*; Editorial Office Director: *Jia-Ping Yan*.

NAME OF JOURNAL

World Journal of Radiology

ISSN

ISSN 1949-8470 (online)

LAUNCH DATE

January 31, 2009

FREQUENCY

Monthly

EDITORS-IN-CHIEF

Thomas J Vogl

EDITORIAL BOARD MEMBERS

<https://www.wjgnet.com/1949-8470/editorialboard.htm>

PUBLICATION DATE

June 28, 2023

COPYRIGHT

© 2023 Baishideng Publishing Group Inc

INSTRUCTIONS TO AUTHORS

<https://www.wjgnet.com/bpg/gerinfo/204>

GUIDELINES FOR ETHICS DOCUMENTS

<https://www.wjgnet.com/bpg/GerInfo/287>

GUIDELINES FOR NON-NATIVE SPEAKERS OF ENGLISH

<https://www.wjgnet.com/bpg/gerinfo/240>

PUBLICATION ETHICS

<https://www.wjgnet.com/bpg/GerInfo/288>

PUBLICATION MISCONDUCT

<https://www.wjgnet.com/bpg/gerinfo/208>

ARTICLE PROCESSING CHARGE

<https://www.wjgnet.com/bpg/gerinfo/242>

STEPS FOR SUBMITTING MANUSCRIPTS

<https://www.wjgnet.com/bpg/GerInfo/239>

ONLINE SUBMISSION

<https://www.f6publishing.com>

Acute pancreatitis: Structured report template of magnetic resonance imaging

Ling-Ji Song, Bo Xiao

Specialty type: Radiology, nuclear medicine and medical imaging

Provenance and peer review:

Invited article; Externally peer reviewed.

Peer-review model: Single blind

Peer-review report's scientific quality classification

Grade A (Excellent): 0
Grade B (Very good): 0
Grade C (Good): B
Grade D (Fair): D
Grade E (Poor): 0

P-Reviewer: Mohey NM, Egypt;
Nakano H, Japan

Received: March 27, 2023

Peer-review started: March 27, 2023

First decision: May 13, 2023

Revised: May 25, 2023

Accepted: June 16, 2023

Article in press: June 16, 2023

Published online: June 28, 2023



Ling-Ji Song, Bo Xiao, Department of Radiology, Sichuan Key Laboratory of Medical Imaging, The Affiliated Hospital of North Sichuan Medical College, Nanchong 637000, Sichuan Province, China

Corresponding author: Bo Xiao, Doctor, MD, PhD, Associate Professor, Department of Radiology, Sichuan Key Laboratory of Medical Imaging, The Affiliated Hospital of North Sichuan Medical College, No. 1 Maoyuan South Street, Nanchong 637000, Sichuan Province, China. xiaoboimaging@163.com

Abstract

Acute pancreatitis (AP) is a common acute abdomen disease of the digestive system. It has a potentially fatal risk because of its variable severity and various complications. With the widespread application of the Revised Atlanta Classification, new requirements for AP imaging reports are introduced. Experts in abdominal radiology and pancreatology in the United States published the first structured computed tomography reporting template for AP in 2020. However, there is no corresponding structured magnetic resonance imaging (MRI) reporting template globally. Therefore, this article focuses on the structured MRI report of AP images from our pancreatitis imaging center, which is intended to improve the systematic understanding of this disease and standardize the writing of MRI structured reports. In the meantime, we aim to promote the clinical diagnosis and assessment of MRI efficacy for AP and its multiple complications. It is further intended to facilitate academic exchanges and scientific research between different medical centers.

Key Words: Magnetic resonance imaging; Acute pancreatitis; Structured reporting; Computed tomography

©The Author(s) 2023. Published by Baishideng Publishing Group Inc. All rights reserved.

Core Tip: Acute pancreatitis (AP) is a common digestive disease. Experts in abdominal radiology and pancreatology in the United States published the first structured computed tomography reporting template for AP in 2020, but there is no corresponding structured magnetic resonance imaging (MRI) reporting template internationally. For this reason, this article focuses on the structured MRI report of AP and its standardization, which is beneficial for clinicians to diagnose and evaluate the MRI efficacy of AP and its multiple complications. At the same time, it will promote academic exchanges between different medical centers as well as scientific research and teaching.

Citation: Song LJ, Xiao B. Acute pancreatitis: Structured report template of magnetic resonance imaging. *World J Radiol* 2023; 15(6): 157-169

URL: <https://www.wjgnet.com/1949-8470/full/v15/i6/157.htm>

DOI: <https://dx.doi.org/10.4329/wjr.v15.i6.157>

INTRODUCTION

Acute pancreatitis (AP) is one of the most common causes of hospitalization due to gastrointestinal disorders and it requires multidisciplinary treatment[1,2]. AP inflammation can be confined to the pancreas itself, and can further involve other tissues and remote organs[3]. Approximately 15%-20% of AP patients will progress to severe acute pancreatitis (SAP)[4], which is potentially lethal and remains one of the most challenging diseases to date. In China, the majority of AP patients are caused by cholelithiasis, alcoholism, and hyperlipidemia[5]. With the in-depth study of pathophysiological mechanisms of AP, traditional terminologies of imaging reports related to AP have been updated in the Revised Atlanta Consensus[6]. In fact, it is both an opportunity and a challenge for radiologists. In 2020, American experts in the field of abdominal radiology and pancreatology first released AP's computed tomography (CT) structured report template[7]. It is designed based on contrast-enhanced CT. But to the best of our knowledge, magnetic resonance imaging (MRI) has additionally important values in the AP severity assessment at early-phase and differential diagnosis of AP-related collection complications [3,8,9]. However, there is a lack of corresponding MRI structured report template in this field. In this article, therefore, we have combined our clinical practice and previous research data to introduce the structured MRI report template for AP. Our aim is to facilitate the standardization of MRI report writing and clinical multidisciplinary team communication for AP patients.

IMAGING INDICATIONS OF ACUTE PANCREATITIS

AP is a dynamically changing disease. In the clinical settings, most AP patients have a typical clinical course, symptoms and signs, and serum enzyme characteristics[10]. Under normal circumstances, imaging examination is not the first or mandatory choice. However, AP patients with the following aspects need to be examined in time: (1) Difficulty in differential diagnosis of other acute abdomen disorders; (2) serum enzymatic levels do not reach the relevant threshold; (3) confirm the clinical prediction of SAP; and (4) suspected cholelithiasis and other neoplastic complications[11]. In addition, the detection of various local complications in the late stage of AP and the evaluation of curative effect after treatment are also indications for AP repeated imaging examination[6,12].

For radiologists, the first step should be to identify the patient's general information (gender, age, inducement, previous history, concomitant diseases, *etc.*). It is essential for the diagnosis and treatment of pancreatic diseases. For instance, men are prone to alcoholic AP due to alcohol abuse, while women are prone to gallstone AP[13]. The occurrence of AP in adolescents may be related to genetic factors and biliopancreatic duct anatomical variants. In contrast, AP in the elderly may be severe and complicated by advanced age factors and the coexistence of multiple underlying diseases. The medical history of pregnancy, trauma, and endoscopic retrograde cholangiopancreatography (ERCP) is also important in determining the etiology of AP. Additionally, Sadr-Azodi *et al*[14] suggest that smoking may be an independent risk factor for AP. Another study further confirmed that smoking was positively associated with the development of pancreatitis[15]. Last but most importantly, patients with underlying renal disease or renal insufficiency need to avoid CT-enhanced examinations[6,16]. Accordingly, the emergence MRI can make up for the deficiency of CT.

IMAGING TECHNIQUES OF ACUTE PANCREATITIS

Early imaging of AP (within 72 h of onset) is frequently deceptive due to underestimate the true extent

of parenchymal involvement and the inability to reliably assess early complications[17,18]. However, revised Atlanta International Consensus still suggests enhanced CT is the primary imaging method for the initial diagnosis of AP patients. It can clearly diagnose AP and provide a better evaluation of pancreatic necrosis, local complications, and the severity of AP. Occasionally, the application of contrast agents has been reported to aggravate the condition of AP[19]. Also, CT examinations have radiation. So accordingly, many studies at domestic and abroad have used conventional MRI sequences combined with diffusion-weighted imaging (DWI) to detect AP. Some scholars have confirmed that the diagnostic value of the DWI technique in AP is equivalent to that of enhanced CT and exceeds the capability of plain CT[20]. They believe that DWI can be used as a powerful tool for evaluating and following up AP [20]. In addition, MRI is feasible for patients with a medical history of iodine allergy or acute renal insufficiency. Moreover, for pregnant women, children, and patients requiring multiple reviews, MRI can be utilized to evaluate the pancreas and peripancreatic conditions.

Taking our unit as an example, we use the following MRI sequences and parameters for comprehensive evaluation of AP (Tables 1 and 2), covering T1-weighted imaging (T1WI) (anatomy, hemorrhage), T2-weighted imaging (T2WI) (effusion, necrosis), DWI (early diffusion restriction), magnetic resonance cholangiopancreatography (MRCP) (observation of the pancreaticobiliary system, effusion), and contrast-enhancement scans (blood supply). Since each medical center has different MRI manufacturers and different imaging protocols, we recommend the mentioned-above sequences for reference. On the basis of our clinical practice, most AP patients are able to complete MRI examinations. Compared to enhanced CT, MRI has the following advantages for AP: (1) MRI is a non-ionizing radiation-free diagnostic imaging that can be used for patients who require multiple follow-up scans; (2) The diagnostic ability of MRI plain scan for pancreatic necrosis is comparable to that of contrast-enhanced CT[20]; (3) Fat-suppressed T1WI is more sensitive than CT for the diagnosis of pancreatic/peripancreatic hemorrhage[21]; (4) Fat-suppressed T2WI is appropriate for the detection of peripancreatic fat necrosis; (5) Fat-suppressed T2WI is significantly better than CT in showing small amounts of "non-liquid" substances within acute necrotic collection (ANC) and walled-off necrosis (WON); (6) MRCP is superior to CT in demonstrating morphological changes of main pancreatic duct (MPD) and the connectivity between the MPD and pseudocyst/WON; and (7) MRI is a reliable modality for staging the severity of AP and has predictive value for disease prognosis. Indeed, MRI has some shortcomings. For example, it is not as good as CT for peripancreatic infection gas findings. MRI needs a long scanning time, and presents difficulty in completing the examination in some SAP patients, as well as a relatively high cost. It is worth mentioning that clinicians need to clarify the advantages and disadvantages of various imaging techniques in order to select the proper examination method for each individual with AP.

STRUCTURED REPORT TEMPLATE OF MRI FOR ACUTE PANCREATITIS

As for the initial CT examination of AP, the Revised Atlanta Consensus recommends that it is better to perform CT 3 d after AP onset[6,22]. At this time, the evaluation of the degree of inflammation and the confirmation of pancreatic necrosis are more reliable, and they may help facilitate the differentiation between acute peripancreatic fluid collection (APFC) and ANC[17]. Furthermore, some scholars have found that MRI performed within 3 d is also helpful in determining the severity of AP and evaluating the prognosis[21].

The MRI structured report for AP should include the description of the pancreas itself, peripancreatic conditions, related complications, and the severity score. Moreover, changes of the lesions before and after treatment need to be described, as shown in Table 3[21,23].

INTERPRETATION AND CLINICAL VALUE OF EVALUATION INDEXES OF STRUCTURED IMAGING REPORT

Pancreatic necrosis

Pancreatic necrosis refers to the pathological accumulation of inactivated pancreatic tissue, which is a relatively common local complication of AP[24]. The extent of pancreatic necrosis can be subdivided according to the anatomical region of the organ and the percentage of unenhanced pancreatic parenchyma, such as < 30%, 31%-50%, and > 50% subcategories[25]. These subcategories are clinically significant because the volume of glandular necrosis can predict serious complications such as infection and organ failure. When talking about necrotizing pancreatitis, we previously always thought of the severity of "pancreas itself" necrosis. This is because of the influence of the scoring system based on the degree of pancreatic parenchymal necrosis proposed by Balthazar. However, the Revised Atlanta Consensus reclassified pancreatic necrosis into three subtypes: (1) Pancreatic and peripancreatic necrosis (mixed type) (Figure 1A and B); (2) peripancreatic necrosis only (Figure 1C and D); and (3) pancreatic necrosis only (Figure 2). Although the mixed type is the most prevalent in clinical practice, the latter two

Table 1 Magnetic resonance imaging sequences and parameters (1.5 Tesla) for acute pancreatitis

Sequence	Repetition time (ms)	Echo time (ms)	Slice thickness (mm)	Slice space (mm)	Matrix	Field of view (mm)	Flip angle
T1WI	6.19	2.86	2.4	0	143 × 272	300 × 400	15°
IP/OP	6.19	4.47	2.4	0	143 × 272	300 × 400	15°
T2WI	2000	78.26	5	1	256 × 152	300 × 380	150°
DWI	3611	64	6	1.2	114 × 144	300 × 380	90°
MRCP	6500	1004	60	60	336 × 336	340 × 340	160°
DCE MRI	6.19	2.86	2.4	0	143 × 272	300 × 400	15°

IP/OP: In-phase/Out-of-phase; DWI: Diffusion-weighted imaging; MRCP: Magnetic resonance cholangiopancreatography; DCE: Dynamic contrast-enhancement.

Table 2 Magnetic resonance imaging sequences and parameters (3.0 Tesla) for acute pancreatitis

Sequence	Repetition time (ms)	Echo time (ms)	Slice thickness (mm)	Slice space (mm)	Matrix	Field of view (mm)	Flip angle
T1WI	3.91	1.42	4.5	0	304 × 274	400 × 300	12°
T2WI	8963	116.16	6	20	256 × 218	380 × 300	90°
DWI	3555	63.8	6.0	20	128 × 101	380 × 300	90°
MRCP	6000	753.6	60	0	368 × 276	300 × 300	180°
DCE MRI	3.91	1.42	4.5	0	304 × 274	400 × 300	12°

DWI: Diffusion-weighted imaging; MRCP: Magnetic resonance cholangiopancreatography; DCE: Dynamic contrast-enhancement.

subtypes also require attention. As proposed by Meyrignac *et al*[26] and Çakar *et al*[27] in recent years, the amount of peripancreatic necrosis was more suitable for AP severity determination and prognostic analysis than the pancreatic necrosis score proposed by Balthazar. And meanwhile, it could better predict organ failure and secondary infection. Cucuteanu *et al*[28] found that extra-pancreatic necrotic volume was the best predictor for evaluating severe pancreatitis with an area under the curve of 0.993. MRI has good soft tissue resolution, so it is accurate to determine the nature of pancreatic necrosis and the measurement of extra-pancreatic necrotic volume.

Pancreatic divisum

Pancreatic divisum is an anatomical variation of the pancreatic duct system, with an incidence of approximately 10% in the general population. About 5% of these patients will present with symptoms [29]. MRI combined with MRCP is the first choice for the diagnosis of pancreatic divisum. It has been estimated that approximately 20% of AP patients with unknown etiology suffer from pancreatic divisum[29]. Therefore, MRI structured report template for AP should include the description of pancreatic divisum.

Peripancreatic changes

As we all know, the term “AP-related hemorrhage” is not mentioned in the Revised Atlanta Classification. Pathologically, AP is still divided into interstitial edematous pancreatitis and hemorrhagic necrotizing pancreatitis (necrotic lesions often accompanied by hemorrhagic foci)[30]. Peripancreatic fatty tissue necrosis is a form of inflammatory extension involving the peripancreatic intra-abdominal fatty tissue and adipose tissue in the retroperitoneal spaces[31]. MRI might show the intra-abdominal inflammatory involvement located in the omental or mesenteric fatty tissue regions. In our clinical practice, we found that peripancreatic fat necrosis combined with hemorrhage could be detected by MRI (patchy T1-hyperintense on fat suppression T1WI). Although early detection of this pathology condition may have no effect on patient management, necrosis combined with hemorrhage may be associated with the prognosis of AP patients. Scholars show that pancreatic/peripancreatic hemorrhage demonstrated on MR imaging (Figure 3A) has a good correlation with the severity of AP[21], which can be useful in prognostic determination.

In addition to the corresponding changes in retroperitoneal spaces in AP, changes in subperitoneal spaces should also be observed. Some scholars have conducted clinical studies on this issue. AP is prone to involve the transverse colonic mesentery (incidence of 61.9%)[32] (Figure 3B). Moreover, AP also easily involved the small intestine mesentery (incidence of 67.9%)[33]. Both the transverse-mesocolon

Table 3 Structured report template of magnetic resonance imaging for acute pancreatitis

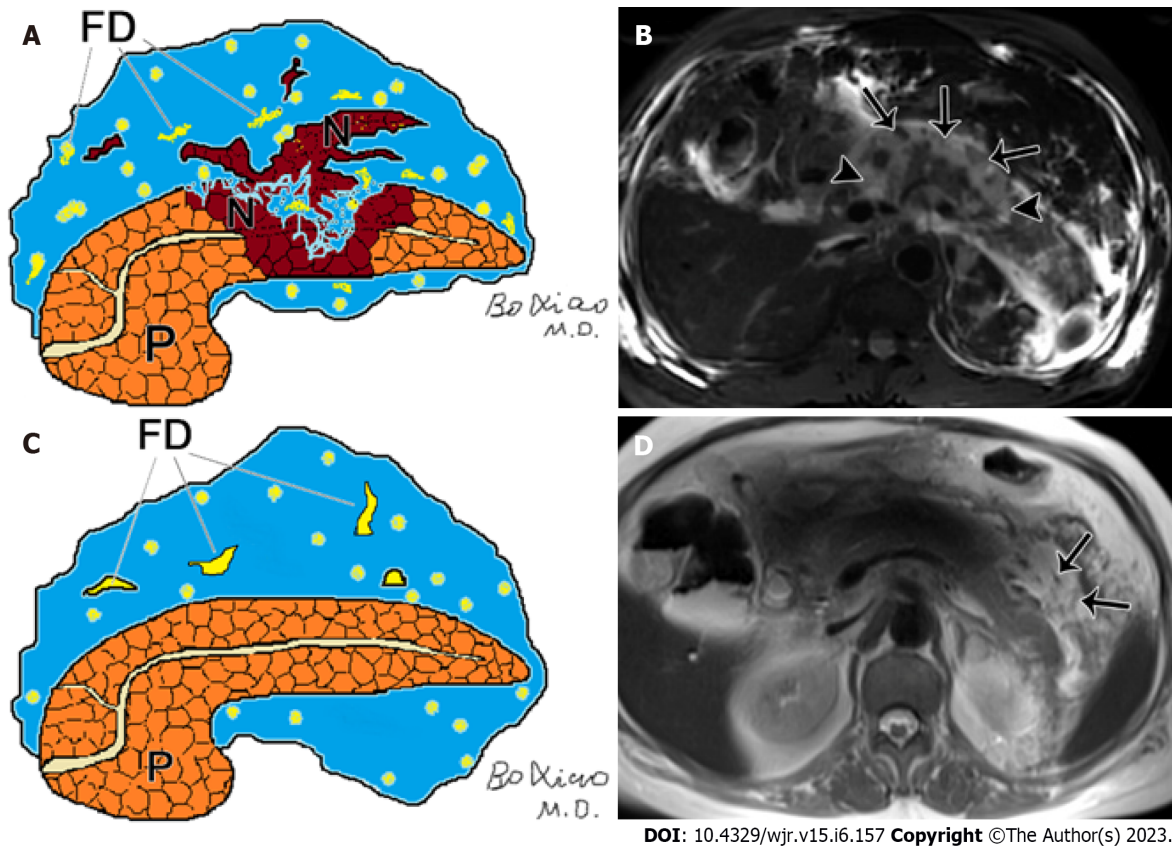
Contents	Descriptions
Pancreas itself	
Enlargement	Diffuse; Focal (head/neck/body/tail)
Edge	Clear; blur
Signal intensity	Variable owing to internal necrosis and/or hemorrhage
Enhancement	Homogeneous; Heterogeneous
Pancreatic duct	Normal; dilated (mm); stricture (mm); calculi (mm)
Pancreatic necrosis	
Position	Head; neck; body; tail
Range ¹	< 30%; 30%-50%; > 50%
Peripancreatic changes	
Renal fascia and peritoneum	Thickening (anterior renal fascia/posterior renal fascia/lateral cone fascia/lateral abdominal wall peritoneum); Enhanced or not?
Peripancreatic fat space	Clear; Blur
Peripancreatic fat necrosis	Site (retroperitoneal space/transverse colonic mesentery/small intestinal mesentery); amount (patchy/large flake); whether combined with hemorrhage (fat-suppressed T1-hyperintense)[21]
Peripancreatic collection	Position ² ; volume (linear/patchy/large); encapsulated round/oval; contents (homogeneous fluid signal/heterogeneous mixed signal)
Local complication	
I Pancreatic/peripancreatic collection (type)	Some of the features can be seen in the above peripancreatic collection
APFC	Yes or no?
ANC	Yes or no?
Pseudocyst	Yes or no? If yes, thickness of the cyst wall (mm, uniform?); Is adjacent to and pushing out adjacent organs (stomach/duodenum, etc.)?
WON	Yes or no? If yes, thickness of the lesion wall (mm); Whether the wall is enhanced and the pattern of enhancement? "Non-liquid substances" within WON (< 10%, 10%-40%, > 40%)[23]; Is WON close to adjacent organs (stomach/duodenum/AC/DC)?
II Infection of collection	
Complicated intestinal fistula	Suggestive signs [bubble sign, air-fluid level sign]
Complicated intestinal fistula	Relationship between collection and the intestinal fistula canal, and the intestinal segment of intestinal fistula (duodenum/AC/DC)
III Pancreatic duct disruption syndrome	
III Pancreatic duct disruption syndrome	Site (head/neck/body); Is MPD dilated on the upstream/caudal side of the interruption (mm)? Relationship with adjacent pseudocyst/WON?
IV Vascular complications	
Venous thrombosis	SV; SMV; PV, etc.
Sinistral portal hypertension	Establishment of collateral vascular network ³
Pseudoaneurysm	Size (mm) and involvement artery ⁴
Organ complications	
Liver	Fatty liver (Signal difference of liver in the in-phase and out-of-phase)
Gallbladder and bile duct	Gallbladder stones (sandy/granular/filled); Common bile duct stones (site, number, size) and maximum duct diameter (mm)
Lung	Extent of pneumonia, pleural effusion
Subcutaneous and intermuscular space	Edema/effusion
Severity image score (MRSI)	(0-10) score
Comparison with previous imaging findings	For AP review, describe the pancreatic/peripancreatic changes after treatment; for surgical treatment, describe the site of the external drainage tube and internal covered metal stent

¹The ratio of the area of pancreatic necrosis in the largest slice to the whole pancreatic area.

²Sites of effusion include: left/right pararenal anterior spaces, perirenal spaces, posterior pararenal spaces, omental sac, bilateral paracolic sulcus, transverse colonic mesentery, small intestinal mesentery, greater omentum, other abdominal spaces, pelvic extraperitoneal spaces, pelvis cavity, thoracic cavity, and mediastinum.

³Such as left/right gastric omental vein, gastrocolic trunk, short gastric vein, submucosal vein of gastric fundus and gastric coronary vein).

⁴Such as splenic artery, pancreaticoduodenal artery, gastroduodenal artery, superior mesenteric artery, and celiac trunk. APFC: Acute peripancreatic fluid collection; ANC: Acute necrotic collection; WON: Walled-off necrosis; AC: Ascending colon; DC: Descending colon; MPD: Main pancreatic duct; SV: Splenic vein; SMV: Superior mesenteric vein; PV: Portal vein; IEP: Interstitial edematous pancreatitis; ANP: Acute necrotizing pancreatitis.



DOI: 10.4329/wjr.v15.i6.157 Copyright ©The Author(s) 2023.

Figure 1 Pancreatic and peripancreatic necrosis. A: Schematic diagram of pancreatic and peripancreatic necrosis (mixed type): pancreatic body necrosis (N) accompanied by peripancreatic fatty tissue debris (FD); B: A 61-year-old male with acute necrotizing pancreatitis (both pancreatic and peripancreatic necrosis). Fat-suppressed axial T1-weighted imaging shows a wide range of necrosis of the head and body of the pancreas (arrowheads), as well as peripancreatic collections containing large amounts of fat necrotic debris (arrows); C: Schematic diagram of necrotizing pancreatitis (peripancreatic necrosis alone): FD and absence of necrosis of pancreatic parenchyma; D: A 65-year-old woman with acute necrotizing pancreatitis (peripancreatic necrosis alone). Magnetic resonance imaging T2WI shows multiple patchy fatty fragments (hypointensity areas) (arrows) surrounding the pancreas.

involvement score and the mesenteric involvement score correlated well with the MRSI score[32,33]. These signs of subperitoneal space invasion can contribute to the prognostic assessment of the disease.

Local complications

The Revised Atlanta Consensus renamed four local fluid collections following AP. Of note, the exact time from the onset of the patient's initial symptoms to the imaging examination needs to be clarified. For radiologists, it is important for the correct nomenclature of peripancreatic fluid collections[2]. Typically, an imaging diagnosis of a pseudocyst or WON is reported equivalent to 4 wk after the onset of APFC (Figure 3C) or ANC (Figure 1). In particular, while characterizing the contents of a WON (Figure 3D), the percentage of solid debris within the overall fluid collection needs to be identified. That can be valuable in the choice of patient treatment decision-making. Rana *et al*[23] performed endoscopic ultrasound-guided treatment in 43 patients with symptomatic WON. When the solid necrotic debris in WON is less than 10%, only one endoscopic drainage is required. Then, at least two endoscopic drainages are required to cure patients if the necrotic debris is between 10% and 40%. If the solid necrotic debris is more than 40%, either endoscopic removal of necrotic tissue under ultrasound or surgical removal of necrotic tissue is additionally required[23]. In other words, with the increase of the amount of solid fragments, the number of transendoscopic operations will increase significantly[23].

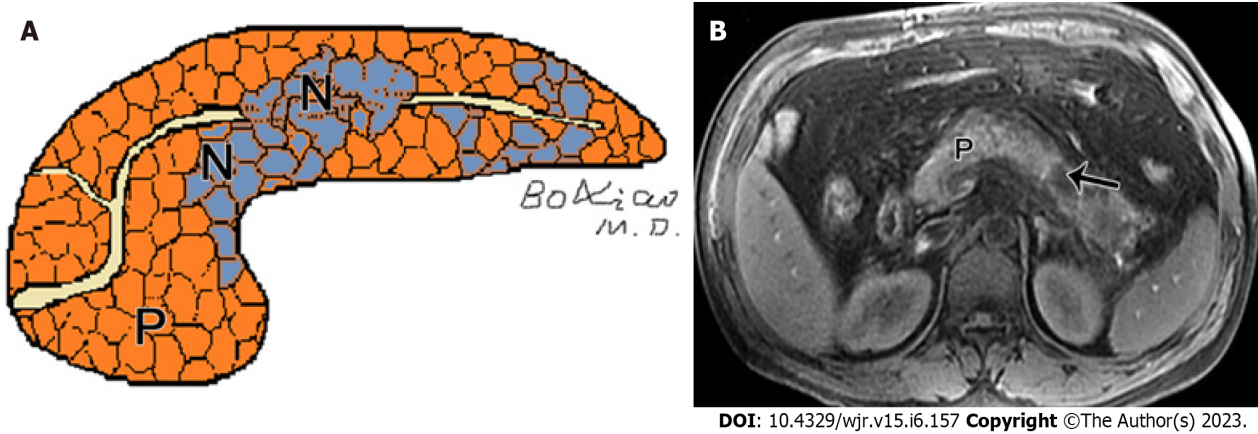


Figure 2 Peripancreatic necrosis only. A: Schematic diagram of necrotizing pancreatitis (pancreatic necrosis alone): Scattered necrotic lesions (N) within the pancreatic parenchyma; B: A 40-year-old man with necrotizing pancreatitis (pancreatic necrosis alone). Magnetic resonance imaging fat-suppressed T1-weighted imaging shows hypointensity area (arrow) in the pancreatic body, as well as absence of peripancreatic fat involvement.

DWI technology has a good ability to distinguish between aseptic, infected or necrotic components in WON[3,9,34]. Therefore, MRI is also a powerful tool for the qualitative and quantitative analysis of solid necrotic debris in WON.

Complications of infection

If peripancreatic fluid collection is complicated with infection, the mortality of AP patients will be significantly increased[6,35]. When gas-bubble or gas-fluid level signs appear in the APFC/ANC or pseudocyst/WON, radiologists need to describe in the MRI report and suggest infectious collections (Figure 3E). Besides, long-term fluid collections in the peripancreatic areas may erode the adjacent digestive tract and cause a secondary intestinal fistula[35]. Therefore, we need to report the segment of the intestinal canal that may be complicated by intestinal fistula. Patients with combined intestinal fistulas are indications for surgical procedures[36].

Disconnected pancreatic duct syndrome

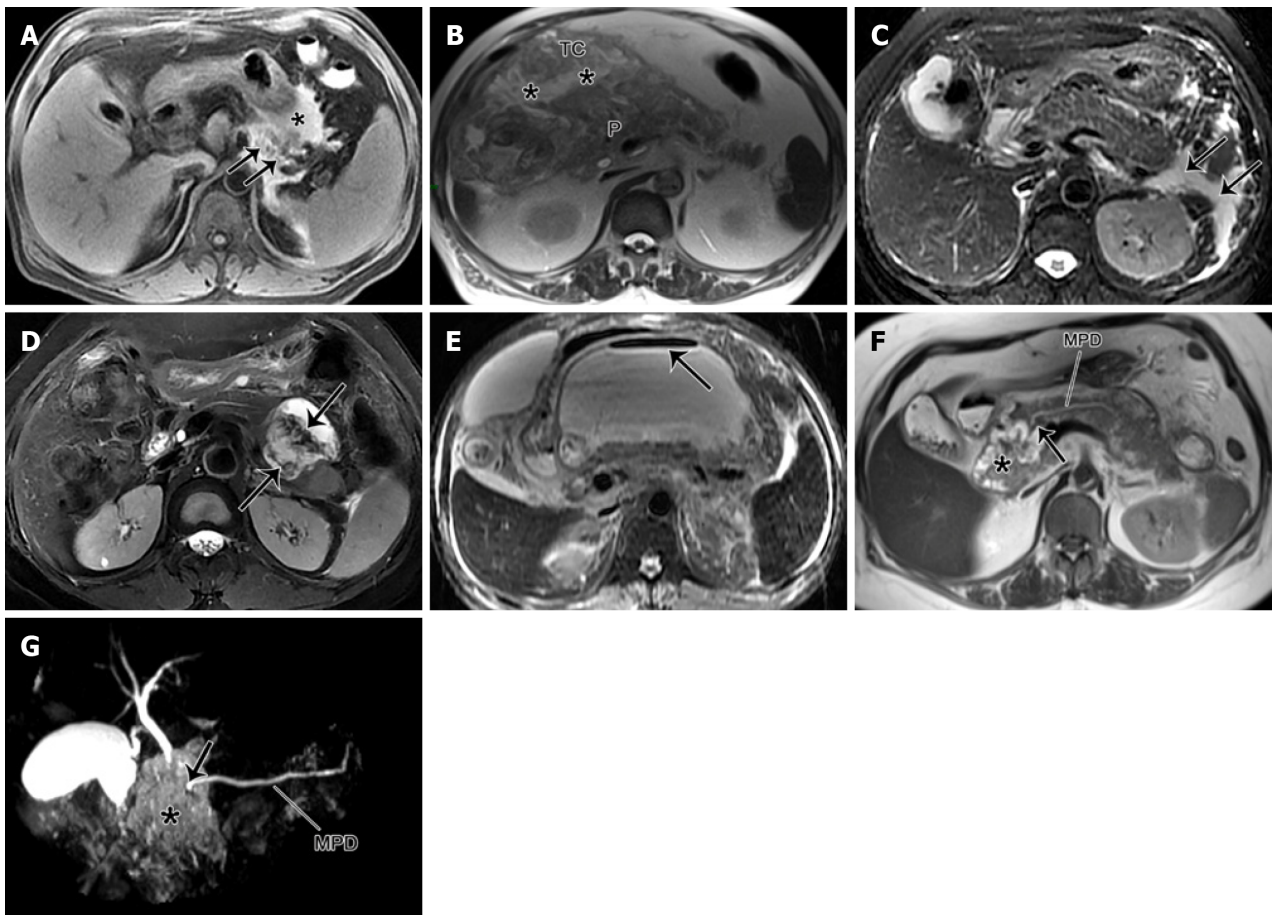
If an encapsulated fluid collection of the pancreas/peripancreatic zones involves the entire length of a pancreas (transmural necrosis), the collection lesion can often disrupt the MPD (Figure 3F and G). That is to say, it can lead to "disconnected pancreatic duct syndrome (DPDS)"[37], which is commonly seen in acute necrotizing pancreatitis. A recent prospective study shows that about 46.2% of patients with necrotizing pancreatitis will develop DPDS[38]. In addition, Maatman *et al*[39] have confirmed that an increased degree of pancreatic glandular necrosis is associated with the development of DPDS. Most importantly, the presence of such complications often requires surgical management. ERCP is the gold standard for diagnosing DPDS with 100% sensitivity, but it is invasive[40]. Magnetic resonance cholangiopancreatography (MRCP) is a non-invasive magnetic resonance technique. A recent study reported 92% sensitivity of combined MRCP and secretin MRCP in diagnosing DPDS[40]. That it can be seen that MRCP technology in MRI plays an irreplaceable role in the diagnosis of DPDS.

Vascular complications

Sinistral portal hypertension: Although chronic pancreatitis and pancreatic cancer are the main causes of sinistral portal hypertension (SPH), AP-related SPH also requires attention[41]. One study[42] found a 3.3% prevalence of SPH in 633 AP patients who underwent MRI. According to MRSI scores, the prevalence of SPH in mild, moderate, and severe AP increased progressively with 0.6%, 2.9%, and 47.8%, respectively[42]. This complication may be associated with late-phase gastrointestinal bleeding in AP patients and is therefore described in the MR structured report.

Pseudoaneurysm: Pseudoaneurysm is a rare but potentially fatal complication of AP, which is caused by reactive local arteritis following pancreatic proteolytic enzyme erosion[43]. The lesion most frequently involves the splenic, gastroduodenal, or pancreaticoduodenal arteries. If a pseudoaneurysm ruptures and bleeds, it may constitute a life-threatening emergency[24]. MRI can directly show the pseudoaneurysm lumen connected to the adjacent artery and the mural thrombus in the pseudoaneurysm lumen. On the enhanced MRI, the enhancement of the pseudoaneurysm lumen corresponds to that of an adjacent artery, while the non-enhanced area shows mural thrombus formation.

Venous thrombosis: Venous thrombosis is the most common vascular complication of AP[24]. The splenic vein is the most frequent vein invaded by inflammatory extension of the pancreas because of its proximity to the pancreas. Furthermore, the portal and superior mesenteric veins may also be involved.



DOI: 10.4329/wjr.v15.i6.157 Copyright ©The Author(s) 2023.

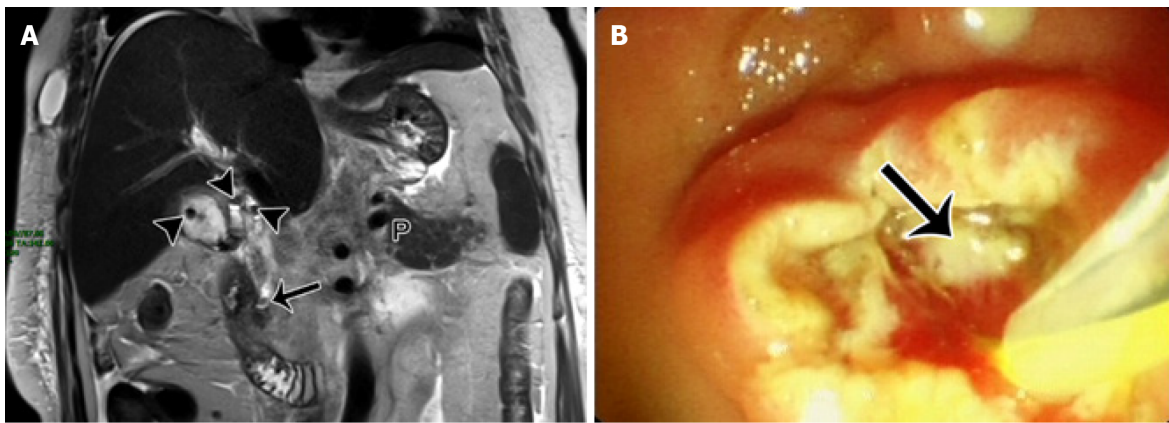
Figure 3 Pancreatic necrosis only. A: A 47-year-old male with acute necrotizing pancreatitis complicated by hemorrhage. Magnetic resonance imaging (MRI) fat-suppressed T1WI depicts a large area of hyperintensity in the pancreatic body (arrow) and peripancreatic areas (*), indicating the presence of pancreatic and peripancreatic fat necrosis with hemorrhage; B: A 73-year-old man with acute necrotizing pancreatitis complicated with transverse mesenteric effusion. MRI T1-weighted imaging (T1WI) demonstrates peripancreatic inflammation spreading from the root of mesentery to the transverse colon along the involved transverse mesentery (*). P: pancreas; C: A 63-year-old woman with acute interstitial pancreatitis with acute peripancreatic fluid collection. MRI fat-suppressed T2WI reveals the uniformly hyperintense fluid collections (arrows) around the pancreas; D: A 53-year-old woman with walled-off necrosis secondary to acute necrotizing pancreatitis (pancreatic and peripancreatic necrosis type). MRI fat-suppressed T2WI shows an enveloped necrotic collection involving the body and tail of the pancreas, with solid necrotic debris (arrows) accounting for more than 40%; E: A 45-year-old man with acute necrotizing pancreatitis accompanied by walled-off necrosis and secondary infection. MRI fat-suppressed T2WI shows extensive walled-off necrosis in the omental sac, as well as a gas-fluid level sign (arrow). Thereafter, the open surgery and drainage for infectious collections was performed; F: A 55-year-old woman with pancreatic duct disruption syndrome secondary to acute necrotizing pancreatitis with walled-off necrosis. MRI T2WI shows an enveloped necrosis lesion (*) in the pancreatic head, and a cut-off sign (arrow) of the main pancreatic duct (MPD) traveling into this lesion (*). G: MRCP reveals that the MPD of the pancreatic body and tail directly enters into the lesion (*) in a right-angle, concomitant with the interrupted MPD.

Dörffel *et al*[44] assessed this issue by color Doppler ultrasonography and found the incidence of venous thrombosis was 30% in acute non-necrotizing pancreatitis and 57% in necrotizing pancreatitis, similar to the conclusion of Jeffrey *et al*[45]. When there is venous thrombosis, MRI shows a loss of the normal vascular flow effect in the involved venous segment. After administration of contrast agent, intravenous filling defects can be seen on the enhanced venous phase images.

Organ complications/comorbidities

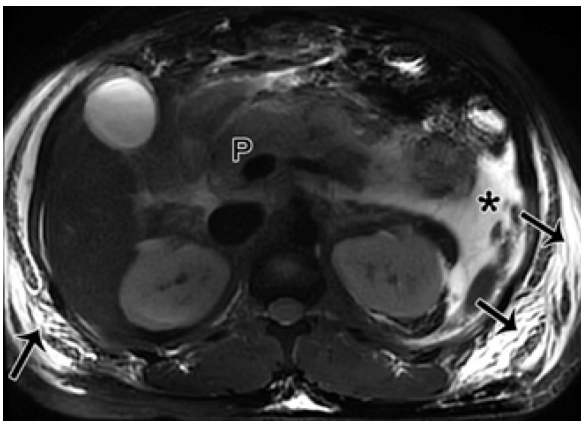
It is well known that three-quarters of the hepatic blood are supplied by the portal system. When AP occurs, many inflammatory factors and free fatty acids could be gathered in the liver during a short period of time, thereafter, MRI manifestations of fatty liver can be seen. Xiao *et al*[46] found that 66% of AP patients could be detected with signs of fatty liver on MRI. And the liver signal difference quantified by in-phase and out-of-phase images was positively correlated with MRSI. With the reduction of plasma triglyceride levels, the performance of the fatty liver on MRI can gradually return to normal[46].

The diagnosis of biliary stones, especially common bile duct stones, is suggestive for the choice of clinical treatment modality[47]. Thus, the MRI report description needs to be focused on gallstone pancreatitis (Figure 4). Furthermore, AP inflammatory exudate has a great impact on the gastrointestinal tract. It often causes damage to the intestinal barrier[48], followed by incomplete intestinal



DOI: 10.4329/wjr.v15.i6.157 Copyright ©The Author(s) 2023.

Figure 4 The magnetic resonance imaging report description needs to be focused on gallstone pancreatitis. A 56-year-old woman with acute gallstone pancreatitis. A: Magnetic resonance imaging T2WI coronal imaging shows multiple hypointensity stones (arrowheads) in the gallbladder and gallbladder duct, and another hypointensity stone (arrow) in the lower level of the common bile duct. The patient was underwent an endoscopic retrograde cholangiopancreatography (ERCP) procedure; B: ERCP shows a stone in the lower part of the common bile duct with suppurative conditions (arrow). P: Pancreas.



DOI: 10.4329/wjr.v15.i6.157 Copyright ©The Author(s) 2023.

Figure 5 Acute pancreatitis can also cause subcutaneous edema and fluid collection changes in the abdominal walls. A 25-year-old man with acute necrotizing pancreatitis and acute necrotic collection accompanied by conspicuous subcutaneous edema. Magnetic resonance imaging fat-suppressed T1-weighted imaging shows a majority of hyperintense fluid collections (*) in the left pararenal anterior space, and large flaps of hyperintense changes (arrows) in subcutaneous tissues of bilateral flanks and abdominal walls. P: Pancreas.

obstruction. This is associated with abdominal distention and increased intra-abdominal pressure in AP patients.

As far as chest CT is concerned, AP is mostly combined with pleural effusion and signs of compressive atelectasis[49]. Some scholars have suggested that this may be related to the presence of respiratory insufficiency (such as acute respiratory distress syndrome) in AP patients[50].

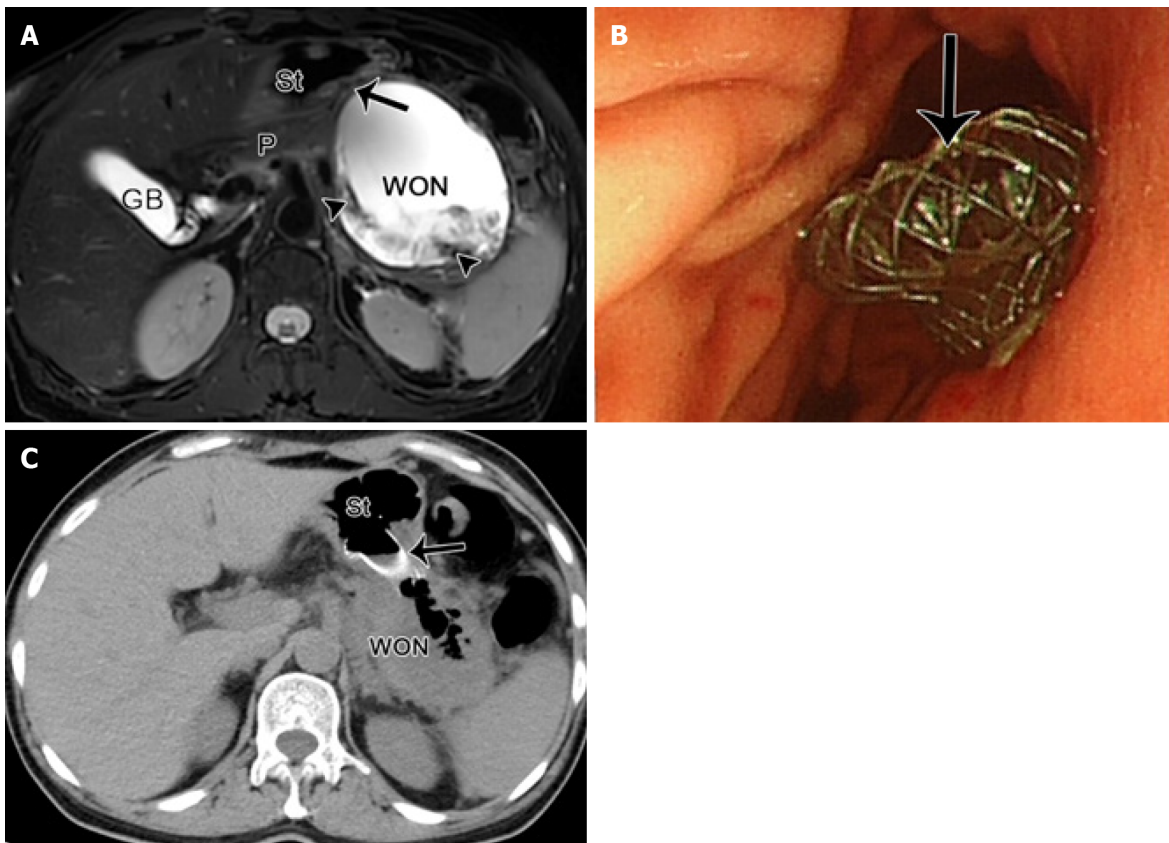
AP can also cause subcutaneous edema and fluid collection changes in the abdominal walls (Figure 5). Yang *et al*[51] found that 53.8% of AP patients showed abdominal wall edema on MRI. The abdominal wall edema score was positively correlated with the MRSI score[51]. Also, the degree of abdominal wall edema could indirectly reflect the severity of AP.

Comparison before and after treatment

The radiological changes in pancreatic/peripancreatic fluid collections before and after treatment should be described emphatically (Figure 6) in order to guide the adjustment of clinical treatment. In the cases of surgical drainage or built-in metal stents[52], the relationship between the site of the placement and the surrounding tissues and organs should be observed.

CONCLUSION

In summary, AP is a systemic and complex disease. The radiologists need to assist the clinicians in



DOI: 10.4329/wjr.v15.i6.157 Copyright ©The Author(s) 2023.

Figure 6 The radiological changes in pancreatic/peripancreatic fluid. A 49-year-old woman with acute necrotizing pancreatitis and pancreatic walled-off necrosis, performed by endoscopic ultrasound drainage. A: Magnetic resonance imaging fat-suppressed T1-weighted imaging shows a walled-off necrosis (WON) with a diameter of 10 cm × 9 cm in the omental sac and pancreatic body and tail, as well as numerous necrotic fragments (arrowheads) within the WON. The WON is adjacent to the gastric body; B: Thereafter, under the guidance of endoscopic ultrasonography, a fully coated mushroom metal stent (arrow) was placed through the stomach for internal drainage; C: Postoperative computed tomography image shows that the WON was apparently decreased, with a large amount of gas and a high-density stent (arrow) in place. St: Stomach, P: Pancreas, GB: Gallbladder.

selecting a reasonable imaging modality. Although enhanced CT is considered to be the main imaging method for the first diagnosis of AP patients, MRI has good soft tissue resolution and various sequence techniques. Thus, it can be better evaluated and follow up the condition of AP patients. In the writing of MR structured imaging report, we need to take into account the systematic description of the pancreas itself, peripancreatic changes, local complications, organ complications, and the dynamic changes after treatment. If the patient's condition is tolerated and the hospital equipment permits, we recommend that the patient be examined by MRI. The MRI structured report template of AP recommended in this paper could be used as a reference for different centers. Indeed, multi-center validation of MR structured report template at domestic and abroad is needed in order to constantly improve and update in the future clinical practice.

FOOTNOTES

Author contributions: Song LJ and Xiao B contributed equally to this work; Xiao B designed the research study; Song LJ performed the research; Song LJ and Xiao B analyzed the data and wrote the manuscript; All authors have read and approve the final manuscript.

Conflict-of-interest statement: All the authors declare that they have no conflict of interest.

Open-Access: This article is an open-access article that was selected by an in-house editor and fully peer-reviewed by external reviewers. It is distributed in accordance with the Creative Commons Attribution NonCommercial (CC BY-NC 4.0) license, which permits others to distribute, remix, adapt, build upon this work non-commercially, and license their derivative works on different terms, provided the original work is properly cited and the use is non-commercial. See: <https://creativecommons.org/licenses/by-nc/4.0/>

Country/Territory of origin: China

ORCID number: Ling-Ji Song 0000-0003-4508-9654; Bo Xiao 0000-0001-5862-974X.

S-Editor: Liu JH

L-Editor: A

P-Editor: Zhao S

REFERENCES

- 1 **Li F**, Zhang F, Wan X, Wu K, Liu Q, Qiu C, Yin H, Lyu J. Infections in Acute Pancreatitis: Organisms, Resistance-Patterns and Effect on Mortality. *Dig Dis Sci* 2023; **68**: 630-643 [PMID: 36562889 DOI: 10.1007/s10620-022-07793-1]
- 2 **Ortiz Morales CM**, Girela Baena EL, Olalla Muñoz JR, Parlorio de Andrés E, López Corbalán JA. Radiology of acute pancreatitis today: the Atlanta classification and the current role of imaging in its diagnosis and treatment. *Radiologia (Engl Ed)* 2019; **61**: 453-466 [PMID: 31153603 DOI: 10.1016/j.rx.2019.04.001]
- 3 **Sureka B**, Rai B, Varshney V, Nag VL, Garg MK, Garg PK, Yadav T, Khera PS, Goel A. Quantitative diffusion-weighted magnetic resonance imaging for prediction of early infection in pancreatic collections: Results of a pilot study. *Saudi J Gastroenterol* 2020; **26**: 20-25 [PMID: 31997778 DOI: 10.4103/sjg.SJG_411_19]
- 4 **Pavlidis ET**, Pavlidis TE. Management of infected acute necrotizing pancreatitis. *World J Clin Cases* 2023; **11**: 482-486 [PMID: 36686342 DOI: 10.12998/wjcc.v11.i2.482]
- 5 **Li YL**, Zhang DD, Xiong YY, Wang RF, Gao XM, Gong H, Zheng SC, Wu D. Development and external validation of models to predict acute respiratory distress syndrome related to severe acute pancreatitis. *World J Gastroenterol* 2022; **28**: 2123-2136 [PMID: 35664037 DOI: 10.3748/wjg.v28.i19.2123]
- 6 **Banks PA**, Bollen TL, Dervenis C, Gooszen HG, Johnson CD, Sarr MG, Tsiotos GG, Vege SS; Acute Pancreatitis Classification Working Group. Classification of acute pancreatitis--2012: revision of the Atlanta classification and definitions by international consensus. *Gut* 2013; **62**: 102-111 [PMID: 23100216 DOI: 10.1136/gutjnl-2012-302779]
- 7 **Khurana A**, Nelson LW, Myers CB, Akisik F, Jeffrey BR, Miller FH, Mittal P, Morgan D, Mortele K, Poulos P, Sahani D, Sandrasegaran K, Tirkes T, Zaheer A, Patel BN. Reporting of acute pancreatitis by radiologists-time for a systematic change with structured reporting template. *Abdom Radiol (NY)* 2020; **45**: 1277-1289 [PMID: 32189022 DOI: 10.1007/s00261-020-02468-9]
- 8 **Türkvan A**, Erden A, Türkoğlu MA, Seçil M, Yener Ö. Imaging of acute pancreatitis and its complications. Part 1: acute pancreatitis. *Diagn Interv Imaging* 2015; **96**: 151-160 [PMID: 24512896 DOI: 10.1016/j.diii.2013.12.017]
- 9 **de Freitas Tertulino F**, Schraibman V, Ardengh JC, do Espírito-Santo DC, Ajzen SA, Torrez FR, Lobo EJ, Szejnfeld J, Goldman SM. Diffusion-weighted magnetic resonance imaging indicates the severity of acute pancreatitis. *Abdom Imaging* 2015; **40**: 265-271 [PMID: 25070771 DOI: 10.1007/s00261-014-0205-y]
- 10 **Szatmary P**, Grammatikopoulos T, Cai W, Huang W, Mukherjee R, Halloran C, Beyer G, Sutton R. Acute Pancreatitis: Diagnosis and Treatment. *Drugs* 2022; **82**: 1251-1276 [PMID: 36074322 DOI: 10.1007/s40265-022-01766-4]
- 11 **Aghdassi AA**, Seidensticker M. [Imaging diagnostics in acute pancreatitis]. *Internist (Berl)* 2021; **62**: 1044-1054 [PMID: 34524469 DOI: 10.1007/s00108-021-01153-3]
- 12 **Brizi MG**, Perillo F, Cannone F, Tuzza L, Manfredi R. The role of imaging in acute pancreatitis. *Radiol Med* 2021; **126**: 1017-1029 [PMID: 33982269 DOI: 10.1007/s11547-021-01359-3]
- 13 **Yadav D**, Lowenfels AB. The epidemiology of pancreatitis and pancreatic cancer. *Gastroenterology* 2013; **144**: 1252-1261 [PMID: 23622135 DOI: 10.1053/j.gastro.2013.01.068]
- 14 **Sadr-Azodi O**, Andrén-Sandberg Å, Orsini N, Wolk A. Cigarette smoking, smoking cessation and acute pancreatitis: a prospective population-based study. *Gut* 2012; **61**: 262-267 [PMID: 21836026 DOI: 10.1136/gutjnl-2011-300566]
- 15 **Ye X**, Lu G, Huai J, Ding J. Impact of smoking on the risk of pancreatitis: a systematic review and meta-analysis. *PLoS One* 2015; **10**: e0124075 [PMID: 25879541 DOI: 10.1371/journal.pone.0124075]
- 16 **Obed M**, Gabriel MM, Dumann E, Vollmer Barbosa C, Weißenborn K, Schmidt BMW. Risk of acute kidney injury after contrast-enhanced computerized tomography: a systematic review and meta-analysis of 21 propensity score-matched cohort studies. *Eur Radiol* 2022; **32**: 8432-8442 [PMID: 35727320 DOI: 10.1007/s00330-022-08916-y]
- 17 **Rocha APC**, Schawkat K, Mortele KJ. Imaging guidelines for acute pancreatitis: when and when not to image. *Abdom Radiol (NY)* 2020; **45**: 1338-1349 [PMID: 31712865 DOI: 10.1007/s00261-019-02319-2]
- 18 **James TW**, Crockett SD. Management of acute pancreatitis in the first 72 hours. *Curr Opin Gastroenterol* 2018; **34**: 330-335 [PMID: 29957661 DOI: 10.1097/MOG.0000000000000456]
- 19 **Shinya S**, Sasaki T, Nakagawa Y, Guiquing Z, Yamamoto F, Yamashita Y. Acute pancreatitis successfully diagnosed by diffusion-weighted imaging: a case report. *World J Gastroenterol* 2008; **14**: 5478-5480 [PMID: 18803364 DOI: 10.3748/wjg.14.5478]
- 20 **Shinya S**, Sasaki T, Nakagawa Y, Guiquing Z, Yamamoto F, Yamashita Y. The efficacy of diffusion-weighted imaging for the detection and evaluation of acute pancreatitis. *HepatoGastroenterology* 2009; **56**: 1407-1410 [PMID: 19950800]
- 21 **Tang MY**, Chen TW, Bollen TL, Wang YX, Xue HD, Jin ZY, Huang XH, Xiao B, Li XH, Ji YF, Zhang XM. MR imaging of hemorrhage associated with acute pancreatitis. *Pancreatol* 2018; **18**: 363-369 [PMID: 29615311 DOI: 10.1016/j.pan.2018.03.004]
- 22 **Foster BR**, Jensen KK, Bakis G, Shaaban AM, Coakley FV. Revised Atlanta Classification for Acute Pancreatitis: A Pictorial Essay. *Radiographics* 2016; **36**: 675-687 [PMID: 27163588 DOI: 10.1148/rg.2016150097]
- 23 **Rana SS**, Bhasin DK, Sharma RK, Kathiresan J, Gupta R. Do the morphological features of walled off pancreatic necrosis on endoscopic ultrasound determine the outcome of endoscopic transmural drainage? *Endosc Ultrasound* 2014; **3**: 118-122 [PMID: 24955341 DOI: 10.4103/2303-9027.131039]

- 24 **Miller FH**, Keppke AL, Dalal K, Ly JN, Kamler VA, Sica GT. MRI of pancreatitis and its complications: part 1, acute pancreatitis. *AJR Am J Roentgenol* 2004; **183**: 1637-1644 [PMID: 15547203 DOI: 10.2214/ajr.183.6.01831637]
- 25 **Liao Q**, Ding L, Xu X, Yu C, Deng F, Xiong H, He W, Xia L, Zeng X, Lu N, Zhu Y. Pancreatic necrosis volume for predicting readmission and reintervention in acute necrotizing pancreatitis. *Eur J Radiol* 2022; **154**: 110419 [PMID: 35878514 DOI: 10.1016/j.ejrad.2022.110419]
- 26 **Meyrignac O**, Lagarde S, Bournet B, Mokrane FZ, Buscail L, Rousseau H, Otal P. Acute Pancreatitis: Extrapancreatic Necrosis Volume as Early Predictor of Severity. *Radiology* 2015; **276**: 119-128 [PMID: 25642743 DOI: 10.1148/radiol.15141494]
- 27 **Çakar İ**, Keven A, Eseroğlu E, Çubuk SM. Role of extrapancreatic necrosis volume in determining early prognosis in patients with acute pancreatitis. *Abdom Radiol (NY)* 2020; **45**: 1507-1516 [PMID: 31428812 DOI: 10.1007/s00261-019-02188-9]
- 28 **Cucuteanu B**, Negru D, Gavrilescu O, Popa IV, Floria M, Mihai C, Cijevschi Prelicean C, Dranga M. Extrapancreatic necrosis volume: A new tool in acute pancreatitis severity assessment? *World J Clin Cases* 2021; **9**: 9395-9405 [PMID: 34877275 DOI: 10.12998/wjcc.v9.i31.9395]
- 29 **Khristenko E**, Tjaden C, Klaufß M. [Pancreas divisum and pancreatitis]. *Radiologe* 2021; **61**: 541-547 [PMID: 33942124 DOI: 10.1007/s00117-021-00848-w]
- 30 **Wessling J**, Peitz U, Hoffmann M, Schreyer AG, Grenacher L. [Acute pancreatitis : Typical findings in computed tomography and magnetic resonance imaging]. *Radiologe* 2021; **61**: 532-540 [PMID: 34061214 DOI: 10.1007/s00117-021-00854-y]
- 31 **Lenhart DK**, Balthazar EJ. MDCT of acute mild (necrotizing) pancreatitis: abdominal complications and fate of fluid collections. *AJR Am J Roentgenol* 2008; **190**: 643-649 [PMID: 18287434 DOI: 10.2214/AJR.07.2761]
- 32 **Chi XX**, Zhang XM, Chen TW, Huang XH, Yang L, Tang W, Xiao B. The normal transverse mesocolon and involvement of the mesocolon in acute pancreatitis: an MRI study. *PLoS One* 2014; **9**: e93687 [PMID: 24705446 DOI: 10.1371/journal.pone.0093687]
- 33 **Chi XX**, Zhang XM, Chen TW, Tang W, Xiao B, Ji YF, Huang XH. Magnetic resonance imaging for the normal mesostenium and involvement of the mesostenium in acute pancreatitis. *Biomed Res Int* 2014; **2014**: 924845 [PMID: 25136639 DOI: 10.1155/2014/924845]
- 34 **Islim F**, Salik AE, Bayramoglu S, Guven K, Alis H, Turhan AN. Non-invasive detection of infection in acute pancreatic and acute necrotic collections with diffusion-weighted magnetic resonance imaging: preliminary findings. *Abdom Imaging* 2014; **39**: 472-481 [PMID: 24441591 DOI: 10.1007/s00261-014-0076-2]
- 35 **Umapathy C**, Gajendran M, Mann R, Boregowda U, Theethira T, Elhanafi S, Perisetti A, Goyal H, Saligram S. Pancreatic fluid collections: Clinical manifestations, diagnostic evaluation and management. *Dis Mon* 2020; **66**: 100986 [PMID: 32312558 DOI: 10.1016/j.disamonth.2020.100986]
- 36 **Banter LR**, Maatman TK, McGuire SP, Ceppa EP, House MG, Nakeeb A, Nguyen TK, Schmidt CM, Zyromski NJ. Duodenal complications in necrotizing pancreatitis: Challenges of an overlooked complication. *Am J Surg* 2021; **221**: 589-593 [PMID: 33218676 DOI: 10.1016/j.amjsurg.2020.11.022]
- 37 **Vanek P**, Urban O, Trikudanathan G, Freeman ML. Disconnected pancreatic duct syndrome in patients with necrotizing pancreatitis. *Surg Open Sci* 2023; **11**: 19-25 [PMID: 36438587 DOI: 10.1016/j.sopen.2022.10.009]
- 38 **Maatman TK**, Roch AM, Lewellen KA, Heimberger MA, Ceppa EP, House MG, Nakeeb A, Schmidt CM, Zyromski NJ. Disconnected Pancreatic Duct Syndrome: Spectrum of Operative Management. *J Surg Res* 2020; **247**: 297-303 [PMID: 31685250 DOI: 10.1016/j.jss.2019.09.068]
- 39 **Maatman TK**, Roch AM, Ceppa EP, Easler JJ, Gromski MA, House MG, Nakeeb A, Schmidt CM, Sherman S, Zyromski NJ. The continuum of complications in survivors of necrotizing pancreatitis. *Surgery* 2020; **168**: 1032-1040 [PMID: 32843212 DOI: 10.1016/j.surg.2020.07.004]
- 40 **Timmerhuis HC**, van Dijk SM, Verdonk RC, Bollen TL, Bruno MJ, Fockens P, van Hooft JE, Voermans RP, Besselink MG, van Santvoort HC; Dutch Pancreatitis Study Group. Various Modalities Accurate in Diagnosing a Disrupted or Disconnected Pancreatic Duct in Acute Pancreatitis: A Systematic Review. *Dig Dis Sci* 2021; **66**: 1415-1424 [PMID: 32594462 DOI: 10.1007/s10620-020-06413-0]
- 41 **Li H**, Yang Z, Tian F. Clinical Characteristics and Risk Factors for Sinistral Portal Hypertension Associated with Moderate and Severe Acute Pancreatitis: A Seven-Year Single-Center Retrospective Study. *Med Sci Monit* 2019; **25**: 5969-5976 [PMID: 31400275 DOI: 10.12659/MSM.916192]
- 42 **Xie CL**, Wu CQ, Chen Y, Chen TW, Xue HD, Jin ZY, Zhang XM. Sinistral Portal Hypertension in Acute Pancreatitis: A Magnetic Resonance Imaging Study. *Pancreas* 2019; **48**: 187-192 [PMID: 30629031 DOI: 10.1097/MPA.0000000000001242]
- 43 **Kalas MA**, Leon M, Chavez LO, Canalizo E, Surani S. Vascular complications of pancreatitis. *World J Clin Cases* 2022; **10**: 7665-7673 [PMID: 36158481 DOI: 10.12998/wjcc.v10.i22.7665]
- 44 **Dörffel T**, Wruck T, Rückert RI, Romaniuk P, Dörffel Q, Wermke W. Vascular complications in acute pancreatitis assessed by color duplex ultrasonography. *Pancreas* 2000; **21**: 126-133 [PMID: 10975705 DOI: 10.1097/00006676-200008000-00004]
- 45 **Easler J**, Muddana V, Furlan A, Dasyam A, Vippera K, Slivka A, Whitcomb DC, Papachristou GI, Yadav D. Portosplenomesenteric venous thrombosis in patients with acute pancreatitis is associated with pancreatic necrosis and usually has a benign course. *Clin Gastroenterol Hepatol* 2014; **12**: 854-862 [PMID: 24161350 DOI: 10.1016/j.cgh.2013.09.068]
- 46 **Xiao B**, Zhang XM, Jiang ZQ, Tang W, Huang XH, Yang L, Feng ZS. Fatty liver in acute pancreatitis: characteristics in magnetic resonance imaging. *J Comput Assist Tomogr* 2012; **36**: 400-405 [PMID: 22805667 DOI: 10.1097/RCT.0b013e31825977c2]
- 47 **Ji YF**, Zhang XM, Li XH, Jing ZL, Huang XH, Yang L, Zhai ZH. Gallbladder patterns in acute pancreatitis: an MRI study. *Acad Radiol* 2012; **19**: 571-578 [PMID: 22366559 DOI: 10.1016/j.acra.2012.01.004]
- 48 **Koh YY**, Jeon WK, Cho YK, Kim HJ, Chung WG, Chon CU, Oh TY, Shin JH. The effect of intestinal permeability and

- endotoxemia on the prognosis of acute pancreatitis. *Gut Liver* 2012; **6**: 505-511 [PMID: 23170158 DOI: 10.5009/gnl.2012.6.4.505]
- 49 **Kumar P**, Gupta P, Rana S. Thoracic complications of pancreatitis. *JGH Open* 2019; **3**: 71-79 [PMID: 30834344 DOI: 10.1002/jgh3.12099]
- 50 **Song LJ**, Xiao B. Medical imaging for pancreatic diseases: Prediction of severe acute pancreatitis complicated with acute respiratory distress syndrome. *World J Gastroenterol* 2022; **28**: 6206-6212 [PMID: 36504558 DOI: 10.3748/wjg.v28.i44.6206]
- 51 **Yang R**, Jing ZL, Zhang XM, Tang W, Xiao B, Huang XH, Yang L, Feng ZS. MR imaging of acute pancreatitis: correlation of abdominal wall edema with severity scores. *Eur J Radiol* 2012; **81**: 3041-3047 [PMID: 22571930 DOI: 10.1016/j.ejrad.2012.04.005]
- 52 **Heckler M**, Hackert T, Hu K, Halloran CM, Büchler MW, Neoptolemos JP. Severe acute pancreatitis: surgical indications and treatment. *Langenbecks Arch Surg* 2021; **406**: 521-535 [PMID: 32910276 DOI: 10.1007/s00423-020-01944-6]

Radiological parameters to predict pancreatic texture: Current evidence and future perspectives

Raja Kalayarasan, Mandalapu Himaja, Ananthkrishnan Ramesh, Kathirvel Kokila

Specialty type: Radiology, nuclear medicine and medical imaging

Provenance and peer review: Invited article; Externally peer reviewed.

Peer-review model: Single blind

Peer-review report's scientific quality classification

Grade A (Excellent): 0
Grade B (Very good): 0
Grade C (Good): C
Grade D (Fair): D
Grade E (Poor): 0

P-Reviewer: Kikuyama M, Japan;
Yang F, China

Received: April 26, 2023

Peer-review started: April 26, 2023

First decision: May 19, 2023

Revised: June 3, 2023

Accepted: June 14, 2023

Article in press: June 14, 2023

Published online: June 28, 2023



Raja Kalayarasan, Mandalapu Himaja, Department of Surgical Gastroenterology, Jawaharlal Institute of Postgraduate Medical Education and Research, Puducherry 605006, India

Ananthkrishnan Ramesh, Kathirvel Kokila, Department of Radiodiagnosis, Jawaharlal Institute of Postgraduate Medical Education and Research, Puducherry 605006, India

Corresponding author: Raja Kalayarasan, MBBS, MS, MCh, FRCS (Ed), Additional Professor, Department of Surgical Gastroenterology, Jawaharlal Institute of Postgraduate Medical Education and Research, Room No. 5442, 4th floor, Super Specialty Block, Puducherry 605006, India. kalayarasanraja@yahoo.com

Abstract

Preoperative prediction of the postoperative pancreatic fistula risk is critical in the current era of minimally invasive pancreatic surgeries to tailor perioperative management, thereby minimizing postoperative morbidity. Pancreatic duct diameter can be readily measured by any routine imaging used to diagnose pancreatic disease. However, radiological evaluation of pancreatic texture, an important determinant of pancreatic fistula, has not been widely used to predict the risk of postoperative pancreatic fistula. Qualitative and quantitative assessment of pancreatic fibrosis and fat fraction provides the basis for predicting pancreatic texture. Traditionally computed tomography has been utilized in identifying and characterizing pancreatic lesions and background parenchymal pathologies. With the increasing utilisation of endoscopic ultrasound and magnetic resonance imaging for evaluating pancreatic pathologies, elastography is emerging as a promising tool for predicting pancreatic texture. Also, recent studies have shown that early surgery for chronic pancreatitis is associated with better pain relief and preservation of pancreatic function. Pancreatic texture assessment can allow early diagnosis of chronic pancreatitis, facilitating early intervention. The present review outlines the current evidence in utilizing various imaging modalities for determining the pancreatic texture based on different parameters and image sequences. However, multidisciplinary investigations using strong radiologic-pathologic correlation are needed to standardize and establish the role of these non-invasive diagnostic tools in predicting pancreatic texture.

Key Words: Pancreatic fistula; Minimally invasive; Pancreaticoduodenectomy; Pancreatic cancer; Neoplasms; Computed tomography; Endoscopic ultrasound; Ultrasonography;

Magnetic resonance imaging

©The Author(s) 2023. Published by Baishideng Publishing Group Inc. All rights reserved.

Core Tip: Preoperative prediction of pancreatic texture and pancreatic fistula risk can guide selecting patients who could derive maximum benefit from minimally invasive pancreatoduodenectomy. Also, pancreatic texture evaluation could facilitate early diagnosis of chronic pancreatitis. Endoscopic ultrasound and magnetic resonance imaging-based elastography has improved the diagnostic accuracy of pancreatic fibrosis. Future studies should focus on combining different radiological modalities and correlating with histological parameters to standardize the radiological evaluation of pancreatic texture.

Citation: Kalayarasan R, Himaja M, Ramesh A, Kokila K. Radiological parameters to predict pancreatic texture: Current evidence and future perspectives. *World J Radiol* 2023; 15(6): 170-181

URL: <https://www.wjgnet.com/1949-8470/full/v15/i6/170.htm>

DOI: <https://dx.doi.org/10.4329/wjr.v15.i6.170>

INTRODUCTION

Pancreatoduodenectomy (PD) is the primary treatment for periampullary and pancreatic malignancies. Advancements in surgical techniques and perioperative management reduced the mortality after PD to less than 5% in high-volume centers[1]. However, PD-related morbidity remains high at 30%-50%[2,3]. Postoperative pancreatic fistula (POPF) is the primary determinant of morbidity and mortality after PD. Hence it is crucial to identify patients at high risk of POPF. Previous studies have identified pancreatic texture, pancreatic duct diameter, pancreatic stump ischemia, and operative blood loss as significant risk factors for POPF[4-8].

Pancreatic texture has been reported as an important predictor of POPF[6,7]. Soft pancreas is associated with increased risk of POPF and a firm pancreas is protective against POPF. The higher the fat fraction in the pancreas, the softer the pancreas is, however it becomes harder with the increasing grade of fibrosis. Traditionally assessment of the pancreatic texture is done by intraoperative palpation or histological evaluation of the operative specimen[7]. However, these assessment techniques cannot be used for the preoperative prediction of POPF. Also, intraoperative assessment of pancreatic texture during minimally invasive surgeries, especially the robotic approach, is challenging. With advancements in surgical techniques and instrumentation, a minimally invasive approach has been increasingly used to perform PD. However, multicenter randomized controlled trials (RCTs), including the recent Chinese trial, have failed to show short-term clinical benefits with minimally invasive PD compared to the open approach[9,10]. The results of these RCTs underscore that in PD, morbidity related to the procedure rather than access determines the short-term outcomes. As most of the morbidity in PD is related to POPF, preoperative prediction of patients with high risk of POPF can guide in adopting the intraoperative and postoperative management to reduce the POPF-related morbidity and thereby reducing the overall morbidity of PD. It also helps select patients at low risk of POPF who will benefit from minimally invasive PD. Hence, attempts have been made to correlate preoperative radiological parameters with pancreatic texture[11-16].

Another application of pancreatic texture evaluation is in patients with chronic pancreatitis. Recent studies have shown that early intervention for patients with chronic pancreatitis is associated with better outcomes than delayed intervention[17,18]. Pancreatic texture evaluation could facilitate the early identification of pancreatic fibrosis. The commonly employed diagnostic modalities for the assessment of pancreatic lesions are ultrasonography (USG), computed tomography (CT), magnetic resonance imaging (MRI), and endoscopic US (EUS). The present review aims to provide an overview of various parameters that can be assessed with each radiological investigation to detect the presence of fatty or fibrotic pancreas and predict the pancreatic texture.

PANCREATIC TEXTURE AND POSTOPERATIVE PANCREATIC FISTULA

The association between pancreatic texture and POPF risk has been documented in multiple retrospective and prospective studies. Kawai *et al*[4] in a multicenter study analyzed the risk factors for POPF in 1239 patients who underwent pancreatoduodenectomy. The authors concluded that soft pancreas was one of the significant risk factors for clinical pancreatic fistula. Patients with soft pancreatic texture are at 2.7 times more risk of developing POPF. Ansorge *et al*[5], in a single-center

prospective study of 164 patients reported that softer pancreatic texture is associated with a significantly higher incidence of POPF ($P < 0.001$) and a higher incidence of symptomatic postoperative peripancreatic collections ($P = 0.071$) compared to those with firm pancreatic texture. Ridolfi *et al*[6] evaluated the morpho histological features of pancreatic stump after pancreatoduodenectomy in 143 patients and found them to be the primary determinant of pancreatic fistula after pancreatoduodenectomy. A soft pancreas was strongly associated with POPF development and with high-grade POPF. In their study 42% of patients with soft pancreas developed a high-grade fistula, compared to 4% of patients with firm pancreatic texture ($P < 0.001$). In their study pancreatic texture was confirmed with histological correlation using fibrosis and inflammation scores. Hu *et al*[7] retrospectively analysed 539 patients who underwent pancreatoduodenectomy and found a significant correlation between pancreatic texture and POPF by univariate and multivariate analysis.

However similar correlation could not be established between pancreatic texture and POPF after distal pancreatectomy. This could be because of a different mechanism for leak and fistula formation from the pancreatic remnant after distal pancreatectomy compared to pancreaticoduodenectomy, which includes pancreatoenteric anastomosis. Chong *et al*[8], in a meta-analysis that included 43 studies with 8864 patients, found no difference in clinically relevant POPF rate between soft pancreas (25.3%, 373/1477) and hard pancreas (13.5%, 72/535) ($P = 0.46$). Pancreatic gland texture and duct size are not associated with the development of pancreatic fistula following distal pancreatectomy, unlike that of pancreatoduodenectomy. Hence, assessment of pancreatic texture is more useful in patients undergoing pancreatoduodenectomy compared to those undergoing distal pancreatectomy.

ULTRASONOGRAPHY ABDOMEN

Transabdominal USG is the commonly used initial investigation to evaluate pancreatic pathology. The grayscale B- mode USG can evaluate the echotexture of the pancreas. The echotexture of the normal pancreas is isoechoic or slightly hyperechoic compared to the normal liver and shows a granular appearance with a smooth or minimally lobulated outline (Figure 1). With age, the echogenicity of the pancreas increases due to atrophy with fatty replacement. A fatty pancreas often occurs at the same time as fatty liver, which makes diagnosis more challenging. The most common limitations in scanning the pancreas by transabdominal approach are abdominal fat in obese patients and bowel air. As predicting pancreatic texture by routine B-mode USG is challenging, USG elastography has recently been used to measure the elasticity of different tissues[19,20].

Elastography

Elastography measures the stiffness of various organs and has been used to evaluate liver fibrosis and breast lesions[19,20]. Elastography of the pancreas can be performed using transabdominal USG, EUS, or MRI[21]. The techniques of USG elastography include strain elastography and shear wave elastography (SWE)[21]. The stiffness of tissue in the strain elastography is estimated by measuring the grade of strain generated by external pressure: the greater the strain, the softer the stiffness of the target tissue. The SWE relies on the principle of acoustic radiation force impulse (ARFI) using a USG probe which propagates through the tissue, and stiffness is estimated by measuring the propagation speed of the shear wave (Figure 1). The shear wave velocity (SWV) depends on the stiffness of the tissue: the higher the SWV, the harder the target tissue[22,23]. As SWE is less operator-dependent, it is preferred over strain elastography. Strain elastography is challenging to measure when the ultrasound probe, the pancreas, and the aorta are not in line. Hence it is easy to get a fine elastogram in the pancreatic body but not in the pancreatic head and tail regions. However, SWE can be easily performed anywhere in the pancreas because ARFI can be emitted wherever desired. Over the last few years, there has been increasing interest in assessing the role of elastography in evaluating pancreatic texture, differentiating benign and malignant pancreatic lesions, and diagnosing chronic pancreatitis[24-28].

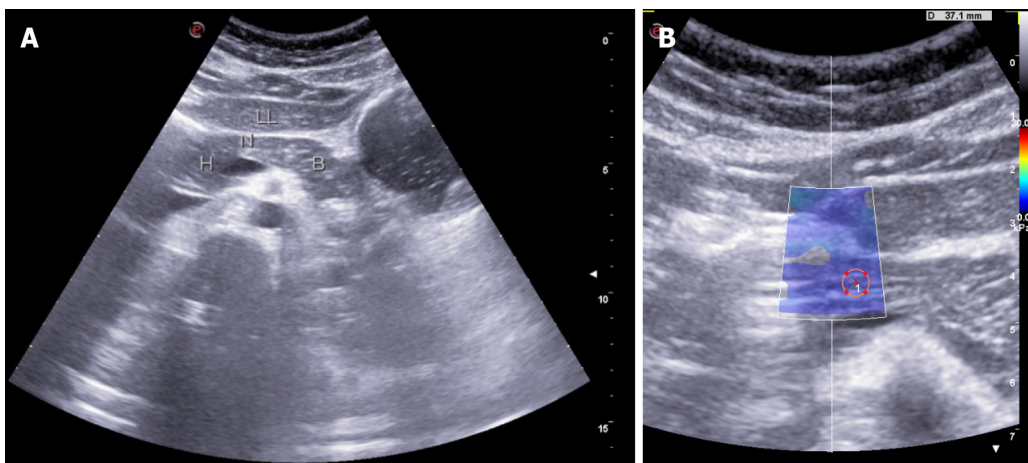
Yashima *et al*[27] used ARFI elastography of the pancreas and reported high elasticity in patients with chronic pancreatitis compared to normal patients. SWV in patients with chronic pancreatitis was significantly higher than that in healthy volunteers in each part of the pancreas (Figure 2). However, the measurement was difficult in the tail of the pancreas (Table 1). Harada *et al*[29] reported a good correlation between SWV and the histological grade of fibrosis. Pancreatic SWV, measured by preoperative ARFI imaging, was shown to have significant correlations with the grade of pathologic fibrosis, influencing the risk of POPF.

Llamoza-Torres *et al*[30], in their study of 33 patients, established the diagnostic accuracy of transabdominal USG-guided elastography in evaluating patients with suspected chronic pancreatitis. Patients included in the study were initially evaluated by EUS and/or MRI to establish their chronic pancreatitis status. Also, none of the included patients were found to have advanced-stage pancreatitis. The study results underscore the role of trans-abdominal USG elastography in assessing patients with early-stage chronic pancreatitis. However, the correlation with histological fibrosis was not evaluated. Further multicenter trials would be crucial to establish the role of transabdominal USG elastography in evaluating pancreatic texture and diagnosing early-stage chronic pancreatitis.

Table 1 Summary of studies evaluating the role of transabdominal ultrasonography in assessing pancreatic texture

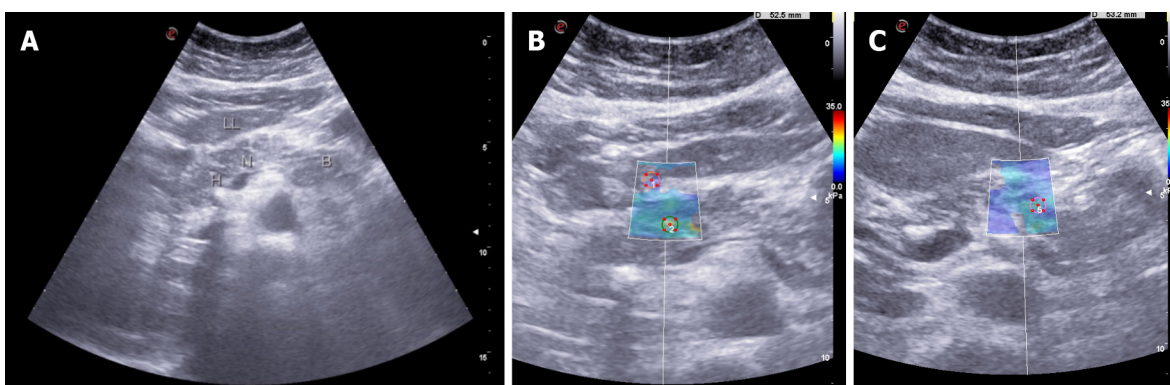
Ref.	Number of patients	Aim	Results	Conclusion	Histological correlation
Yashima <i>et al</i> [27], 2012	98	Efficacy of elastography to diagnose chronic pancreatitis	SWV cut off – 1.40 m/s; Sensitivity 75%; Specificity 72%; PPV 69%; NPV 78%	SWV in chronic pancreatitis patients higher than healthy volunteers	Not evaluated
Harada <i>et al</i> [29], 2016	68	Correlation of SWV with pathological degree of fibrosis	SWV cut off – 1.54 m/s; Sensitivity 91%; Specificity 75%; PPV 67%; NPV 93%	SWV significantly correlated with grade of fibrosis and postoperative pancreatic fistula	Good
Llamoza-Torres <i>et al</i> [30], 2016	33	Accuracy of elastography to diagnose chronic pancreatitis	SWV cut off – 1.4 m/s; Sensitivity 58%; Specificity 81%; PPV 76%; NPV 65%	SWV significantly correlated with EUS findings	Not evaluated

SWV: Shear wave velocity; PPV: Positive predictive value; NPV: Negative predictive value; EUS: Endoscopic ultrasonography.



DOI: 10.4329/wjr.v15.i6.170 Copyright ©The Author(s) 2023.

Figure 1 Transabdominal ultrasonography. A: Grayscale appearance of the normal pancreas (LL- Left lobe of liver, H- Head of pancreas, N- neck of pancreas, B-Body of pancreas). The pancreas is isoechoic compared to normal liver and shows a granular appearance and smooth outline; B: 2D Shear wave elastography measurement from the normal pancreas-neck region (3.84 ± 0.45 kPa).



DOI: 10.4329/wjr.v15.i6.170 Copyright ©The Author(s) 2023.

Figure 2 Shear wave velocity in patients with chronic pancreatitis was significantly higher than that in healthy volunteers in each part of the pancreas. A: Grayscale appearance of the pancreas in chronic calcific pancreatitis. (LL- Left lobe of liver, H- Head of pancreas, N- neck of pancreas, B-Body of pancreas). It shows a focal hyperechoic signal compared to normal liver and a mildly lobulated outline, a focus of calcification in the head region with posterior acoustic shadowing; B: 2D Shear wave elastography measurement of the pancreas in chronic calcific pancreatitis - head region (15.55 ± 2.64 kPa); C: 2D Shear wave elastography measurement of the pancreas in chronic calcific pancreatitis - region (11 ± 2.07 kPa).

COMPUTED TOMOGRAPHY ABDOMEN

Pancreatic texture on CT abdomen can be predicted based on the patterns of attenuation and enhancement of its parenchyma on various phases. They were evaluated as preoperative predictors of POPF in several studies[11-15]. While pancreatic attenuation index (PAI) like Liver Attenuation Index can measure pancreatic fat, pancreatic enhancement ratio (PER) can be measured to grade the pancreatic fibrosis (Figure 3). The higher the PER, the firmer the gland is. The presence of a higher PER and lower PAI can be considered to be associated with the low risk of development of POPF after PD.

Pancreatic attenuation index

PAI has been proposed as a simple tool by Yardimci *et al*[31] to assess pancreatic fat fraction by evaluating 76 patients who underwent PD. PAI was calculated with non-enhanced computed tomography by dividing the pancreas density measured in Household Units by the spleen density. They reported that higher PAI was associated with a high POPF rate and determined the value of 0.67 as an optimum cut-off value for predicting POPF. PAI has been reported to be useful in assessing pancreatic fat fraction by few other studies as well[11,12]. However, Gnanasekaran *et al*[32] reported that PAI was not helpful in predicting CR-POPF. Also, in their study, PAI did not correlate with histological estimation of pancreatic fat fraction. It might be due to the use of a region of interest-based assessment. In future studies, area-based assessment for the pancreatic fat fraction should be correlated with histopathological fat fraction.

Pancreatic enhancement ratio

An increase in the fibrosis of the pancreas makes the pancreatic texture hard. A fibrotic pancreas shows delayed enhancement in the pancreatic phase and nearly normal enhancement in the hepatic phase on dual-phase CT[33]. In contrast, the normal pancreas shows maximum enhancement in the pancreatic phase and washout in the hepatic phase[33]. Thus, predicting the degree of pancreatic fibrosis may be possible on analysis of enhancement patterns on pancreatic protocol CT done routinely to evaluate pancreatic tumors.

Kang *et al*[15] determined a PER cut-off of 1.10 as a useful predictor for POPF based on their retrospective analysis of 146 patients. PER on the equilibrium phase was significantly higher in the patients without POPF compared to patients with POPF (2.26 ± 3.63 vs 1.04 ± 0.51 , $P = 0.001$). In the logistic regression analyses, PER was an independent predictor for the development of POPF (odds ratio = 0.243, $P = 0.002$). Maehira *et al*[13] retrospectively analysed 115 patients and concluded the pancreatic enhancement pattern as a reliable predictor for the development of POPF. Gnanasekaran *et al*[32] showed a positive correlation of PER with pancreatic fibrosis. Their study utilised a PER cut-off value of 0.661 which was 78% sensitive and 55 % specific in predicting POPF (Table 2). In the same study, PAI is reported to have negative correlation with PER, indicating that the pancreatic fat content and fibrosis are inversely related. However, the estimation of PER depends on the perfusion of organs with injected contrast which relies upon the hemodynamic status of the subjects. In comparison, PAI is independent of contrast injection.

MAGNETIC RESONANCE IMAGING

MRI allows the detection of fibrotic change of pancreatic parenchyma and hence can predict the risk of POPF. A normal pancreas shows hyperintensity on T1-weighted images irrespective of fat saturation. The fibrosis makes the pancreatic parenchyma to lose its high signal intensity (SI) owing to the replacement of the high protein content of the pancreas by fibrosis.

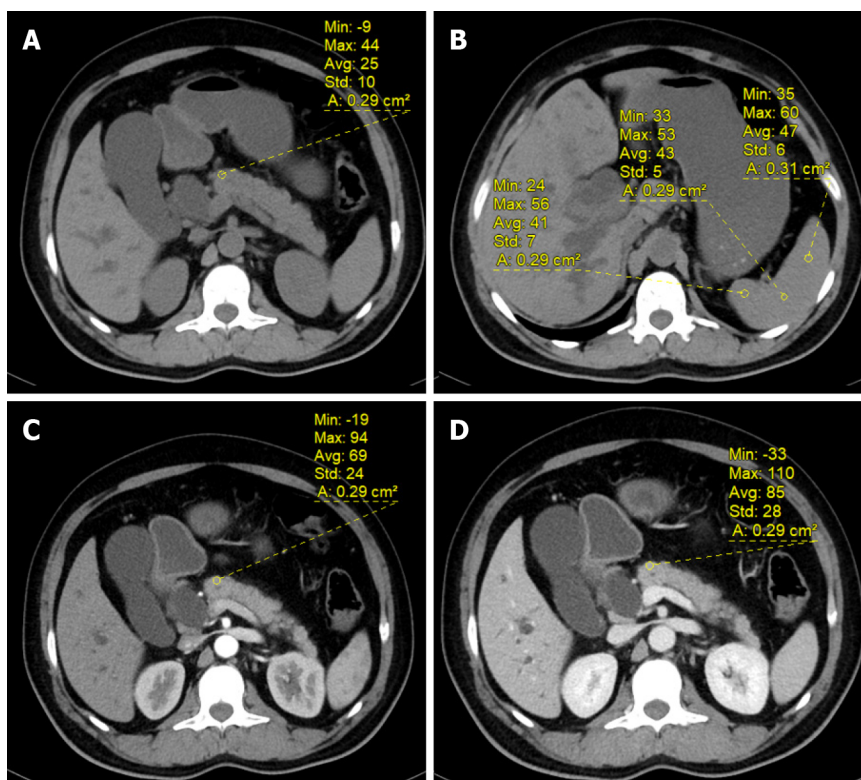
Winston *et al*[34] reported that the SI of pancreatic parenchyma, compared to that of the liver, decreases on fat-saturated T1-weighted images in patients with type 2 diabetes. Noda *et al*[35] found that the pancreatic fibrosis grade was negatively correlated with the SI ratio on in-phase T1-weighted images ($r = -0.67$, $P = -0.0002$). Another retrospective study by Watanabe *et al*[36] on 29 patients demonstrated that the SI ratio on T1-weighted images constantly decreased as the pancreatic fibrosis progressed. The higher risk of POPF is associated with a high SI ratio. Multiple regression analysis showed that pancreas-to-muscle SI ratios on T1-weighted images and apparent diffusion coefficient (ADC) values were independently associated with pancreatic fibrosis ($r(2) = 0.66$, $P < 0.001$) and with activated pancreatic stellate cell expression ($r(2) = 0.67$, $P < 0.001$). The mean pancreas-to-muscle SI ratio (\pm standard deviation) on T1-weighted images was higher ($P = 0.0029$) for patients with POPF (1.6 ± 0.2) than for those without (1.2 ± 0.2), and the odds ratio for POPF was 21.3 in patients with an SI ratio of 1.41 and higher[36].

Kim *et al*[16], in their pilot study, studied the correlation of pancreatic fibrosis with POPF after PD with the use of breath-hold unenhanced fat-suppressed T1 weighted images. The pancreas-to-liver SI ratio between the fistula and no fistula groups was -0.0009 ± 0.2 and -0.1297 ± 0.2 , respectively ($P = 0.0004$). Each group's pancreas-to-spleen SI ratio was 0.423 ± 0.25 and 0.288 ± 0.32 , respectively ($P = 0.014$). Using qualitative analysis where the pancreas SI was qualitatively assessed relative to liver and

Table 2 Summary of studies evaluating the role of computed tomography abdomen in assessing pancreatic texture

Ref.	Number of patients	PER calculation	Results	Histological correlation
Kang <i>et al</i> [15], 2017	146	1 Equilibrium phase -Pre contrast/ Pre contrast (EP- Pre/Pre); 2 Equilibrium phase -Pre contrast/ Arterial phase - Pre contrast (EP-Pre/AP-Pre)	Mean PER was significantly higher in patients without POPF than in patients with POPF. PER cut off: EP- Pre/Pre -1.10; Pre/AP-Pre - 0.60	Not evaluated
Maehira <i>et al</i> [13], 2019	115	1 Arterial phase/Portal phase (A/P); 2 Portal phase/Late phase (P/L)	Enhancement ratio is significantly higher in POPF group. PER cut off: A/P - 1.19; P/L - 1.17	Not evaluated
Gnanasekaran S <i>et al</i> [32], 2022	61	Equilibrium phase -Pre contrast/ Arterial phase - Pre contrast (EP-Pre/AP-Pre)	PER was significantly higher in patients without POPF than in patients with POPF, PER cut off - 0.673	PER correlated well with fibrosis

PER: Pancreatic enhancement ratio; POPF: Postoperative pancreatic fistula.



DOI: 10.4329/wjr.v15.i6.170 Copyright ©The Author(s) 2023.

Figure 3 Calculation of pancreatic attenuation index and pancreatic enhancement ratio. A: Hounsfield unit (HU) of the pancreatic neck in the plain phase; B: HU of the spleen in plain phase; C: HU of the pancreatic neck in the arterial phase; D: HU of the pancreatic neck in the equilibrium phase. ROI: Region of interest.

spleen SI using a five-point scale (-2, -1, 0, 1, 2), the SI ratios were 1.27 and 0.66 in each group ($P = 0.013$). The diagnostic performance for preoperative predictions of POPF was better with the qualitative analysis ($Az = 0.653$) than with the pancreas-to-liver SI ratio ($Az = 0.640$) and pancreas-spleen SI ratio ($Az = 0.613$); although, statistically significant difference was not found in each MRI parameter.

Yoon *et al*[37] reported that multiparametric MR imaging of the pancreas, including imaging with the T2*-corrected Dixon technique and intravoxel incoherent motion diffusion-weighted imaging (DWI), may yield quantitative information regarding pancreatic steatosis and fibrosis. The mean pancreas-to-muscle SI ratio on T1-weighted MRI values for F0, F1, and the cut-off value for predicting POPF was 1.51, 1.48, and 1.40, respectively (Table 3). Fukada *et al*[38], in their single-center retrospective study comprising 117 patients, reported 1.37 as the cut-off value for the pancreas-to-muscle SI ratio for predicting POPF.

Table 3 Summary of studies evaluating the role of magnetic resonance imaging abdomen signal intensity in assessing pancreatic texture

Ref.	Number of patients	Aim	Parameter studied	Results	Conclusion	Histological correlation
Winston <i>et al</i> [34], 1995	89	Correlation of pancreatic SI to predict the presence of pancreatic disease	PLSI	Accuracy -86%; PPV- 88	Pancreatic SI less than that of liver correlates highly with pancreatic disease, especially in younger patients	Not evaluated
Kim <i>et al</i> [16], 2009	43	Accuracy of non-enhanced fat-suppressed T1W MRI in predicting POPF	PLSI, PSSI	PLSI cut off -0.12097 (sensitivity -36%, specificity - 89%); PSSI cut off -0.29979 (sensitivity-79%, specificity-45%)	PLSI, PSSI significantly differed between POPF group and non POPF group, hence, can be useful in predicting POPF	Good
Watanabe <i>et al</i> [36], 2014	29	Efficacy of MRI in assessing degrees of pancreatic fibrosis and predicting POPF	PMSI in unenhanced T1W and T2 W images	Odds ratio of PMSI in T1 W for POPF was 21.3 in patients with an SI ratio of 1.41 and higher	T1W SI ratio and ADC measurements useful to detect advanced pancreatic fibrosis and occurrence of POPF	Good
Noda <i>et al</i> [35], 2016	29	Evaluate the noncontrast-enhanced MRI to grade pancreatic fibrosis and correlate with HbA1c values	PMSI on in- and opposed-phase T1W images	The pancreatic fibrosis grade and HbA1c value were negatively correlated with the SI ratio on opposed-phase T1W images	PMSI could be a potential biomarker for pancreatic fibrosis and elevated HbA1c values	Good
Yoon <i>et al</i> [37], 2016	165	Evaluate the multiparametric pancreatic MRI in the quantification of pancreatic fibrosis and determine relation with POPF	PMSI on in- and opposed-phase T1, IVIM DW imaging; Perfusion fraction (<i>f</i>)	Mean SI ratio for fibrosis; F0 - 1.51; F1 - 1.48; SI ratio cutoff for POPF - 1.40; Odds of developing POPF for a 1% increase in <i>f</i> were 1.17	Multiparametric MR imaging of the pancreas may quantify pancreatic steatosis and fibrosis, and <i>f</i> was significantly associated with POPF	Good
Fukada <i>et al</i> [38], 2022	117	Predictive ability of SI ratio on T1W MRI for POPF after distal pancreatectomy	PMSI on T1W	SI ratio cutoff for POPF - 1.37; Sensitivity- 96.3% Specificity- 52.0%	PMSI is a quantitative biomarker for pancreatic characteristics	Good

T1W: T1 weighted; T2W: T2 Weighted; MRI: Magnetic resonance imaging; POPF: Postoperative pancreatic fistula; PLSI: Pancreas-to-liver signal intensity ratio; PSSI: Pancreas-to-spleen signal intensity ratio; PMSI: Pancreas-to-muscle signal intensity ratio; SI: Signal intensity; IVIM: Intravoxel incoherent motion.

Diffusion-weighted imaging

DWI is used to evaluate fibrosis using ADC values. In the fibrotic pancreas, diffusion is restricted because of the replacement of normal pancreatic parenchyma with fibrous tissue. ADC values can be used to identify the presence of fibrosis and to grade its extent. Studies have reported lower ADC values in chronic pancreatitis patients[39]. Bieliuniene *et al*[40] identified a significant negative correlation between ADC value and histologically determined pancreatic fibrosis (PF) ($r = -0.752$, $P < 0.001$). In addition, a significant negative correlation was observed between T1SI and histologically determined pancreatic fibrosis ($r = -0.631$, $P < 0.001$). Also, by combining the ADC and T1SI measurements, PF can be detected with greater sensitivity and specificity during the early stages of the disease when other clinical signs are absent.

Tirkes *et al*[41] conducted a multi institutional, prospective study to evaluate the diagnostic value of four quantitative MRI parameters in chronic pancreatitis: T1 relaxation time, extracellular fraction, fat signal fraction and ADC. Except ADC, all the parameters were reported to be significantly higher in the patients with chronic pancreatitis and also were showed to have moderately high diagnostic value after adjustment for covariates. A Q-MRI score has been proposed by combining these three MR parameters which was shown to have improved diagnostic performance. However, ADC values were reported to be not helpful for diagnosing chronic pancreatitis.

Magnetic resonance elastography

Magnetic resonance elastography (MRE) can also be used to estimate pancreatic stiffness. The technique of MRE involves three steps similar to transabdominal and EUS elastography: Generation of shear waves in the tissue, acquisition of MR images depicting the propagation of the induced shear waves, and generation of elastograms, the quantitative maps of tissue stiffness by processing the acquired images of the shear waves.

Patients with chronic pancreatitis were reported to have significantly higher stiffness values than normal people (1.53 vs 1.11 kPa)[42]. Wang *et al*[43] reported the usefulness of MRE for the assessment

of the severity of chronic pancreatitis and showed that the pancreatic stiffness was significantly low in healthy controls (mean -1.21 kPa), when compared to patients with a mild degree of chronic pancreatitis (mean - 1.50 kPa), and also those with a moderate/severe degree of chronic pancreatitis (mean - 1.90 kPa).

ENDOSCOPIC ULTRASONOGRAPHY ELASTOGRAPHY

EUS elastography is a novel diagnostic tool to assess pancreatic fibrosis. Like transabdominal ultrasound, EUS elastography can be strain elastography or SWE.

Strain elastography

In strain elastography, the target tissue is compressed with a EUS probe to create a stain, which is reflected on ultrasound images. Softer tissue has a larger strain when compared to harder tissues. However, this gives only qualitative estimation of tissue elasticity. Second-generation EUS elastography has been developed, giving two semi-quantitative tissue stiffness measures[28]. The strain ratio (SR), one of two semi quantitative measure is based on comparing stiffness between specific regions of interest in two tissue areas and is expressed as a relative ratio. The strain histogram (SH) is another semi-quantitative parameter representing the selected area's mean strain value.

Six articles reported the diagnostic performance of EUS strain elastography for chronic pancreatitis; three reported SR, and three used SH (Table 4)[28,44-48]. Of them two SR articles reported that EUS elastography is helpful for differentiating the normal pancreas from chronic pancreatitis[28,47]. Two of the SH articles also reported the usefulness of EUS elastography in differentiating between normal pancreas and chronic pancreatitis[44,48]. One report showed that the SH elastography values significantly correlated with the degree of fibrosis assessed on histology of the surgical specimens[45].

Shear wave elastography

Acoustic radiation force is sent to the region of interest, and this push pulse generates a shear wave at the edge. The shear wave propagates faster in harder tissues. EUS-SWE is has better diagnostic value in chronic pancreatitis than strain elastography by providing the absolute values of pancreatic hardness.

Since it is a novel investigation, only two articles report the utility of EUS-SWE[49,50]. For diagnosis of chronic pancreatitis, a SWV cut-off value of 2.19 (Rosemont criteria) and 1.96 (Japan Pancreatic Society criteria) had a sensitivity of 100% and 83%, respectively, and specificity of 94% and 100%. EUS-SWE values correlate well with the stage of chronic pancreatitis and predicted exocrine dysfunction compared to transabdominal ultrasound. EUS-SWE data are better than those published using transabdominal ultrasound[30]. However, EUS is an invasive technique compared to trans-abdominal ultrasound.

FUTURE PERSPECTIVES

Identifying potential preoperative predictors for POPF is a critical step in our journey to improve perioperative outcomes after PD. Also, early diagnosis of chronic pancreatitis is essential to improve long-term outcomes of patients undergoing surgery for chronic pancreatitis. Recent studies have shown that pancreatic texture parameters like mean positive pixel before initiating neoadjuvant therapy, kurtosis and changes in kurtosis during neoadjuvant therapy can be used in predicting response to neoadjuvant therapy[51,52]. While the current evidence suggests the promising role of radiological parameters in predicting pancreatic texture, it is essential to understand the limitations of available evidence. Most of the studies had a smaller sample size. Hence, studies with larger sample sizes and multicentric studies are required for all the radiological modalities to determine the reference values for the normal and diseased pancreas. Also, socio-demographic variables need to be correlated with the pancreatic texture in all age groups to determine appropriate reference standards for all the available radiological modalities.

Most studies have assessed individual radiological parameter's role in predicting pancreatic texture. However, studies comparing different radiological parameters are not available. Hence future studies are required to study the efficacy of one imaging modality over the other and the effectiveness of combining several radiological modalities to devise a quantitative variable such as fistula risk score based on texture.

The accepted gold standard to find the pancreatic texture is histology. Since there can be an uneven distribution of pancreatic fatty infiltration or fibrosis, using the same focal area of the pancreas in imaging modalities and histology in future studies will provide a better correlation of pancreatic texture. Also, it is essential to understand that multiple factors influence POPF. Hence, a homogenous patient population and standardized surgical techniques are prerequisites for future studies. However, it isn't easy to achieve and reproduce that in complex procedures like PD. Nevertheless, identifying

Table 4 Summary of studies evaluating the role of endoscopic ultrasonography strain elastography in assessing pancreatic texture

Ref.	Parameter used	Inference
Machado <i>et al</i> [44], 2012	SH	EUS is useful in differentiating normal pancreas and chronic pancreatitis
Iglesias-Garcia <i>et al</i> [28], 2013	SR	EUS is useful in differentiating normal pancreas and chronic pancreatitis; SR EUS elastography correlated with number of Rosemont criteria ratio
Itoh <i>et al</i> [45], 2014	SH	SH EUS elastography values significantly correlated with fibrosis on histology
Dominguez-Muñoz <i>et al</i> [46], 2015	SR	SR EUS elastography values significantly correlated with exocrine dysfunction
Kim <i>et al</i> [47], 2017	SR	EUS is useful in differentiating normal pancreas and chronic pancreatitis
Kuwahara <i>et al</i> [48], 2017	SH	EUS is useful in differentiating normal pancreas and chronic pancreatitis; SH EUS elastography correlated with number of Rosemont criteria ratio

SR: Strain ratio; SH: Strain histogram; EUS: Endoscopic ultrasonography.

potential preoperative predictors for POPF is vital in decreasing the morbidity associated with PD.

CONCLUSION

Pancreatic texture can be assessed using radiological parameters derived from preoperative imaging modalities. With advancements in imaging techniques, the accuracy of preoperative prediction of the fatty or fibrotic pancreas has improved. However, more studies are required comparing different imaging modalities to standardize their measurement. Also, the correlation of radiological parameters with histological findings is required to improve predictive accuracy.

FOOTNOTES

Author contributions: Himaja M and Kokila K did the literature search and wrote the first draft of the review; Kalayarasan R and Ramesh A conceptualized the work, supervised the writing, gave intellectual inputs, and critically revised the manuscript.

Conflict-of-interest statement: All authors have no conflicts of interest to report.

Open-Access: This article is an open-access article that was selected by an in-house editor and fully peer-reviewed by external reviewers. It is distributed in accordance with the Creative Commons Attribution NonCommercial (CC BY-NC 4.0) license, which permits others to distribute, remix, adapt, build upon this work non-commercially, and license their derivative works on different terms, provided the original work is properly cited and the use is non-commercial. See: <https://creativecommons.org/licenses/by-nc/4.0/>

Country/Territory of origin: India

ORCID number: Raja Kalayarasan 0000-0003-4056-8672; Mandalapu Himaja 0009-0004-8267-2018; Ananthkrishnan Ramesh 0000-0002-1404-6400; Kathirvel Kokila 0000-0002-9157-9067.

S-Editor: Liu JH

L-Editor: A

P-Editor: Liu JH

REFERENCES

- 1 **Poon RT**, Fan ST, Lo CM, Ng KK, Yuen WK, Yeung C, Wong J. External drainage of pancreatic duct with a stent to reduce leakage rate of pancreaticojejunostomy after pancreaticoduodenectomy: a prospective randomized trial. *Ann Surg* 2007; **246**: 425-33; discussion 433 [PMID: 17717446 DOI: 10.1097/sla.0b013e3181492c28]
- 2 **Greenblatt DY**, Kelly KJ, Rajamanickam V, Wan Y, Hanson T, Rettammel R, Winslow ER, Cho CS, Weber SM. Preoperative factors predict perioperative morbidity and mortality after pancreaticoduodenectomy. *Ann Surg Oncol* 2011; **18**: 2126-2135 [PMID: 21336514 DOI: 10.1245/s10434-011-1594-6]
- 3 **Tzeng CW**, Katz MH, Fleming JB, Lee JE, Pisters PW, Holmes HM, Varadhachary GR, Wolff RA, Abbruzzese JL,

- Vauthey JN, Aloia TA. Morbidity and mortality after pancreaticoduodenectomy in patients with borderline resectable type C clinical classification. *J Gastrointest Surg* 2014; **18**: 146-55; discussion 155 [PMID: 24129825 DOI: 10.1007/s11605-013-2371-6]
- 4 **Kawai M**, Kondo S, Yamaue H, Wada K, Sano K, Motoi F, Unno M, Satoi S, Kwon AH, Hatori T, Yamamoto M, Matsumoto J, Murakami Y, Doi R, Ito M, Miyakawa S, Shinchi H, Natsugoe S, Nakagawara H, Ohta T, Takada T. Predictive risk factors for clinically relevant pancreatic fistula analyzed in 1,239 patients with pancreaticoduodenectomy: multicenter data collection as a project study of pancreatic surgery by the Japanese Society of Hepato-Biliary-Pancreatic Surgery. *J Hepatobiliary Pancreat Sci* 2011; **18**: 601-608 [PMID: 21491103 DOI: 10.1007/s00534-011-0373-x]
 - 5 **Ansorge C**, Strömmer L, Andrén-Sandberg Å, Lundell L, Herrington MK, Segersvärd R. Structured intraoperative assessment of pancreatic gland characteristics in predicting complications after pancreaticoduodenectomy. *Br J Surg* 2012; **99**: 1076-1082 [PMID: 22556164 DOI: 10.1002/bjs.8784]
 - 6 **Ridolfi C**, Angiolini MR, Gavazzi F, Spaggiari P, Tinti MC, Uccelli F, Madonini M, Montorsi M, Zerbi A. Morphohistological features of pancreatic stump are the main determinant of pancreatic fistula after pancreatoduodenectomy. *Biomed Res Int* 2014; **2014**: 641239 [PMID: 24900974 DOI: 10.1155/2014/641239]
 - 7 **Hu BY**, Wan T, Zhang WZ, Dong JH. Risk factors for postoperative pancreatic fistula: Analysis of 539 successive cases of pancreaticoduodenectomy. *World J Gastroenterol* 2016; **22**: 7797-7805 [PMID: 27678363 DOI: 10.3748/wjg.v22.i34.7797]
 - 8 **Chong E**, Ratnayake B, Lee S, French JJ, Wilson C, Roberts KJ, Loveday BPT, Manas D, Windsor J, White S, Pandanaboyana S. Systematic review and meta-analysis of risk factors of postoperative pancreatic fistula after distal pancreatectomy in the era of 2016 International Study Group pancreatic fistula definition. *HPB (Oxford)* 2021; **23**: 1139-1151 [PMID: 33820687 DOI: 10.1016/j.hpb.2021.02.015]
 - 9 **Wang M**, Li D, Chen R, Huang X, Li J, Liu Y, Liu J, Cheng W, Chen X, Zhao W, Tan Z, Huang H, Zhu F, Qin T, Ma J, Yu G, Zhou B, Zheng S, Tang Y, Han W, Meng L, Ke J, Feng F, Chen B, Yin X, Chen W, Ma H, Xu J, Lin R, Dong Y, Yu Y, Zhang H, Qin R; Minimally Invasive Treatment Group in the Pancreatic Disease Branch of China's International Exchange and Promotion Association for Medicine and Healthcare (MITG-P-CPAM). Laparoscopic versus open pancreatoduodenectomy for pancreatic or periampullary tumours: a multicentre, open-label, randomised controlled trial. *Lancet Gastroenterol Hepatol* 2021; **6**: 438-447 [PMID: 33915091 DOI: 10.1016/S2468-1253(21)00054-6]
 - 10 **van Hilst J**, de Rooij T, Bosscha K, Brinkman DJ, van Dieren S, Dijkgraaf MG, Gerhards MF, de Hingh IH, Karsten TM, Lips DJ, Luyer MD, Busch OR, Festen S, Besselink MG; Dutch Pancreatic Cancer Group. Laparoscopic versus open pancreatoduodenectomy for pancreatic or periampullary tumours (LEOPARD-2): a multicentre, patient-blinded, randomised controlled phase 2/3 trial. *Lancet Gastroenterol Hepatol* 2019; **4**: 199-207 [PMID: 30685489 DOI: 10.1016/S2468-1253(19)30004-4]
 - 11 **Tranchart H**, Gaujoux S, Rebours V, Vullierme MP, Dokmak S, Levy P, Couvelard A, Belghiti J, Sauvanet A. Preoperative CT scan helps to predict the occurrence of severe pancreatic fistula after pancreaticoduodenectomy. *Ann Surg* 2012; **256**: 139-145 [PMID: 22609844 DOI: 10.1097/SLA.0b013e318256c32c]
 - 12 **Lim S**, Bae JH, Chun EJ, Kim H, Kim SY, Kim KM, Choi SH, Park KS, Florez JC, Jang HC. Differences in pancreatic volume, fat content, and fat density measured by multidetector-row computed tomography according to the duration of diabetes. *Acta Diabetol* 2014; **51**: 739-748 [PMID: 24671510 DOI: 10.1007/s00592-014-0581-3]
 - 13 **Machira H**, Iida H, Mori H, Kitamura N, Miyake T, Shimizu T, Tani M. Computed Tomography Enhancement Pattern of the Pancreatic Parenchyma Predicts Postoperative Pancreatic Fistula After Pancreaticoduodenectomy. *Pancreas* 2019; **48**: 209-215 [PMID: 30589830 DOI: 10.1097/MPA.0000000000001229]
 - 14 **Hashimoto Y**, Sclabas GM, Takahashi N, Kirihara Y, Smyrk TC, Huebner M, Farnell MB. Dual-phase computed tomography for assessment of pancreatic fibrosis and anastomotic failure risk following pancreatoduodenectomy. *J Gastrointest Surg* 2011; **15**: 2193-2204 [PMID: 21948179 DOI: 10.1007/s11605-011-1687-3]
 - 15 **Kang JH**, Park JS, Yu JS, Chung JJ, Kim JH, Cho ES, Yoon DS. Prediction of pancreatic fistula after pancreatoduodenectomy by preoperative dynamic CT and fecal elastase-1 levels. *PLoS One* 2017; **12**: e0177052 [PMID: 28493949 DOI: 10.1371/journal.pone.0177052]
 - 16 **Kim Z**, Kim MJ, Kim JH, Jin SY, Kim YB, Seo D, Choi D, Hur KY, Kim JJ, Lee MH, Moon C. Prediction of post-operative pancreatic fistula in pancreaticoduodenectomy patients using pre-operative MRI: a pilot study. *HPB (Oxford)* 2009; **11**: 215-221 [PMID: 19590650 DOI: 10.1111/j.1477-2574.2009.00011.x]
 - 17 **Willner A**, Bogner A, Müsle B, Teske C, Hempel S, Kahlert C, Distler M, Weitz J, Welsch T. Disease duration before surgical resection for chronic pancreatitis impacts long-term outcome. *Medicine (Baltimore)* 2020; **99**: e22896 [PMID: 33126342 DOI: 10.1097/MD.00000000000022896]
 - 18 **Issa Y**, Kempeneers MA, Bruno MJ, Fockens P, Poley JW, Ahmed Ali U, Bollen TL, Busch OR, Dejong CH, van Duijvendijk P, van Dullemen HM, van Eijck CH, van Goor H, Hadithi M, Haveman JW, Keulemans Y, Nieuwenhuijs VB, Poen AC, Rauws EA, Tan AC, Thijs W, Timmer R, Witteman BJ, Besselink MG, van Hooft JE, van Santvoort HC, Dijkgraaf MG, Boermeester MA; Dutch Pancreatitis Study Group. Effect of Early Surgery vs Endoscopy-First Approach on Pain in Patients With Chronic Pancreatitis: The ESCAPE Randomized Clinical Trial. *JAMA* 2020; **323**: 237-247 [PMID: 31961419 DOI: 10.1001/jama.2019.20967]
 - 19 **Forestier N**, Gaus A, Herrmann E, Sarrazin C, Bojunga J, Poynard T, Albert J, Gerber L, Schneider MD, Dultz G, Zeuzem S, Friedrich-Rust M. Acoustic radiation force impulse imaging for evaluation of antiviral treatment response in chronic hepatitis C. *J Gastrointest Liver Dis* 2012; **21**: 367-373 [PMID: 23256119]
 - 20 **Itoh A**, Ueno E, Tohno E, Kamma H, Takahashi H, Shiina T, Yamakawa M, Matsumura T. Breast disease: clinical application of US elastography for diagnosis. *Radiology* 2006; **239**: 341-350 [PMID: 16484352 DOI: 10.1148/radiol.2391041676]
 - 21 **Kawada N**, Tanaka S. Elastography for the pancreas: Current status and future perspective. *World J Gastroenterol* 2016; **22**: 3712-3724 [PMID: 27076756 DOI: 10.3748/wjg.v22.i14.3712]
 - 22 **Yin M**, Venkatesh SK, Grimm RC, Rossman PJ, Manduca A, Ehman RL. Assessment of the pancreas with MR elastography. Proceedings of the International Society for Magnetic Resonance in Medicine; Toronto, Canada' 2008: 2627

- [DOI: [10.1109/iembs.1996.651961](https://doi.org/10.1109/iembs.1996.651961)]
- 23 **Kawada N**, Tanaka S, Uehara H, Ohkawa K, Yamai T, Takada R, Shiroeda H, Arisawa T, Tomita Y. Potential use of point shear wave elastography for the pancreas: a single center prospective study. *Eur J Radiol* 2014; **83**: 620-624 [PMID: [24445135](https://pubmed.ncbi.nlm.nih.gov/24445135/) DOI: [10.1016/j.ejrad.2013.11.029](https://doi.org/10.1016/j.ejrad.2013.11.029)]
 - 24 **Iglesias-Garcia J**, Larino-Noia J, Abdulkader I, Forteza J, Dominguez-Munoz JE. Quantitative endoscopic ultrasound elastography: an accurate method for the differentiation of solid pancreatic masses. *Gastroenterology* 2010; **139**: 1172-1180 [PMID: [20600020](https://pubmed.ncbi.nlm.nih.gov/20600020/) DOI: [10.1053/j.gastro.2010.06.059](https://doi.org/10.1053/j.gastro.2010.06.059)]
 - 25 **Ris MM**, Deitrich RA, Von Wartburg JP. Inhibition of aldehyde reductase isoenzymes in human and rat brain. *Biochem Pharmacol* 1975; **24**: 1865-1869 [PMID: [18](https://pubmed.ncbi.nlm.nih.gov/18/) DOI: [10.1016/0006-2952\(75\)90405-0](https://doi.org/10.1016/0006-2952(75)90405-0)]
 - 26 **Halaris AE**, Belendiuk KT, Freedman DX. Antidepressant drugs affect dopamine uptake. *Biochem Pharmacol* 1975; **24**: 1896-1897 [PMID: [19](https://pubmed.ncbi.nlm.nih.gov/19/) DOI: [10.1016/0006-2952\(75\)90412-8](https://doi.org/10.1016/0006-2952(75)90412-8)]
 - 27 **Yashima Y**, Sasahira N, Isayama H, Kogure H, Ikeda H, Hirano K, Mizuno S, Yagioka H, Kawakubo K, Sasaki T, Nakai Y, Tada M, Yoshida H, Omata M, Koike K. Acoustic radiation force impulse elastography for noninvasive assessment of chronic pancreatitis. *J Gastroenterol* 2012; **47**: 427-432 [PMID: [22065162](https://pubmed.ncbi.nlm.nih.gov/22065162/) DOI: [10.1007/s00535-011-0491-x](https://doi.org/10.1007/s00535-011-0491-x)]
 - 28 **Iglesias-Garcia J**, Domínguez-Muñoz JE, Castiñeira-Alvaríño M, Luaces-Regueira M, Lariño-Noia J. Quantitative elastography associated with endoscopic ultrasound for the diagnosis of chronic pancreatitis. *Endoscopy* 2013; **45**: 781-788 [PMID: [24019131](https://pubmed.ncbi.nlm.nih.gov/24019131/) DOI: [10.1055/s-0033-1344614](https://doi.org/10.1055/s-0033-1344614)]
 - 29 **Harada N**, Ishizawa T, Inoue Y, Aoki T, Sakamoto Y, Hasegawa K, Sugawara Y, Tanaka M, Fukayama M, Kokudo N. Acoustic radiation force impulse imaging of the pancreas for estimation of pathologic fibrosis and risk of postoperative pancreatic fistula. *J Am Coll Surg* 2014; **219**: 887-94.e5 [PMID: [25262282](https://pubmed.ncbi.nlm.nih.gov/25262282/) DOI: [10.1016/j.jamcollsurg.2014.07.940](https://doi.org/10.1016/j.jamcollsurg.2014.07.940)]
 - 30 **Llamoza-Torres CJ**, Fuentes-Pardo M, Álvarez-Higuera FJ, Alberca-de-Las-Parras F, Carballo-Álvarez F. Usefulness of percutaneous elastography by acoustic radiation force impulse for the non-invasive diagnosis of chronic pancreatitis. *Rev Esp Enferm Dig* 2016; **108**: 450-456 [PMID: [27459032](https://pubmed.ncbi.nlm.nih.gov/27459032/) DOI: [10.17235/reed.2016.4103/2015](https://doi.org/10.17235/reed.2016.4103/2015)]
 - 31 **Yardimci S**, Kara YB, Tuney D, Attaallah W, Ugurlu MU, Dulundu E, Yegen ŞC. A Simple Method to Evaluate Whether Pancreas Texture Can Be Used to Predict Pancreatic Fistula Risk After Pancreatoduodenectomy. *J Gastrointest Surg* 2015; **19**: 1625-1631 [PMID: [25982120](https://pubmed.ncbi.nlm.nih.gov/25982120/) DOI: [10.1007/s11605-015-2855-7](https://doi.org/10.1007/s11605-015-2855-7)]
 - 32 **Gnanasekaran S**, Durgesh S, Gurram R, Kalayarasan R, Pottakkat B, Rajeswari M, Srinivas BH, Ramesh A, Sahoo J. Do preoperative pancreatic computed tomography attenuation index and enhancement ratio predict pancreatic fistula after pancreaticoduodenectomy? *World J Radiol* 2022; **14**: 165-176 [PMID: [35978980](https://pubmed.ncbi.nlm.nih.gov/35978980/) DOI: [10.4329/wjr.v14.i6.165](https://doi.org/10.4329/wjr.v14.i6.165)]
 - 33 **Takahashi N**, Fletcher JG, Hough DM, Fidler JL, Kawashima A, Mandrekar JN, Chari ST. Autoimmune pancreatitis: differentiation from pancreatic carcinoma and normal pancreas on the basis of enhancement characteristics at dual-phase CT. *AJR Am J Roentgenol* 2009; **193**: 479-484 [PMID: [19620446](https://pubmed.ncbi.nlm.nih.gov/19620446/) DOI: [10.2214/AJR.08.1883](https://doi.org/10.2214/AJR.08.1883)]
 - 34 **Winston CB**, Mitchell DG, Outwater EK, Ehrlich SM. Pancreatic signal intensity on T1-weighted fat saturation MR images: clinical correlation. *J Magn Reson Imaging* 1995; **5**: 267-271 [PMID: [7633102](https://pubmed.ncbi.nlm.nih.gov/7633102/) DOI: [10.1002/jmri.1880050307](https://doi.org/10.1002/jmri.1880050307)]
 - 35 **Noda Y**, Goshima S, Tanaka K, Osada S, Tomita H, Hara A, Horikawa Y, Takeda J, Kajita K, Watanabe H, Kawada H, Kawai N, Kanematsu M, Bae KT. Findings in pancreatic MRI associated with pancreatic fibrosis and HbA1c values. *J Magn Reson Imaging* 2016; **43**: 680-687 [PMID: [26201823](https://pubmed.ncbi.nlm.nih.gov/26201823/) DOI: [10.1002/jmri.25019](https://doi.org/10.1002/jmri.25019)]
 - 36 **Watanabe H**, Kanematsu M, Tanaka K, Osada S, Tomita H, Hara A, Goshima S, Kondo H, Kawada H, Noda Y, Tanahashi Y, Kawai N, Yoshida K, Moriyama N. Fibrosis and postoperative fistula of the pancreas: correlation with MR imaging findings--preliminary results. *Radiology* 2014; **270**: 791-799 [PMID: [24475834](https://pubmed.ncbi.nlm.nih.gov/24475834/) DOI: [10.1148/radiol.13131194](https://doi.org/10.1148/radiol.13131194)]
 - 37 **Yoon JH**, Lee JM, Lee KB, Kim SW, Kang MJ, Jang JY, Kannengiesser S, Han JK, Choi BI. Pancreatic Steatosis and Fibrosis: Quantitative Assessment with Preoperative Multiparametric MR Imaging. *Radiology* 2016; **279**: 140-150 [PMID: [26566228](https://pubmed.ncbi.nlm.nih.gov/26566228/) DOI: [10.1148/radiol.2015142254](https://doi.org/10.1148/radiol.2015142254)]
 - 38 **Fukada M**, Murase K, Higashi T, Fujibayashi S, Kuno M, Yasufuku I, Sato Y, Kiyama S, Tanaka Y, Okumura N, Matsuhashi N, Takahashi T. The pancreas-to-muscle signal intensity ratio on T(1)-weighted MRI as a predictive biomarker for postoperative pancreatic fistula after distal pancreatectomy: a single-center retrospective study. *World J Surg Oncol* 2022; **20**: 250 [PMID: [35932021](https://pubmed.ncbi.nlm.nih.gov/35932021/) DOI: [10.1186/s12957-022-02718-8](https://doi.org/10.1186/s12957-022-02718-8)]
 - 39 **Nissan N**. Modifications of pancreatic diffusion MRI by tissue characteristics: what are we weighting for? *NMR Biomed* 2017; **30** [PMID: [28470823](https://pubmed.ncbi.nlm.nih.gov/28470823/) DOI: [10.1002/nbm.3728](https://doi.org/10.1002/nbm.3728)]
 - 40 **Bieluniene E**, Frøkjær JB, Pockevicius A, Kemesiene J, Lukosevicius S, Basevicius A, Barauskas G, Dambrauskas Z, Gulbinas A. Magnetic Resonance Imaging as a Valid Noninvasive Tool for the Assessment of Pancreatic Fibrosis. *Pancreas* 2019; **48**: 85-93 [PMID: [30451794](https://pubmed.ncbi.nlm.nih.gov/30451794/) DOI: [10.1097/MPA.0000000000001206](https://doi.org/10.1097/MPA.0000000000001206)]
 - 41 **Tirkes T**, Yadav D, Conwell DL, Territo PR, Zhao X, Persohn SA, Dasyam AK, Shah ZK, Venkatesh SK, Takahashi N, Wachsmann A, Li L, Li Y, Pandol SJ, Park WG, Vege SS, Hart PA, Topazian M, Andersen DK, Fogel EL; Consortium for the Study of Chronic Pancreatitis, Diabetes, Pancreatic Cancer (CPDPC). Quantitative MRI of chronic pancreatitis: results from a multi-institutional prospective study, magnetic resonance imaging as a non-invasive method for assessment of pancreatic fibrosis (MINIMAP). *Abdom Radiol (NY)* 2022; **47**: 3792-3805 [PMID: [36038644](https://pubmed.ncbi.nlm.nih.gov/36038644/) DOI: [10.1007/s00261-022-03654-7](https://doi.org/10.1007/s00261-022-03654-7)]
 - 42 **An H**, Shi Y, Guo Q, Liu Y. Test-retest reliability of 3D EPI MR elastography of the pancreas. *Clin Radiol* 2016; **71**: 1068.e7-1068.e12 [PMID: [27132114](https://pubmed.ncbi.nlm.nih.gov/27132114/) DOI: [10.1016/j.crad.2016.03.014](https://doi.org/10.1016/j.crad.2016.03.014)]
 - 43 **Wang M**, Gao F, Wang X, Liu Y, Ji R, Cang L, Shi Y. Magnetic resonance elastography and T(1) mapping for early diagnosis and classification of chronic pancreatitis. *J Magn Reson Imaging* 2018 [PMID: [29537715](https://pubmed.ncbi.nlm.nih.gov/29537715/) DOI: [10.1002/jmri.26008](https://doi.org/10.1002/jmri.26008)]
 - 44 **Machado MC**, Coelho AM, Carneiro D'Albuquerque LA, Jancar S. Effect of ageing on systemic inflammatory response in acute pancreatitis. *Int J Inflam* 2012; **2012**: 270319 [PMID: [22292125](https://pubmed.ncbi.nlm.nih.gov/22292125/) DOI: [10.1155/2012/270319](https://doi.org/10.1155/2012/270319)]
 - 45 **Itoh Y**, Itoh A, Kawashima H, Ohno E, Nakamura Y, Hiramatsu T, Sugimoto H, Sumi H, Hayashi D, Kuwahara T, Morishima T, Funasaka K, Nakamura M, Miyahara R, Ohmiya N, Katano Y, Ishigami M, Goto H, Hirooka Y. Quantitative analysis of diagnosing pancreatic fibrosis using EUS-elastography (comparison with surgical specimens). *J*

- Gastroenterol* 2014; **49**: 1183-1192 [PMID: 24026103 DOI: 10.1007/s00535-013-0880-4]
- 46 **Dominguez-Muñoz JE**, Iglesias-García J, Castiñeira Alvariño M, Luaces Regueira M, Lariño-Noia J. EUS elastography to predict pancreatic exocrine insufficiency in patients with chronic pancreatitis. *Gastrointest Endosc* 2015; **81**: 136-142 [PMID: 25088920 DOI: 10.1016/j.gie.2014.06.040]
- 47 **Kim SY**, Cho JH, Kim YJ, Kim EJ, Park JY, Jeon TJ, Kim YS. Diagnostic efficacy of quantitative endoscopic ultrasound elastography for differentiating pancreatic disease. *J Gastroenterol Hepatol* 2017; **32**: 1115-1122 [PMID: 27862278 DOI: 10.1111/jgh.13649]
- 48 **Kuwahara T**, Hirooka Y, Kawashima H, Ohno E, Ishikawa T, Kawai M, Suhara H, Takeyama T, Hashizume K, Koya T, Tanaka H, Sakai D, Yamamura T, Furukawa K, Funasaka K, Nakamura M, Miyahara R, Watanabe O, Ishigami M, Hashimoto S, Goto H. Quantitative diagnosis of chronic pancreatitis using EUS elastography. *J Gastroenterol* 2017; **52**: 868-874 [PMID: 27995327 DOI: 10.1007/s00535-016-1296-8]
- 49 **Yamashita Y**, Tanioka K, Kawaji Y, Tamura T, Nuta J, Hatamaru K, Itonaga M, Yoshida T, Ida Y, Maekita T, Iguchi M, Kitano M. Utility of Elastography with Endoscopic Ultrasonography Shear-Wave Measurement for Diagnosing Chronic Pancreatitis. *Gut Liver* 2020; **14**: 659-664 [PMID: 31722469 DOI: 10.5009/gnl19170]
- 50 **Yamashita Y**, Tanioka K, Kawaji Y, Tamura T, Nuta J, Hatamaru K, Itonaga M, Ida Y, Maekita T, Iguchi M, Kitano M. Endoscopic ultrasonography shear wave as a predictive factor of endocrine/exocrine dysfunction in chronic pancreatitis. *J Gastroenterol Hepatol* 2021; **36**: 391-396 [PMID: 32511808 DOI: 10.1111/jgh.15137]
- 51 **Kim BR**, Kim JH, Ahn SJ, Joo I, Choi SY, Park SJ, Han JK. CT prediction of resectability and prognosis in patients with pancreatic ductal adenocarcinoma after neoadjuvant treatment using image findings and texture analysis. *Eur Radiol* 2019; **29**: 362-372 [PMID: 29931561 DOI: 10.1007/s00330-018-5574-0]
- 52 **Borhani AA**, Dewan R, Furlan A, Seiser N, Zureikat AH, Singhi AD, Boone B, Bahary N, Hogg ME, Lotze M, Zeh HJ III, Tublin ME. Assessment of Response to Neoadjuvant Therapy Using CT Texture Analysis in Patients With Resectable and Borderline Resectable Pancreatic Ductal Adenocarcinoma. *AJR Am J Roentgenol* 2020; **214**: 362-369 [PMID: 31799875 DOI: 10.2214/AJR.19.21152]

Retrospective Study

Computed tomography angiographic study of surgical anatomy of thyroid arteries: Clinical implications in neck dissection

Yashu Bhardwaj, Brijendra Singh, Pooja Bhadoria, Rashmi Malhotra, Swarnava Tarafdar, Kanchan Bisht

Specialty type: Anatomy and morphology**Provenance and peer review:** Unsolicited article; Externally peer reviewed.**Peer-review model:** Single blind**Peer-review report's scientific quality classification**Grade A (Excellent): 0
Grade B (Very good): 0
Grade C (Good): C, C
Grade D (Fair): D
Grade E (Poor): 0**P-Reviewer:** Taydas O, Turkey;
Yang L, China**Received:** March 1, 2023**Peer-review started:** March 1, 2023**First decision:** April 13, 2023**Revised:** April 27, 2023**Accepted:** May 30, 2023**Article in press:** May 30, 2023**Published online:** June 28, 2023**Yashu Bhardwaj, Brijendra Singh, Pooja Bhadoria, Rashmi Malhotra, Kanchan Bisht**, Department of Anatomy, All India Institute of Medical Sciences, Rishikesh 249203, Uttarakhand, India**Swarnava Tarafdar**, Department of Radiodiagnosis, All India Institute of Medical Sciences, Rishikesh 249203, Uttarakhand, India**Corresponding author:** Rashmi Malhotra, MS, Additional Professor, Department of Anatomy, All India Institute of Medical Sciences, Rishikesh, Veerbhadra Road, Rishikesh 249201, Uttarakhand, India. rashmi.ana@aiimsrishikesh.edu.in**Abstract****BACKGROUND**

The course and variations of thyroid arteries must be understood by surgeons to prevent bleeding during operative procedures of the thyroid gland. There is limited scientific literature regarding the radiological anatomy of thyroid arteries in this geographical area, the Garhwal region of Sub-Himalayan belt, which is considered to be the endemic belt of goiter. Computed tomography angiography provides a three-dimensional orientation of the vascular and surgical anatomy of the entire cervical region.

AIM

To estimate the proportion of variation in origin of thyroid arteries using Computed Tomography Angiography.

METHODS

Using Computed Tomography Angiography, the presence and origin of the superior thyroid artery, inferior thyroid artery, and thyroid ima artery were observed and assessed.

RESULTS

Out of total 210 subjects, superior thyroid artery was seen to be emerging from external carotid artery in 77.1% cases. The artery was found to be originating at the level of bifurcation of common carotid artery in 14.3% cases, whereas in 8.6% cases, it emerged as a direct branch of the common carotid artery. Similarly, the inferior thyroid artery was observed to be emerging from thyrocervical trunk, subclavian artery and vertebral artery in 95.7% cases, 3.3% and 1% cases, respectively. Thyroid ima artery was also reported in a subject, arising from the brachiocephalic trunk.

CONCLUSION

To avoid vascular injuries, excessive and uncontrollable bleeding, intra-operative difficulties, and post-operative issues, it is imperative for surgeons to be aware of the course and variations of thyroid arteries

Key Words: Thyroid arteries; Computed tomography angiography; Origin; Variation

©The Author(s) 2023. Published by Baishideng Publishing Group Inc. All rights reserved.

Core Tip: To avoid vascular injuries, excessive and uncontrollable bleeding, intra-operative difficulties, and post-operative issues, it is imperative for surgeons to be aware of the course and variations of thyroid arteries. The current study will assist the surgeons in understanding the variation in thyroid arteries among people of Garhwal and west Uttar Pradesh region in a non-invasive manner using computed tomography angiography.

Citation: Bhardwaj Y, Singh B, Bhadoria P, Malhotra R, Tarafdar S, Bisht K. Computed tomography angiographic study of surgical anatomy of thyroid arteries: Clinical implications in neck dissection. *World J Radiol* 2023; 15(6): 182-190

URL: <https://www.wjgnet.com/1949-8470/full/v15/i6/182.htm>

DOI: <https://dx.doi.org/10.4329/wjr.v15.i6.182>

INTRODUCTION

The thyroid gland is an endocrine gland, which is essential for the normal metabolism and growth of an individual. Conditions affecting the thyroid gland range from simple goiter to malignant thyroid nodule and thyroid carcinoma. Thyroidectomy or hemithyroidectomy is occasionally indicated to remove a malignant thyroid tumor. The neck is also explored for surgical procedures, such as lobectomy, selective embolization of the thyroid, emergency cricothyroidotomy, radical neck dissection, diagnostic and therapeutic catheterization, reconstruction of the aneurysm, and carotid endarterectomy[1]. Bleeding during the operative procedure of the thyroid gland may compress the trachea causing difficulty in breathing[2].

Thyroid is a richly vascularized gland, which is supplied by superior thyroid artery (STA), inferior thyroid artery (ITA) and thyroid ima artery (TIA). The superior thyroid artery usually arises from external carotid artery and runs in close proximity to external branch of superior laryngeal nerve, before entering the fascia of thyroid and giving anterior and posterior branch.

Inferior thyroid artery usually commences from thyrocervical trunk[3]. Occasionally there is presence of a single minor artery, thyroid ima artery in 10% of the individuals[4].

The course and variations of the thyroid arteries must be understood by surgeons to prevent bleeding during the operative procedure of the thyroid gland.

There is limited scientific literature regarding the radiological anatomy of thyroid arteries in this geographical area, the Garhwal region of Sub-Himalayan belt, which is considered to be the endemic belt of goiter[5]. Computed tomography (CT) angiography provides a three-dimensional orientation of the vascular and surgical anatomy of the entire cervical region. For vascular mapping, radiography is a non-invasive multiplanar imaging method[6]. The present study investigated the origin and variation of thyroid arteries with the help of CT angiography.

MATERIALS AND METHODS

The proposed study was done in the Department of Anatomy in collaboration with the Department of Radiodiagnosis over a period of 18 months. A total of 210 samples were included as per inclusion and exclusion criteria. Patients above 18 years who underwent CT angiography were included. Patients who had undergone previous common carotid occlusions or known vascular abnormalities (carotid hypoplasia, plaque in the carotid bifurcation, aneurysms) were excluded. Following the approval of Institutional Ethics Committee, with ethical clearance number AIIMS/IEC/21/323, CT angiographic data from 64-slice CT scanner and 128-slice CT scanner were collected from the Department of Radiodiagnosis. Reconstruction of the three-dimensional views of the images were done using RadiAnt DICOM Viewer (RadiAnt ©), a software installed in the MSI laptop PC. The images, thus obtained, were observed and evaluated for variations. The images were analyzed as per the general anatomical course

and branches of vessels and variations, if present, were noted. The statistical analysis was done using the chi square test and the Stuart–Maxwell test.

Study sample size

The sample size for the proposed study was 208, considering our primary objective, which was to study variation in origin of superior thyroid artery. Previous studies have shown that the percentage of variation in the superior thyroid artery ranged from 6.5%–18.5%. We selected 6.5% to calculate our sample size with 10% (65) of relative procedure and finite population correction factor as 216 with 95% of confidence level and alpha error as 5%. The calculated sample size was 208. We used Open Epi, Version 3, open source calculator for the calculation of same.

RESULTS

We collected 210 samples; however, the calculated sample size for the present study was 208. Out of total 210 participants, 162 (77.1%) participants had the superior thyroid artery originating from the external carotid artery. Participants with superior thyroid artery originating from level of bifurcation of common carotid artery were 30 (14.3%), whereas participants who had origin of superior thyroid artery from common carotid artery were 18 (8.6%). **Figure 1** represents the CT angiographic image of various origin of superior thyroid artery in the axial plane.

Participants who had origin of inferior thyroid artery from thyrocervical trunk, subclavian artery, and vertebral artery were 201 (95.7%), 7 (3.3%), and 2 (1.0%), respectively. **Figure 2** represent the origin of inferior thyroid artery from left & right subclavian arteries and thyrocervical trunk respectively.

Out of total 210 cases, we observed one case that had origin of thyroid ima artery from brachiocephalic trunk (**Figure 3**).

The overall difference in the origin of superior thyroid artery was statistically significant (Stuart–Maxwell test: $\chi^2 = 11.632$, $P = 0.003$) (**Table 1**).

The overall difference in the origin of inferior thyroid artery was not statistically significant (Stuart–Maxwell test: $\chi^2 = 5.000$, $P = 0.082$) (**Table 2**).

The following variables were significantly associated ($P < 0.05$) with the variable 'Gender':

The association between “gender” and the “origin of STA” was investigated using the χ^2 test (**Table 3**).

Regarding the distribution of the origin of the STA, there was no discernible difference between the various groups ($\chi^2 = 1.409$, $P = 0.494$).

Cramer’s V value for the strength of association between the two variables is 0.08, which is considered to have little or no association in this study.

The distribution of the origin of ITA did not significantly differ across the different groups ($\chi^2 = 2.059$, $P = 0.545$) (**Table 4**).

The connection of the two variables for Cramer’s V strength was 0.1, which is considered to be little or no association in this study.

DISCUSSION

The STA is considered to be a branch of external carotid artery (ECA) in normal anatomy. The STA can also originate from common carotid artery or bifurcation of common carotid artery, according to studies that have investigated the variability in the origin site of the superior thyroid artery from the carotid arteries. The inferior thyroid artery is generally considered a branch of the thyrocervical trunk, while it can also originate from subclavian artery, vertebral artery and common carotid artery according to previous research[7]. Although thyroid ima artery is considered to originate from brachiocephalic trunk, in some cases it originates directly from arch of aorta[8].

In the present study, we have observed that the STA originated from ECA, common carotid artery (CCA) and bifurcation of common carotid artery (CCB) in 77%, 14.3% and 8.6% of the cases, respectively. However, in the case of ITA the variation in origin was seen only in 3.3% of cases from subclavian artery (SA) and in 1% case from vertebral artery (VA) with varying level of origin of thyrocervical trunk (TCT).

Sreedharan *et al*[7] in 2018 did a cadaveric study depending on the frequency of origin of STA coming from ECA, CCB, or CCA. With an incidence of 88.33%, the STA originated from ECA in 53 of the 60 hemi-neck specimens. A total of 5 out of 60 hemi-necks showed that STA appeared at the CCB in 8.33% of cases. The STA developed from the CCA in 2 of the 60 patients, with an incidence of 3.33%. In the present study the overall difference in the origin of STA was statistically significant (Stuart–Maxwell test: $\chi^2 = 11.632$, $P = 0.003$) on right and left sides, which is shown in **Table 1**.

Anagnostopoulou *et al*[9] in 2014 conducted a study on 68 formalin-embalmed adult cadavers regarding superior thyroid artery only and categorized their result in three major groups. Type A consisted of cases in which the STA originates from ECA, Type B includes cases in which STA originates

Table 1 Comparison between the origin of superior thyroid arteries on right and left side (n = 105), n (%)

Origin of superior thyroid artery	Category			Chi-squared test	
	Right	Left	Total	χ^2	P value
Bifurcation of common carotid artery	7 (6.7)	23 (21.9)	30 (14.3)	10.756	0.005
Common carotid artery	8 (7.6)	10 (9.5)	18 (8.6)		
External carotid artery	90 (85.7)	72 (68.6)	162 (77.1)		
Total	105 (100.0)	105 (100.0)	210 (100.0)		

Table 2 Comparison between the origin of inferior thyroid arteries on right and left side (n = 105), n (%)

Origin of inferior thyroid artery	Category			Fisher's exact test	
	Right	Left	Total	χ^2	P value
Subclavian artery	1 (1.0)	6 (5.7)	7 (3.3)	3.696	0.119
Thyrocervical trunk	103 (98.1)	98 (93.3)	201 (95.7)		
Vertebral artery	1 (1.0)	1 (1.0)	2 (1.0)		
Total	105 (100.0)	105 (100.0)	210 (100.0)		

Table 3 Association between gender and the origin of superior thyroid artery (n = 210), n (%)

Origin of STA	Gender			Chi-squared test	
	Male	Female	Total	χ^2	P value
External carotid Artery	89 (79.5)	73 (74.5)	162 (77.1)	1.409	0.494
Bifurcation of CCA	13 (11.6)	17 (17.3)	30 (14.3)		
CCA	10 (8.9)	8 (8.2)	18 (8.6)		
Total	112 (100.0)	98 (100.0)	210 (100.0)		

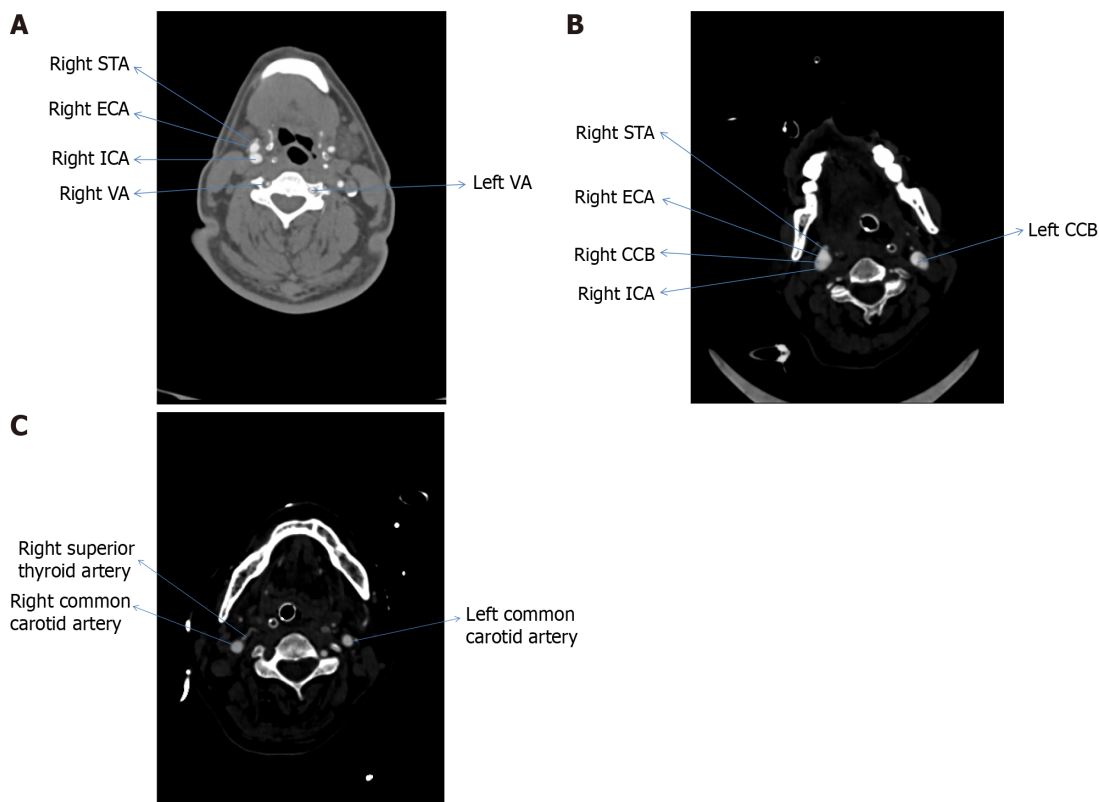
CCA: Common carotid artery; STA: Superior thyroid artery.

Table 4 Association between gender and the origin of inferior thyroid artery (n = 210), n (%)

Origin of ITA	Gender			Fisher's exact test	
	Male	Female	Total	χ^2	P value
Thyrocervical Trunk	107 (95.5)	94 (95.9)	201 (95.7)	2.059	0.545
SA	3 (2.7)	4 (4.1)	7 (3.3)		
VA	2 (1.8)	0 (0.0)	2 (1.0)		
Total	112 (100.0)	98 (100.0)	210 (100.0)		

ITA: Inferior thyroid artery; SA: Subclavian artery; VA: Vertebral artery.

from CCA and Type C constitutes cases in which STA originates from the level of CCB. In 36.8% (25/68) of the patients, Type A was found on the right side, and in 42.6% (29/68) of the cases, on the left. In 32.4% (22/68) and 38.2% (26/68) of the individuals, type B was seen on the right and left side, respectively. In 19.1% (13/68) and 30.9% (21/68) of cases, Type C variation was noted on the right and left sides. In our study, superior thyroid artery originated from ECA in majority of cases followed by level of CCB and then CCA, on left side with 72 (68.6%), 23 (21.9%) and 10 (9.5%) cases, respectively and on the right side the order of frequency of origin of superior thyroid artery is from ECA, CCA and then CCB contrary to study done by Anagnostopoulou *et al*[9].



DOI: 10.4329/wjr.v15.i6.182 Copyright ©The Author(s) 2023.

Figure 1 Computed tomography angiographic image (axial section). A: Showing the origin of the right superior thyroid artery from the external carotid artery; B: Bifurcation of the common carotid artery; C: Common carotid artery. STA: Superior thyroid artery; ECA: External carotid artery; ICA: Internal carotid artery; VA: Vertebral artery; CCB: Bifurcation of common carotid artery.

Shankar *et al*[10] in 2017 did a cadaveric study on 80 superior thyroid arteries with 40 right and 40 Left arteries, and found that it originated from the external carotid artery in 43 (53.75%), from CCB in 12 (15%), and the CCA in 25 (31.265%) cases[6]. The results of this study are similar to that of the present study as in the present study STA arose from ECA in 90 (85.7%) and 72 (68.6%) cases, on the right and left sides respectively, as the most common site of origin on both sides.

Esen *et al*[11] in 2017 did an angiographic study on 640 patients in which on the right (64.5%) and left (39.7%) sides, the STA was frequently originated from the ECA. In their study, there were 608 (95%) and 578 (90.3%) right and left ITAs emerging from the thyrocervical trunk, respectively. A single root from the SA gave rise to 18 (2.8%) right and 13 (2.0%) left ITAs. The VA was the origin of four left ITAs. In 15 patients (2.3%), the TIA was identified. A total of 12 of these were brachiocephalic arteries, 2 were right CCAs, and 1 was an aortic arch[7]. In present study the right and left STA arises from ECA in 90 (85.7%) and 72 (68.6%) cases respectively, whereas in the remaining 30 (14.3%) and 18 (8.6%) cases the STA originates from the level of CCB and main trunk of CCA respectively. However, ITA arise from TCT in 103 (98.1%) cases on right and 98 (93.3%) cases on left and among remaining cases 7 (3.3%) arise from SA and 2 (1.0%) arise from VA. We found TIA in 1 case originating from BT.

Tsegay *et al*[12] performed a cadaveric study in 2019 and observed that, the ECA was identified as the most frequent location of STA origin. The TCT gave rise to the ITA in each case, while in the present study the result for STA corresponds with the given study as in majority of cases the STA arises from ECA on both the sides, whereas in the case of ITA present study does not correspond with given study as in present study the ITA takes origin from thyrocervical trunk, SA, and VA in 201 (95.7%), 7 (3.3%) and 2 (1.0%) cases, respectively.

Gupta *et al*[13] performed an angiographic study in 2020, on 15 Indian patients indigenously from New Delhi region who were examined with a total of 25 selective STA angiograms. ECA was the primary source of STA on both sides. Ten patients (71.5%) had right STAs with ECA origins, while eight (72.5%) had left STAs with ECA origins. The bifurcation of the CCA accounted for 3 (21%) right STA and 2 (18.5%) left STA, making it the second most frequent site of STA genesis. CCA (right STA) and internal carotid artery (left STA) were the least frequent sites of origin, each accounting for one instance. In the present study, we considered a sample size of 210 patients from population of Uttarakhand, India. Gupta *et al*[13] in their study used DSA technique and also noted the branching patterns of STA only but in our study we observed the CT angiographic data and evaluated STA, ITA as well as TIA.

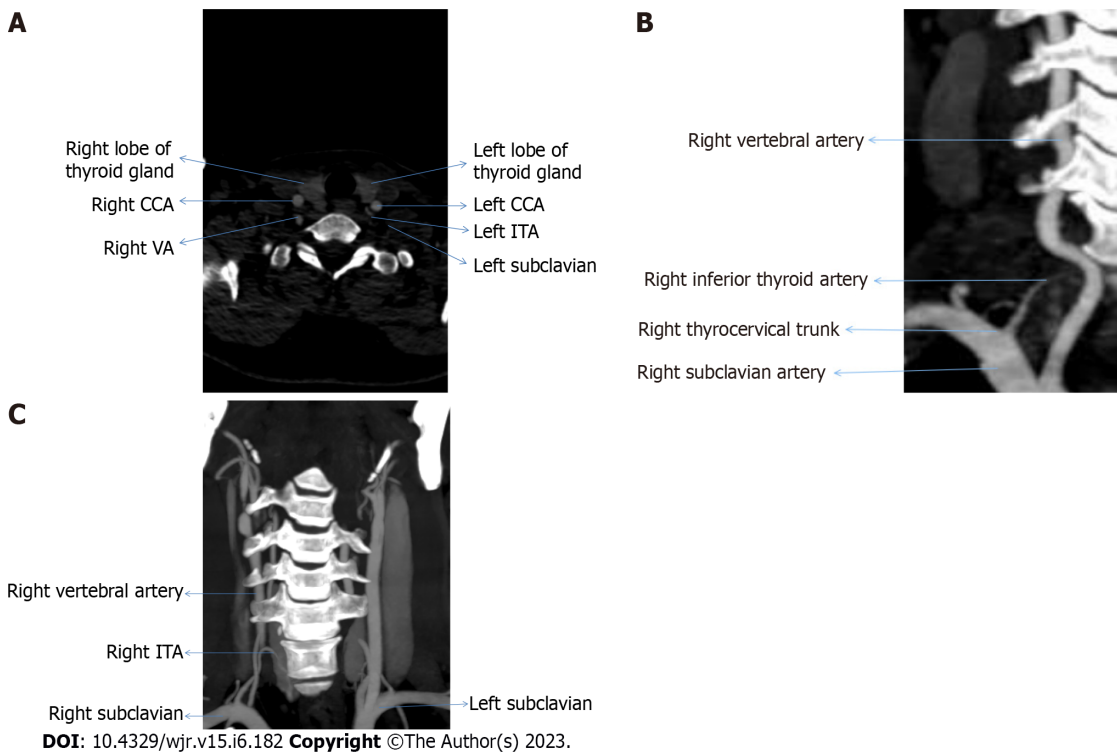


Figure 2 Computed tomography. A: Origin of inferior thyroid artery from left subclavian artery; B: Right subclavian artery; C: Right thyrocervical trunk. ITA: Inferior thyroid artery; VA: Vertebral artery; CCA: Common carotid artery.

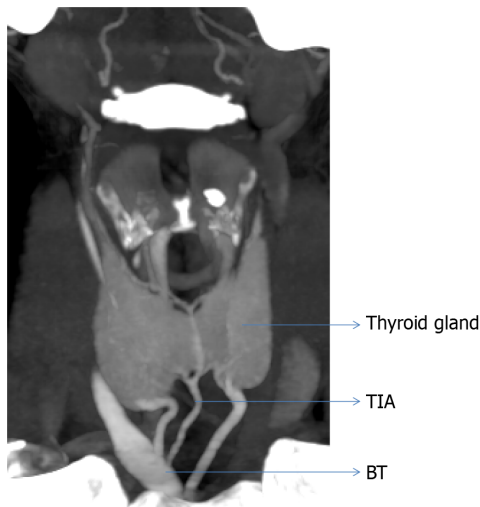


Figure 3 Showing origin of thyroid ima artery from the brachiocephalic trunk. TIA: Thyroid ima artery; BT: Brachiocephalic trunk.

Dhindsa *et al*[14] in 2014 found during a routine cadaveric dissection on male cadaver that STA on left side was arising from CCA, while on right it was originating from ECA only[10]. In the present study, we evaluated the data of 112 male patients and found that in 89 (79.5%) cases the STA arose from ECA, in 13 (11.6%) cases STA originated from level of CCB and in 10 (8.9%) cases the STA originated from CCA main trunk.

Vázquez *et al*[15] performed a cadaveric study and indicated that there are four different types of origin of STA. In type 1 STA originated from the level of CCB in 102 (49%) of cases. Type 2 was when STA originated from CCA in 55 (27%) of cases. There is a statistically significant difference between the frequency of type 2 origins on the left and right. On the other hand, there was no statistically significant distinction between male and female Type 2 origins. In Type 3, the STA arose from ECA in 48 (23%) cases. In our study we did not categorize the types, but we found that STA arose 120 from CCA, level of CCB and ECA in 18 (8.6%), 30 (14.3%), and 162 (77.1%) cases, respectively and in our study the overall difference in the origin of STA was statistically significant (Stuart-Maxwell test: $\chi^2 = 11.632$, $P = 0.003$)

on right and left sides which is shown in [Table 1](#).

In the present study the measurement of the thyroid arteries was not done.

CONCLUSION

In our study, 77% of the cases had ECA as the source of STA and in more than 22% of cases variation were seen in the origin of STA, from CCA and CCB. Variation in the level of bifurcation of CCA was also seen, which greatly changes the course of STA. The present study reveals the variation in origin of ITA is 4%, while its course varied with varying level of origin of TCT. We found that thyroid ima artery is not frequently present, but was present in only one case and can lead to severe hemorrhagic condition if remains unnoticed.

ARTICLE HIGHLIGHTS

Research background

An individual's normal growth and metabolism depend on the thyroid gland, an endocrine organ. Simple goiter, thyroid cancer, and malignant thyroid nodules are just a few of the conditions that can affect the thyroid gland. Sometimes it is necessary to perform a thyroidectomy or hemithyroidectomy in order to remove a malignant thyroid tumor. Additionally, the neck is examined for surgical treatments such as lobectomy, carotid endarterectomy, emergency cricothyroidotomy, radical neck dissection, diagnostic and therapeutic catheterization, and selective thyroid embolization. Breathing difficulties may result from tracheal compression brought on by bleeding during the thyroid gland surgery.

Research motivation

To avoid complications during thyroid surgeries, surgeons must be aware of the path and variations of the thyroid arteries. The Garhwal region of the Sub-Himalayan belt, which is thought to be the endemic zone of goitre, has little scientific literature on the radiological anatomy of thyroid arteries. A three-dimensional orientation of the vascular and surgical anatomy of the entire cervical region is provided by computed tomography angiography.

Research objectives

Radiography is a non-invasive multiplanar imaging technique for vascular mapping. The objective of the current research was to examine the origin and variation of thyroid arteries, with the aid of Computed Tomography angiography, Surgeons must be familiar with the course and variations of the thyroid arteries to prevent difficulties during thyroid operations.

Research methods

Patients with known vascular anomalies (carotid hypoplasia, plaque in the carotid bifurcation, aneurysms) or past common carotid occlusions were excluded. Following the Institutional Ethics Committee's consent, the Department of Radiodiagnosis obtained computed tomography (CT) angiographic data from 64-slice and 128-slice CT scanners. RadiAnt DICOM Viewer (RadiAnt), a programme installed on the MSI laptop PC, was used to reconstruct the three-dimensional views of the photos. The Stuart-Maxwell test and the chi square test were employed in the statistical study.

Research results

Out of 210 individuals, 77.1% of the time the superior thyroid artery was observed to be arising from the external carotid artery. In 14.3% of cases, the artery was shown to originate at the point where the common carotid artery splits, whereas in 8.6% of cases, it was discovered to be a direct branch of the common carotid artery. Similar to this, in 95.7%, 3.3%, and 1% of cases, respectively, the inferior thyroid artery was seen to be arising from the thyrocervical trunk, subclavian artery, and vertebral artery. Another person was found to have a thyroid ima artery that emerged from the brachiocephalic trunk.

Research conclusions

In our study, superior thyroid artery (STA) originated from external carotid artery in 77% of instances, and the common carotid artery (CCA) and common carotid bifurcation were the sources of STA in more than 22% of cases. Variation in the degree of CCA bifurcation was also observed, which significantly alters the path of STA. The current study shows that there is a 4% variance in inferior thyroid artery origin, whereas its course varies depending on the level of thyrocervical trunk origin. We discovered that the thyroid ima artery is only occasionally present in a small number of cases—it was only present in one case—and that if it goes unnoticed, it can cause serious hemorrhagic disease.

Research perspectives

The Garhwal region of the Sub-Himalayan belt, which is thought to be the endemic zone of goitre, has little scientific literature on the radiological anatomy of thyroid arteries. A three-dimensional orientation of the vascular and surgical anatomy of the entire cervical region is provided by computed tomography angiography. The objective of the current research was to examine the origin and variation of thyroid arteries, with the aid of Computed Tomography angiography, Surgeons must be familiar with the course and variations of the thyroid arteries to prevent difficulties during thyroid operations. Additional research in this area using even better methods can further add to the existing knowledge on thyroid arteries.

ACKNOWLEDGEMENTS

We would like to thank the attendants and fellows from the Radiology department of AIIMS Rishikesh as well as the laboratory staff, Mr. Devender, for their continued support and assistance during data collection.

FOOTNOTES

Author contributions: All the authors have contributed significantly to this work; Singh B, Bhadoria P and Malhotra R designed the research study; Bhardwaj Y and Tarafdar S performed the research; Bhardwaj Y, Malhotra R and Bisht K analyzed the data and wrote the manuscript; All authors have read and approved the final manuscript.

Institutional review board statement: Following the approval of Institutional Ethics Committee, with ethical clearance number AIIMS/IEC/21/323, CT angiographic data from 64-slice CT scanner and 128-slice CT scanner were collected from the Department of Radiodiagnosis.

Informed consent statement: A waiver was granted by our Institutional Ethics committee as this is a retrospective study.

Conflict-of-interest statement: The authors declare no conflict of interest.

Data sharing statement: Anonymization of data will be maintained.

Open-Access: This article is an open-access article that was selected by an in-house editor and fully peer-reviewed by external reviewers. It is distributed in accordance with the Creative Commons Attribution NonCommercial (CC BY-NC 4.0) license, which permits others to distribute, remix, adapt, build upon this work non-commercially, and license their derivative works on different terms, provided the original work is properly cited and the use is non-commercial. See: <https://creativecommons.org/licenses/by-nc/4.0/>

Country/Territory of origin: India

ORCID number: Yashu Bhardwaj 0009-0008-0506-2899; Brijendra Singh 0000-0002-3501-0896; Pooja Bhadoria 0000-0001-9617-6526; Rashmi Malhotra 0000-0002-5633-5446; Swarnava Tarafdar 0000-0003-3582-8871; Kanchan Bisht 0000-0002-4615-1352.

S-Editor: Liu JH

L-Editor: A

P-Editor: Zhao S

REFERENCES

- 1 **Kaplan E**, Angelos P, Applewhite M, Mercier F, Grogan RH. Chapter 21. Surgery of the Thyroid. In: Feingold KR, Anawalt B, Blackman MR, Boyce A, Chrousos G, Corpas E, *et al*, editors. South. Dartmouth (MA). 2000 [DOI: 10.1016/s1530-891x(20)44840-2]
- 2 **Lemke J**, Schreiber MN, Henne-Bruns D, Cammerer G, Hillenbrand A. Thyroid gland hemorrhage after blunt neck trauma: case report and review of the literature. *BMC Surg* 2017; **17**: 115 [PMID: 29183351 DOI: 10.1186/s12893-017-0322-y]
- 3 **Allen E**, Fingeret A. Anatomy, head and neck, thyroid. InStatPearls [DOI: 10.1201/b19589-27]
- 4 **Gray's Anatomy**, 39th Edition: The Anatomical Basis of Clinical Practice. Vol. *American Journal of Neuroradiology* 2005; 2703-2704 [DOI: 10.1177/0310057x0503300431]
- 5 **Sareen N**, Kapil U, Nambiar V, Pandey RM, Khenduja P. Iodine nutritional status in Uttarakhand State, India. *Indian J Endocrinol Metab* 2016; **20**: 171-176 [PMID: 27042411 DOI: 10.4103/2230-8210.176363]

- 6 **Kumamaru KK**, Hoppel BE, Mather RT, Rybicki FJ. CT angiography: current technology and clinical use. *Radiol Clin North Am* 2010; **48**: 213-235, vii [PMID: 20609871 DOI: 10.1016/j.rcl.2010.02.006]
- 7 **Sreedharan R**, Krishna L, Shetty A. Origin of superior thyroid artery: under the surgeon's knife. *J Vasc Bras* 2018; **17**: 290-295 [PMID: 30787946 DOI: 10.1590/1677-5449.004218]
- 8 **Jayaraju RM**, Mohiyuddin A, Merchant S, Raj S, Sasidharan B. Thyroidea ima artery: a report of two cases. *Int J Head Neck Surg* 2015; **5**: 89-90 [DOI: 10.5005/jp-journals-10001-1188]
- 9 **Anagnostopoulou S**, Mavridis I. Emerging patterns of the human superior thyroid artery and review of its clinical anatomy. *Surg Radiol Anat* 2014; **36**: 33-38 [PMID: 23783368 DOI: 10.1007/s00276-013-1149-6]
- 10 **Shankar VV**, N K, Shetty S. A cross-sectional study of superior thyroid artery in human cadavers. *Int J Anat Res* 2017; **5**: 4751-4755 [DOI: 10.16965/ijar.2017.463]
- 11 **Esen K**, Ozgur A, Balci Y, Tok S, Kara E. Variations in the origins of the thyroid arteries on CT angiography. *Jpn J Radiol* 2018; **36**: 96-102 [PMID: 29204764 DOI: 10.1007/s11604-017-0710-3]
- 12 **Tsegay AT**, Berhe T, Amdeklase F, Hayelom H. Variations on arterial supply of thyroid gland and its clinical significance in selected universities of North Ethiopia. *Int J Anat Res* 2019; **7**: 6830-6834 [DOI: 10.16965/ijar.2019.237]
- 13 **Gupta P**, Bhalla AS, Thulkar S, Kumar A, Mohanti BK, Thakar A, Sharma A. Variations in superior thyroid artery: A selective angiographic study. *Indian J Radiol Imaging* 2014; **24**: 66-71 [PMID: 24851008 DOI: 10.4103/0971-3026.130701]
- 14 **Dhindsa GS**, Sodhi S. Variation in the origin of superior thyroid artery. *J Evol Med Dent Sci* 2014; **3**: 5969-5972 [DOI: 10.14260/jemds/2014/2691]
- 15 **Vázquez T**, Cobiella R, Maranillo E, Valderrama FJ, McHanwell S, Parkin I, Sañudo JR. Anatomical variations of the superior thyroid and superior laryngeal arteries. *Head Neck* 2009; **31**: 1078-1085 [PMID: 19340860 DOI: 10.1002/hed.21077]

Observational Study

Role of contrast-enhanced serial/spot abdominal X-rays in perioperative follow-up of patients undergoing abdominal surgery: An observational clinical study

Osman Nuri Dilek, Arif Atay, Orgun Gunes, Furkan Karahan, Şebnem Karasu

Specialty type: Surgery

Provenance and peer review:

Invited article; Externally peer reviewed.

Peer-review model: Single blind

Peer-review report's scientific quality classification

Grade A (Excellent): 0

Grade B (Very good): B

Grade C (Good): C, C

Grade D (Fair): D, D

Grade E (Poor): 0

P-Reviewer: Amagai T, Japan; Ghimire R, Nepal; Giacomelli L, Italy

Received: March 13, 2023

Peer-review started: March 13, 2023

First decision: May 9, 2023

Revised: May 17, 2023

Accepted: June 16, 2023

Article in press: June 16, 2023

Published online: June 28, 2023



Osman Nuri Dilek, Arif Atay, Furkan Karahan, Department of Surgery, İzmir Katip Celebi University, School of Medicine, İzmir 35150, Turkey

Orgun Gunes, Department of Surgery, İzmir Atatürk Education and Research Hospital, İzmir 35150, Turkey

Şebnem Karasu, Department of Radiology, İzmir Katip Celebi University, School of Medicine, İzmir 35150, Turkey

Corresponding author: Osman Nuri Dilek, FACS, Professor, Surgeon, Department of Surgery, İzmir Katip Celebi University, School of Medicine, Basın Sitesi, İzmir 35150, Turkey. osmannuridilek@gmail.com

Abstract

BACKGROUND

Many imaging methods such as ultrasonography, computed tomography (CT), magnetic resonance imaging, and endoscopy are used to identify the problems or complications that occur in the perioperative period and to determine the appropriate therapeutic approach. Specialists at surgical clinics and intensive care units sometimes need diagnostic procedures that can give quick results or reveal unexpected results. In particular, rapid on-site evaluation of patients followed under intensive care conditions has several advantages.

AIM

To determine the problems developing in patients in the perioperative period by contrast-enhanced abdominal X-ray (CE-AXR), revealing their current status or defining the effectiveness of CE-AXR.

METHODS

The files of the patients who underwent hepatopancreatobiliary or upper gastrointestinal surgery, whose CE-AXR film was taken, were reviewed retrospectively. Abdominal X-ray radiographs taken after ingestion of a water-soluble contrast agent (iohexol, 300 mg, 50 cc vial) and its application in a drain, nasogastric tube, or stent were evaluated. The contribution of the data obtained in patients who underwent CE-AXR to the diagnosis, follow-up, and treatment processes and the effectiveness of the application were investigated.

RESULTS

CE-AXR was applied to 131 patients in our clinic, most of whom underwent hepatopancreatobiliary or upper gastrointestinal surgery. It was determined that the data obtained from CE-AXR films taken in 98 (74.8%) of the patients contributed to the diagnosis, treatment, and follow-up expectations and positively affected the clinical processes.

CONCLUSION

CE-AXR is a simple procedure that can be applied anywhere, especially in intensive care patients and at bedside, with a portable X-ray device. The simplicity of the procedure, less radiation exposure for the patients, less time wastage, reduction in the CT and endoscopy procedure burden and costs, quick results, rapid assessment of the situation, and enabling the monitoring of processes with repetitive procedures are important advantages. X-rays taken will be useful in terms of being a reference value during the follow-up period of the patient and determining the situation in medicolegal processes.

Key Words: Abdominal X-rays; Contrast medium; Diagnosis; Complication; Leakage; Radiation exposure

©The Author(s) 2023. Published by Baishideng Publishing Group Inc. All rights reserved.

Core Tip: Specialists at surgical clinics and intensive care units sometimes need diagnostic procedures that can give quick results or reveal unexpected results. In this study, contrast-enhanced abdominal X-ray (CE-AXR) was used to evaluate diagnosis and treatment efficacy in 131 patients. We sought to determine the problems developing in patients in the perioperative period, revealing their current condition or defining the effectiveness of CE-AXR. It was found that CE-AXR accelerated and facilitated decision-making processes in selected patient groups and did not require further investigation. It was determined that the data obtained from CE-AXR contributed to the diagnosis, treatment, and follow-up expectations in 98 patients (74.8%) and also had a positive impact on clinical processes. CE-AXR is a procedure that can be performed almost anywhere with a portable X-ray machine, particularly at bedside, and in intensive care units and clinics.

Citation: Dilek ON, Atay A, Gunes O, Karahan F, Karasu Ş. Role of contrast-enhanced serial/spot abdominal X-rays in perioperative follow-up of patients undergoing abdominal surgery: An observational clinical study. *World J Radiol* 2023; 15(6): 191-200

URL: <https://www.wjgnet.com/1949-8470/full/v15/i6/191.htm>

DOI: <https://dx.doi.org/10.4329/wjr.v15.i6.191>

INTRODUCTION

A wide variety of imaging methods is used to identify the problems encountered during the follow-up of patients in surgery. Ultrasonography (USG), magnetic resonance imaging (MRI), computed tomography (CT), and endoscopic interventions are the most commonly used methods. It has been reported that interpretations in diagnostic procedures can be very variable and erroneous reporting (diagnosis) is made in 2%-20% of cases in the literature[1]. On the other hand, most diagnostic devices, except USG and mobile X-ray devices, can be used with limitations of place, time, device, and technical staff.

Direct abdominal X-ray (AXR) radiographs are one of the diagnostic devices that can be used almost everywhere in hospitals with the use of mobile X-ray devices, especially in emergency services[2]. It has also been frequently used to control subclavian, jugular, percutaneous endoscopic gastrostomy, nasogastric tube, or peritoneal dialysis catheter positions. It has been reported that while AXR detects foreign bodies with a sensitivity of 90%, it shows intestinal obstructions with a sensitivity of 49%[3]. It has been reported that the data obtained from approximately half of the patients who underwent AXR in the emergency department have no relation with the definitive diagnosis[4]. The use of mobile X-ray devices can play a vital role in the identification and decision-making of developing pathologies, especially in patients followed in intensive care units.

There are not enough studies in the literature on the use of direct/spot contrast-enhanced AXR (CE-AXR) following contrast agent administration. In this observational clinical study, we aimed to examine our CE-AXR application results in the definition and follow-up of clinical manifestations in patients hospitalized in intensive care units and clinics, mostly with hepatopancreatobiliary and upper abdominal surgery, in the light of the literature.

MATERIALS AND METHODS

Study population and data collection

The data was obtained by retrospectively examining the files of the patients who had CE-AXR films in the surgical clinic (125 beds) of our university hospital (1100 beds) between 2017 and 2021. Since hepatopancreatobiliary (HPB) and upper gastrointestinal surgeries are mainly performed in our clinic, the patients participating in the study mainly underwent pancreatic, liver, biliary tract, esophagus, and stomach surgeries. Most of the patients who underwent major surgery were followed in the intensive care unit in the early postoperative period (1-5 d). Those who were followed in the clinic or the outpatient clinic or who applied to the emergency department with serious complications were also followed in the intensive care unit. Along with conventional diagnostic tools in our hospital, mobile ultrasound and mobile X-ray devices are constantly used.

Study assessment and criteria

CE-AXR scans were performed on selected patients to control and confirm the efficacy of surgeries or to evaluate unexpected results. Outpatient X-ray devices were used in stable patients and mobile X-ray devices were used in patients hospitalized in the clinic. CE-AXR images were taken with mobile X-ray machines at bedside for patients who were thought to be evaluated in the intensive care unit. More complicated patients were transported to the radiology service with their beds and mobile life support units for conventional CT or MRI examination. In case of insufficient data obtained with CE-AXR or in patients with an unexpected pathological condition (anastomotic leakage, stricture, *etc.*), it was decided to perform MRI, magnetic resonance cholangiopancreatography (MRCP), or CT first. Data on conventional cholangiography and other conventional contrast-enhanced imaging methods were not included in the study.

Techniques

AXR radiographs taken following the ingestion of a water-soluble contrast agent (iohexol, 300 mg, 50 cc vial) in the preoperative or postoperative period and its application in a drain or stent were evaluated. CE-AXRs were taken in the early or late periods following the application according to the characteristics of the case and expectations. In patients with percutaneous transhepatic biliary drainage (PTBD), AXR imaging was performed by administering the contrast material through the catheter on postoperative 5th-10th days. While a single spot AXR radiography may be sufficient in most cases, in some of the cases, 2-3 spot AXRs were taken intermittently to monitor the intestinal passage.

In the evaluation of the results, statistical analysis methods were not used, except for numerical and proportional data for the evaluation of whether the procedure contributed to the diagnosis and treatment process.

The study was carried out in accordance with the principles of the Helsinki Declaration. As a routine procedure, written informed consent was obtained from each patient for all procedures and publications. Ethics committee approval was received for this study (2022/GOKAE/0542) from the Clinical Trials Ethics Committee.

RESULTS

CE-AXR images of 131 cases included in the study were evaluated retrospectively (Table 1). CE-AXR images taken to evaluate the patency of anastomoses, which were initially performed in our clinic only in selected patients with PTBD and have started to be applied in more patients in the last two years. CE-AXR was taken at bedside in 67 patients in the intensive care unit during their follow-up. Patients who could not be evaluated with the obtained CE-AXR images were sent to the relevant units for endoscopy, CT, or other diagnostic examinations.

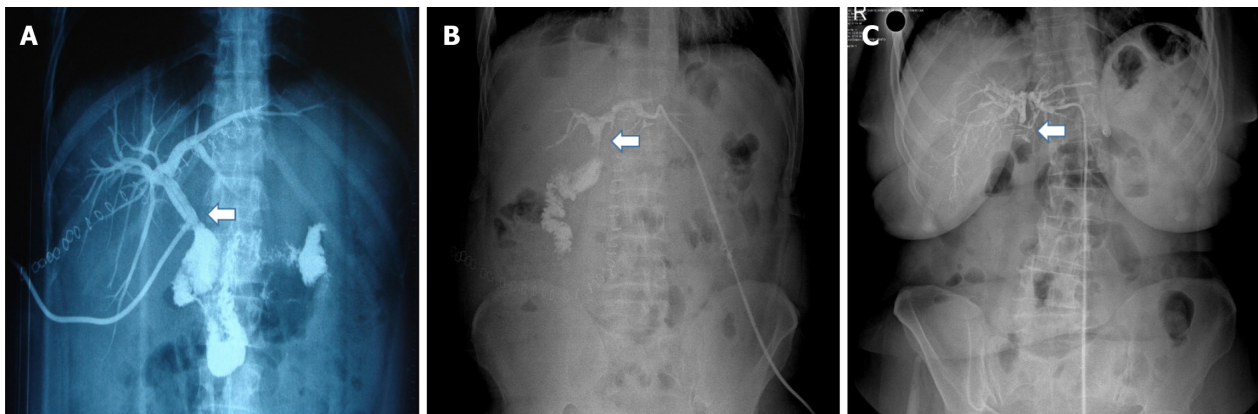
Anastomosis could be evaluated in 29 (80%) patients in CE-AXR radiographs taken with the contrast medium given through the PTBD catheter among 36 patients who underwent hepaticojejunostomy or portoenterostomy (Figure 1). Anastomotic leakage was detected in two patients, while stricture developed in two patients. It was decided to perform MRCP in seven patients who developed complications and could not be evaluated due to insufficient images.

Oral fluid-food intake is started after the routine evaluation of CE-AXR radiographs taken on the 3rd or 4th postoperative days of our patients who underwent esophagectomy (+ gastric pull-up) or total gastrectomy (+ Roux-n-Y reconstruction) (Figure 2). A descriptive image was obtained in 27 of 34 patients (79%) who underwent CE-AXR, and anastomotic leakage was detected in two of the cases (Table 1) (Figure 3). Adequate radiological imaging (Figure 4) was obtained in 15 of 18 patients (78%) with sleeve gastrectomy in our series, no complications were detected in any of them, and the patients were discharged with full recovery.

CE-AXR examinations were performed (Figure 5) to describe the continuity of the gastrointestinal transition in patients ($n = 43$) receiving chemotherapy or developing acute abdomen (intestinal obstruction), or postoperative patients. Definitive diagnosis was made in 27 cases (62%), and additional

Table 1 Characteristics of patients with contrast-enhanced abdominal X-ray (*n* = 131)

Procedure	<i>n</i>	Positive results (Success) <i>n</i> , %
Patency of hepaticojejunostomy (stricture? leakage?)	21	17
Patency of portoenterostomy (stricture? leakage?)	15	12
Esophagectomy + Gastric pull-up	9	7
Total proximal gastrectomies	14	11
Bariatric surgery	18	15
Gastrointestinal anastomosis	11	9
Intestinal obstruction (etiology? levels?)	9	7
Acute abdomen? Etiology? (Perforation? leakage?)	8	4
Dysfunctional ostomies	2	-
Postoperative vomiting	13	7
Persistent vomiting (chemotherapy/follow-up period)	11	9
Total	131	98 (74.8)



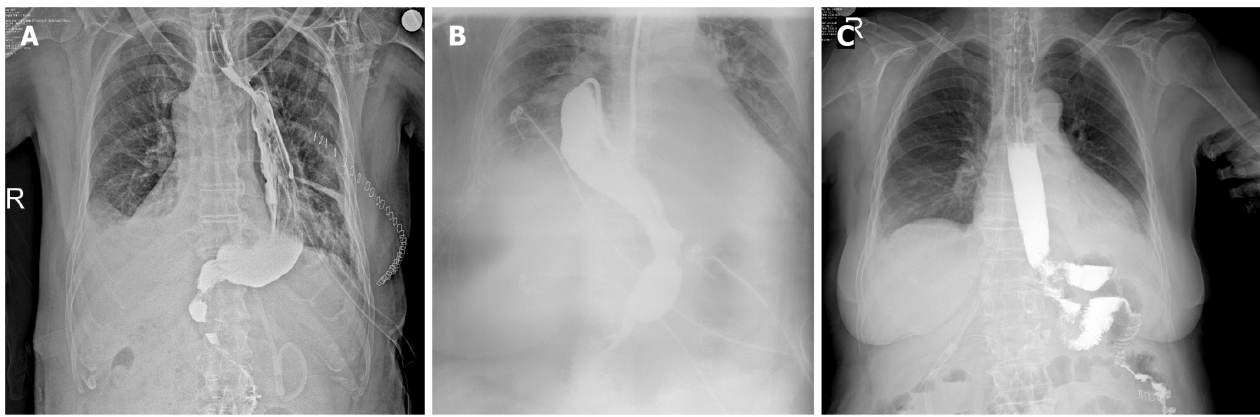
DOI: 10.4329/wjor.v15.i6.191 Copyright ©The Author(s) 2023.

Figure 1 Postoperative contrast-enhanced abdominal X-ray images following hepaticojejunostomy for the reconstruction of the biliary tract. A: Postoperative 14th day contrast-enhanced abdominal X-ray in a 42-year-old man with major bile duct trauma (Strasberg Bismuth E1) who underwent T-tube reconstruction; the biliary tract and anastomosis was normal; B: The anastomosis and bile flow patency was normal in a 47-year-old woman who underwent hepaticojejunostomy for major bile duct trauma (Strasberg Bismuth E2); C: The stricture (arrow) in the common hepatic duct was detected in a 38-year-old woman who developed jaundice after biliary tract trauma (Strasberg Bismuth E2) and underwent percutaneous transhepatic biliary drainage.

radiological imaging was required for a definitive diagnosis in 16 cases (Table 1). For patients who were consulted to our clinic with the suspicion of intestinal obstruction, in addition to the routine procedures applied, the passage was evaluated objectively by taking 2-3 spot images with CE-AXR. Medical treatment protocols were applied to cases with the open passage with CE-AXR, and surgical treatment for patients with CE-AXR obstruction (Figure 6). Twenty-two patients were followed with suspected nausea and vomiting (*n* = 13) or intestinal obstruction (*n* = 9); 12 of them were radiologically normal, and intestinal obstruction was found in two patients (Figure 7). Additional examinations (CT, gastroscopy, and colonoscopy) were performed on other patients for whom sufficient information could not be obtained with CE-AXR.

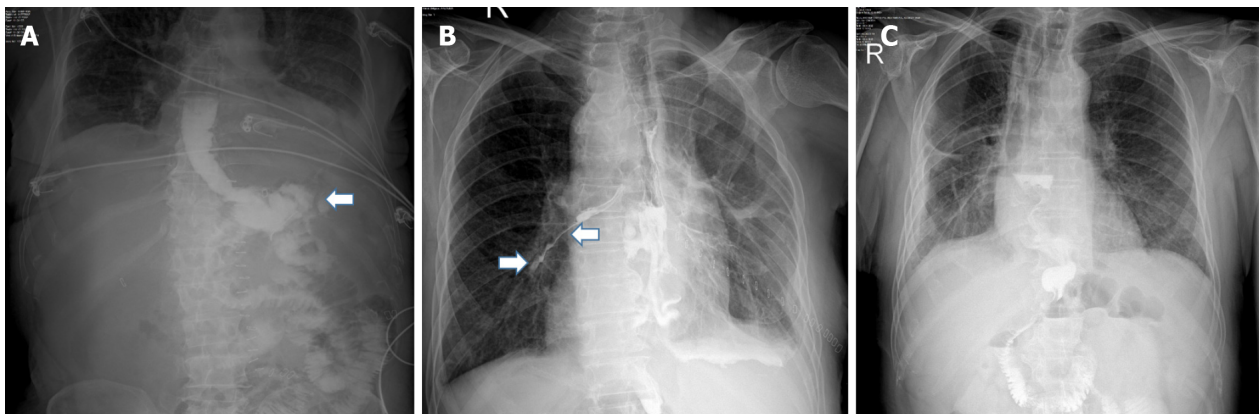
The most common causes of failure in imaging on X-rays taken to detect the presence of anastomotic stenosis or leakage were found to be lack of contrast material (amount or concentration) and timing problems (early-late). It was calculated that imaging data contributed positively to the diagnosis, follow-up, and treatment processes in 98 (74.8%) of the patients with CE-AXR.

Allergic or renal problems or technical problems related to the administration of contrast material were not encountered.



DOI: 10.4329/wjr.v15.i6.191 Copyright ©The Author(s) 2023.

Figure 2 Contrast-enhanced abdominal X-ray images following gastrointestinal reconstruction for stomach/esophagus tumors. A: A 67-year-old man and a 78-year-old woman who underwent esophagectomy + gastric pull-up for distal esophageal tumor. The esophagogastric passage was normal without any findings of fistula or leakage at the sites of anastomoses on the postoperative 4th day; C: The position of the jejunal loop/stump and the passage was normal in a 72-year-old woman who underwent total gastrectomy and Roux-n-Y anastomosis for cardia tumor.



DOI: 10.4329/wjr.v15.i6.191 Copyright ©The Author(s) 2023.

Figure 3 Contrast-enhanced abdominal X-ray images showing anastomotic leakage. A: Anastomotic leakage in a 77-year-old man with total gastric resection and Roux-n-Y anastomosis (arrows) for gastric cancer on the 6th postoperative day; B: Anastomotic leakage detected in a 63-year-old man on the postoperative 4th day who underwent esophagectomy + gastric pull-up for distal esophagus tumor; C: Repeated control contrast-enhanced abdominal X-ray showed healing in the same patient on postoperative 30th day.

DISCUSSION

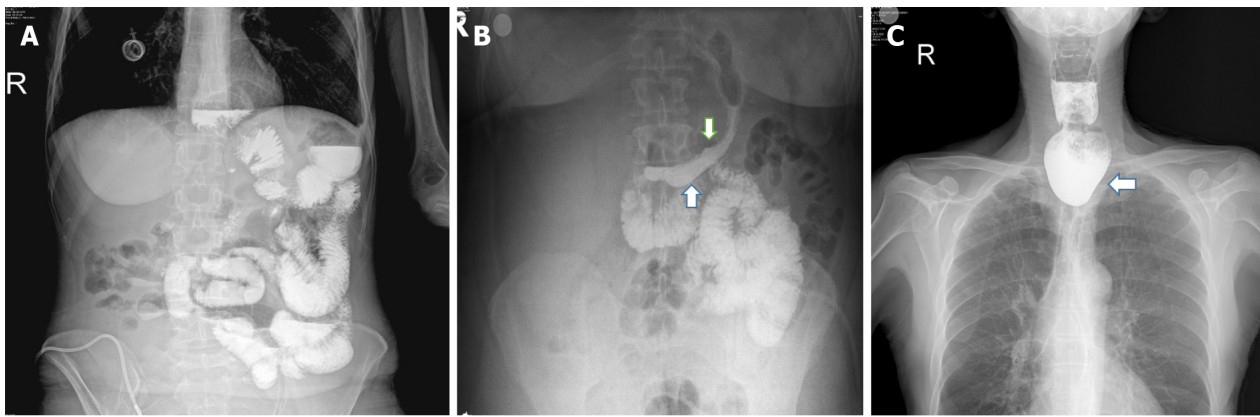
Specialists at surgical clinics and intensive care units sometimes need diagnostic procedures that can give quick results or reveal unexpected results. Radiological examinations are the most widely used and accessible diagnostic tools today[5]. Endoscopists and surgeons often make use of scope imaging during their procedures.

Direct/spot AXRs are mostly used in emergency departments to elucidate the etiology of pain[1,2,6].

AXRs are typically taken in about half of patients suffering from abdominal pain[4,5]. It has also been reported that most AXRs in emergency departments are unnecessary. It has been reported in the literature that positive X-ray results are detectable in 15.8% to 25% of patients undergoing AXRs[2-4]. Today, a wide variety of contrast agents is also used to eliminate the disadvantages of direct imaging, to obtain better images with modern imaging devices, and to make more accurate interpretations. The use of contrast media has become a common procedure in CT, MR, and USG examinations to better define organ and tissue limits. Positive results were obtained in most of the cases ($n = 98$, 74.8%) with CE-AXR in our series (Table 1).

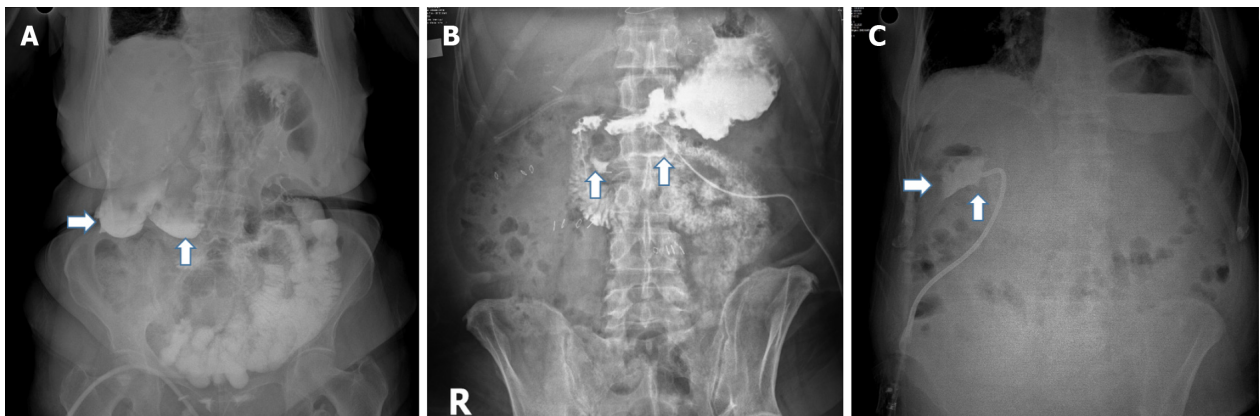
CE-AXRs were originally made to understand the status (patency, stenosis, or leak) of hepaticojejunostomy or portoenterostomies performed only in selected patients undergoing HPB surgery (Figure 1). It has also been used later to describe the current state of patients and when quick decision-making is required.

The major cause of morbidity and mortality after esophagectomy or total gastric resection is asymptomatic anastomotic leakage. Although routine radiological follow-up is not performed in the early postoperative period, it has been reported that anastomotic leakage can be overlooked even in



DOI: 10.4329/wjr.v15.i6.191 Copyright ©The Author(s) 2023.

Figure 4 Functionality of the gastrointestinal passage and patency of anastomosis on contrast-enhanced abdominal X-rays. A: A 57-year-old woman whose esophagojejunal anastomosis functionality and passage continuity were investigated and evaluated as normal on the 4th postoperative day; B: The gastric remnant, position, and functionality were normal in a 37-year-old woman (BMI-47.2) on the 3rd postoperative day after sleeve gastrectomy; C: Zenker's diverticulum that was unexpectedly detected in a 44-year-old man with gastric resection for gastric cancer, who presented with dysphagia in the postoperative follow-up period.



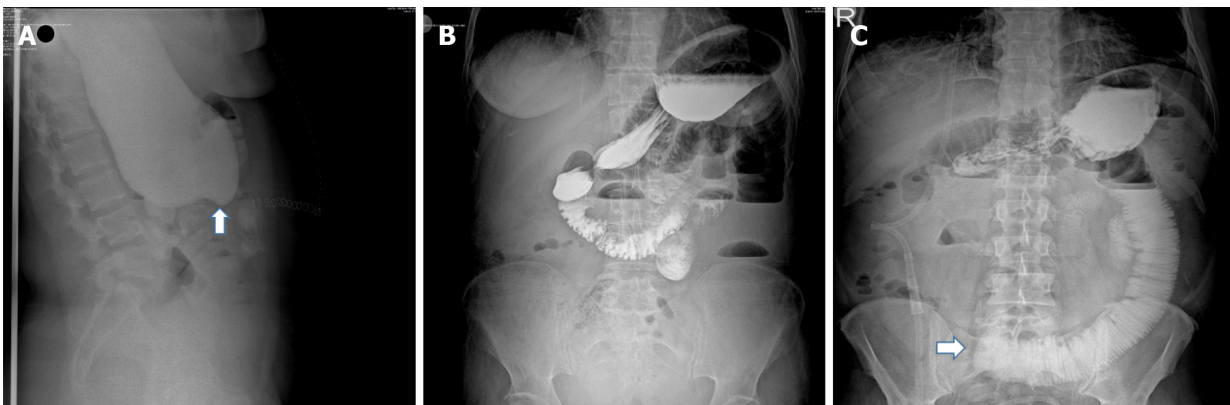
DOI: 10.4329/wjr.v15.i6.191 Copyright ©The Author(s) 2023.

Figure 5 Leakage and perforation on contrast-enhanced abdominal X-rays. A: Contrast material leakage into the abdominal cavity (arrows) due to the peptic ulcer perforation seen on contrast-enhanced abdominal X-ray (CE-AXR) in a 76-year-old woman who cannot be diagnosed by clinical findings; B: CE-AXR in a 57-year-old woman who underwent laparoscopic stromal tumor resection and developed unexpected abdominal pain on the 5th postoperative day showed an opening at the suture line and contrast material leakage (arrows); C: In a 68-year-old woman who underwent hilar resection and portoenterostomy for Klatskin tumor, CE-AXR obtained by administering contrast material through the drain showed the biliary fistula tract and subhepatic pouch (arrows).

routine detailed scans[7]. CE-AXR examinations, which we previously performed in selected patients, have recently begun to be routinely performed (Figures 2-4). In patients with fistula, CE-AXR can guide the location, depth, dimensions, and treatment planning of the fistula.

Intraoperative methylene blue injection through the nasogastric tube is a widely used method[8,9] for checking the tightness of the staple line (leakage) in bariatric and gastrointestinal surgery. Recently, intraoperative indocyanine green has been used for the same purpose[9]. Studies also report a high rate of false negativity in postoperative routine endoscopy or anastomotic leakage screening with methylene blue[10]. In our clinic, methylene blue is routinely used in surgery for the control of tightness in patients undergoing bariatric surgery. While patients were previously given methylene blue on the 3rd or 4th postoperative day, they have recently been evaluated with CE-AXR taken with oral contrast (Figure 4). We believe that it is a more objective method than evaluation with methylene blue. CE-AXR taken on the 3rd or 4th postoperative day also gives information about the resection margins (leakage), stomach balance, and passage status at the patient's discharge time. It also has advantages such as documenting the final status of the patient with the CE-AXR taken and having reference data in the controls to be made.

The continuity of the passage and the presence of perforation can be questioned with a water-soluble radiopaque contrast material to be drunk or administered through a nasogastric tube in patients who are elderly, have cooperation problems, have faint physical examination findings, and whose etiology of the acute abdomen cannot be adequately evaluated. We had cases diagnosed with peptic ulcer



DOI: 10.4329/wjr.v15.i6.191 Copyright ©The Author(s) 2023.

Figure 6 Contrast-enhanced abdominal X-rays showing intestinal obstruction. A: Lateral contrast-enhanced abdominal X-ray (CE-AXR) showed gastric dilation due to gastric outlet obstruction (Arrow) in a 48-year-old woman with persistent nausea and vomiting after pylorus-preserving pancreatoduodenectomy; B: Abdominal cocoon was detected on CE-AXR in a 67-year-old woman who suffered from acute abdomen; C: CE-AXR showed a 74-year-old man who was thought to develop intestinal obstruction due to adhesions (arrow).



DOI: 10.4329/wjr.v15.i6.191 Copyright ©The Author(s) 2023.

Figure 7 Non-surgical patients' contrast-enhanced abdominal X-rays for evaluations of intestinal passage continuity. A: A 69-year-old man underwent pancreatoduodenectomy for a pancreas tumor in the 6th postoperative year and presented with persistent nausea and vomiting due to incarcerated intestinal loops collected in a giant incisional hernia; B: It was seen in the right lower quadrant of the abdomen and the intestinal passage was evaluated as normal; C: Normal passage of the contrast material was seen on contrast-enhanced abdominal X-ray in a 59-year-old woman who was treated with chemotherapy and presented with persistent nausea and vomiting.

perforation by administering an oral contrast agent in drinking water in patients followed up with the diagnosis of acute abdomen and the cause of which could not be identified. Unexpected fistula cases were also detected (Figure 5). CE-AXR may contribute to the reduction of unnecessary laparotomy. On the other hand, it can prevent complications due to delays in diagnosis and treatment.

Gastric emptying difficulty is a serious problem in patients who have undergone major surgery, especially after pancreatoduodenectomy[11-13]. Patients receiving adjuvant chemotherapy may also experience severe nausea and vomiting from time to time. The underlying cause should be studied in certain patients receiving chemotherapy at the oncology clinic who have treatment-resistant nausea and vomiting. Delayed healing of wounds may occur because of wide incisions, high risk of infection, and chemotherapy, and patients with pancreatoduodenectomy may have more incisional hernias that can reach large sizes. Continuity of transition may be assessed with CE-AXR in patients with giant incisional hernias (Figure 7) and complaints of nausea and vomiting. CE-AXR can also prevent unnecessary surveys, procedures, and laparotomies. There may be evidence to show that the patient has recovered or improved after surgery.

Nowadays, the largest source of radiation exposure is X-ray imaging equipment used in diagnostic and therapeutic procedures. According to the global calculations, the average amount of natural radiation or exposure to Radon per person is calculated as 2.4 mSv/year (Table 2)[14-19]. More than 500 million radiological imaging examinations are performed annually in the United States. It is calculated that radiation exposure will increase progressively[14,20]. According to BEIR reports, it has been calculated that abdominal sarcoma/carcinoma may develop in one of 550-600 patients who received 20 mSv of radiation in conventional computed tomography scans[15,21]. The amount of radiation exposure

Table 2 Effective doses of radiation for various radiological procedures and activities

Form of exposure to radiation	Effective dose (mSv)
Natural background radiation for 1 yr	1.3-4.1 (mean 2.4)
Airline passenger with Subsonic flight at 36.000 feet from New York to Istanbul	0.04
Abdominal/pelvic X-ray	0.7
Barium meal/enema	3-10
Hiroshima (measured from the jawbone, 1997)	9460
Average personal dose received by Turkish people due to the Chernobyl accident	0.5
Mammogram	0.4
Chest X-ray	0.02
Intravenous pyelography-IVP	6
Abdominal CT (± contrast)	10-30
Chest/cardiac CT	7.8/16
Pelvic CT	10
Angiography/venography	11-33
CT-guided intervention	11-17
Nuclear stress test with Tc-99m/thallium	11-22
Ultrasonography	0
Abdominal MRI	0

Figures are average data compiled from different reports and may vary according to country, age, gender, devices, and other variables. 1 Gy = 1 Sv = 1000 mSv = 100 Rem. CT: Computed tomography; MRI: Magnetic resonance imaging.

caused by AXR (0.7 mSv) is higher than that by chest X-ray (0.02 mSv)[5,21,22]. The amount of radiation exposure with CE-AXR is significantly lower than that with fluoroscopy and CT (Table 2). It has been determined that CE-AXR can be taken with mobile X-ray devices at bedside and in intensive care units. It also accelerates and facilitates decision-making processes and requires no further review.

CONCLUSION

Simple and mobile devices can also play a significant role in managing medical and surgical processes. Important data can be obtained using CE-AXR to confirm clinical results, determine status, or rule out a diagnosis or event. In selected cases and series, CE-AXR has many clinical benefits and contributions. These are: (1) Very handy and quick results are available; (2) It is possible to determine whether the entities in question are present or not; (3) It is more appropriate in intensive care units and at bedside; (4) The workload in radiology (CT/MRI) and endoscopy units is reduced; (5) Exposure to irradiation is reduced; (6) The use of radiopaque substances, which have toxic effects on the kidneys and have allergic properties, will decrease; and (7) It may be a benchmark for future medical follow-ups and medicolegal proceedings.

ARTICLE HIGHLIGHTS

Research background

Although abdominal X-rays are one of the most frequently used imaging methods in emergencies, they are not as reliable as expected.

Research motivation

The desire to quickly evaluate and know the developments in patients being followed in the surgery clinic and intensive care units prompted us to conduct this study.

Research objectives

It has been designed especially for imaging at bedside in order to learn the result of the procedure or the existence and dimensions of undesirable situations in a short time.

Research methods

Initially, contrast-enhanced abdominal X ray (CE-AXR) was performed to evaluate only biliary tract anastomoses (cholangiography). Evaluation of images (CE-AXR) obtained by the application of catheters, drains, nasogastric tube, or oral contrast agent (iohexol, 300 mg, 50 cc vial) mixed with saline or water in very different clinical situations with satisfactory results (stenosis, patency, functionality, fistula, obstruction, *etc.*) was performed. File data of patients who underwent CE-AXR in the retrospective observational study were evaluated.

Research results

As a result of examining the data of a total of 131 patients, it was determined that CE-AXR, which was performed after liver, biliary tract, pancreas, esophagus, and stomach operations, provided adequate imaging in 74.8% of the cases and contributed to the diagnosis and treatment process. No complications related to the procedure were observed.

Research conclusions

CE-AXR is a very simple imaging method that has no side effects. It can be very useful in clinics and intensive care units because it can be done with mobile X-ray devices at bedside and give fast results. It also has advantages such as reducing the burden of the radiology unit and exposure to radiation.

Research perspectives

CE-AXR can contribute to the diagnosis and treatment process in patients with upper gastrointestinal (esophagus and stomach) and hepatopancreatobiliary surgeries, chemotherapy patients, and cases with persistent nausea-vomiting complaints and suspected intestinal obstruction. Prospective clinical studies are needed to better understand the effectiveness of CE-AXR.

FOOTNOTES

Author contributions: Dilek ON was the designer of the study and revised the article critically for scientific content and collected the images; Güneş Ö and Atay A participated in the acquisition, analysis, and interpretation of the data, and drafted the initial manuscript; Karahan F and Karasu Ş collected and reported the patients' data and images.

Institutional review board statement: The study was carried out in accordance with the principles of the Helsinki Declaration. As a routine procedure, written informed consent was obtained from each patient for all procedures and publications. Ethics committee approval was received for this study (2022/GOKAE/0542) from the Clinical Trials Ethics Committee.

Informed consent statement: All study participants, or their legal guardians, provided informed written consent before study enrollment. The data used in this study did not involve the patients' privacy information, so the informed consent was waived by the Ethics Committee of University Hospital. All patient data obtained, recorded, and managed were only used for this study, and all patient information is strictly confidential, without any harm to the patient.

Conflict-of-interest statement: All of the authors declare that there are no conflicts of interest in connection with this paper, and the material described is not under publication or consideration for publication elsewhere.

Data sharing statement: All of the authors declare that there are no shared data in this paper, and the material described is not under publication or consideration for publication elsewhere.

STROBE statement: The authors have read the STROBE Statement – checklist of items, and the manuscript was prepared and revised according to the STROBE Statement – checklist of items.

Open-Access: This article is an open-access article that was selected by an in-house editor and fully peer-reviewed by external reviewers. It is distributed in accordance with the Creative Commons Attribution NonCommercial (CC BY-NC 4.0) license, which permits others to distribute, remix, adapt, build upon this work non-commercially, and license their derivative works on different terms, provided the original work is properly cited and the use is non-commercial. See: <https://creativecommons.org/licenses/by-nc/4.0/>

Country/Territory of origin: Turkey

ORCID number: Osman Nuri Dilek 0000-0002-6313-3818; Arif Atay 0000-0001-8163-2357; Orgun Gunes 0000-0002-0576-

6086; Furkan Karahan 0000-0003-0384-8181; Şebnem Karasu 0000-0002-0106-5901.

S-Editor: Liu JH**L-Editor:** Wang TQ**P-Editor:** Zhao S

REFERENCES

- 1 **Egri C**, Darras KE, Scali EP, Harris AC. Classification of Error in Abdominal Imaging: Pearls and Pitfalls for Radiologists. *Can Assoc Radiol J* 2018; **69**: 409-416 [PMID: 30318459 DOI: 10.1016/j.carj.2018.06.006]
- 2 **Smith JE**, Hall EJ. The use of plain abdominal x rays in the emergency department. *Emerg Med J* 2009; **26**: 160-163 [PMID: 19234001 DOI: 10.1136/emj.2008.059113]
- 3 **Hassan T**, Kumwenda M, Qutab S, Naqvi SZ, Rashid H, Johnson S. Are we following iRefer guidelines from the royal college of radiology when requesting abdominal x-rays? *Cureus* 2022; **14**: e31050. [PMID: 36349071 DOI: 10.7759/cureus.31050]
- 4 **Campbell JP**, Gunn AA. Plain abdominal radiographs and acute abdominal pain. *Br J Surg* 1988; **75**: 554-556 [PMID: 3395821 DOI: 10.1002/bjs.1800750616]
- 5 **Fernandez M**, Craig S. Appropriateness of adult plain abdominal radiograph requesting in a regional Emergency Department. *J Med Imaging Radiat Oncol* 2019; **63**: 175-182 [PMID: 30628194 DOI: 10.1111/1754-9485.12847]
- 6 **Rosenbaum HD**, Lieber A, Hanson DJ, Pellegrino ED. A routine survey roentgenogram of the abdomen on 500 consecutive patients over 40 years of age. *Am J Roentgenol Radium Ther Nucl Med* 1964; **91**: 903-909 [PMID: 14139923]
- 7 **Kang H**, Ben-David K, Sarosi GA, Thomas RM. Routine Radiologic Assessment for Anastomotic Leak Is Not Necessary in Asymptomatic Patients After Esophagectomy for Esophageal Cancer. *J Gastrointest Surg* 2022; **26**: 279-285 [PMID: 35037179 DOI: 10.1007/s11605-021-05219-3]
- 8 **Kirby GC**, Macano CAW, Nyasavajjala SM, Sahloul M, Nijjar R, Daskalakis M, Richardson M, Singhal R. The Birmingham experience of high-pressure methylene blue dye test during primary and revisional bariatric surgery: A retrospective cohort study. *Ann Med Surg (Lond)* 2017; **23**: 32-34 [PMID: 29071067 DOI: 10.1016/j.amsu.2017.09.015]
- 9 **Hagen ME**, Diaper J, Douissard J, Jung MK, Buehler L, Aldenkortt F, Barcelos GK, Morel P. Early Experience with Intraoperative Leak Test Using a Blend of Methylene Blue and Indocyanine Green During Robotic Gastric Bypass Surgery. *Obes Surg* 2019; **29**: 949-952 [PMID: 30607685 DOI: 10.1007/s11695-018-03625-2]
- 10 **Nelson L**, Moon RC, Teixeira AF, Jawad MA. Methylene Blue or Upper GI, Which is More Effective for Detecting Leaks in Gastric Bypass Patients? *Surg Laparosc Endosc Percutan Tech* 2015; **25**: 451-454 [PMID: 26271023 DOI: 10.1097/SLE.0000000000000191]
- 11 **Panwar R**, Pal S. The International Study Group of Pancreatic Surgery definition of delayed gastric emptying and the effects of various surgical modifications on the occurrence of delayed gastric emptying after pancreatoduodenectomy. *Hepatobiliary Pancreat Dis Int* 2017; **16**: 353-363 [PMID: 28823364 DOI: 10.1016/S1499-3872(17)60037-7]
- 12 **Nojiri M**, Yokoyama Y, Maeda T, Ebata T, Igami T, Sugawara G, Yamaguchi J, Nagino M. Impact of the gastrojejunal anatomic position as the mechanism of delayed gastric emptying after pancreatoduodenectomy. *Surgery* 2018; **163**: 1063-1070 [PMID: 29325788 DOI: 10.1016/j.surg.2017.11.016]
- 13 **Tani M**, Terasawa H, Kawai M, Ina S, Hirono S, Uchiyama K, Yamaue H. Improvement of delayed gastric emptying in pylorus-preserving pancreaticoduodenectomy: results of a prospective, randomized, controlled trial. *Ann Surg* 2006; **243**: 316-320 [PMID: 16495694 DOI: 10.1097/01.sla.0000201479.84934.ca]
- 14 **Lim H**, Choi J, Kim JH, Cheong HK, Ha M. Estimation of Cancer Incidence and Mortality Risks Attributed to Diagnostic Medical Radiation Exposure in Korea, 2013. *J Korean Med Sci* 2018; **33**: e211 [PMID: 30008633 DOI: 10.3346/jkms.2018.33.e211]
- 15 **National Cancer Institute**, National Institute of Health. Radiation Risk Assessment Tool-lifetime cancer risk from ionizing radiation. (Accessed Dec 24, 2022). Available from: <https://radiationcalculators.cancer.gov/radtrat/about/>
- 16 **Canadian Nuclear Safety Commission**. Radiation doses. (Accessed Dec 24, 2022). Available from: <https://nuclearsafety.gc.ca/eng/resources/radiation/introduction-to-radiation/radiation-doses.cfm>
- 17 **United Nations Scientific Committee on the Effects of Atomic Radiation**. UNSCEAR 2008 report to the general assembly, with scientific annexes. (Accessed Dec 24, 2022). Available from: http://www.unscear.org/unscear/en/publications/2008_1.html
- 18 **Nesterenko AV**, Nesterenko VB, Yablokov AV. 12. Chernobyl's radioactive contamination of food and people. *Ann N Y Acad Sci* 2009; **1181**: 289-302 [PMID: 20002056 DOI: 10.1111/j.1749-6632.2009.04837.x]
- 19 **Brooks AL**, Hoel DG, Preston RJ. The role of dose rate in radiation cancer risk: evaluating the effect of dose rate at the molecular, cellular and tissue levels using key events in critical pathways following exposure to low LET radiation. *Int J Radiat Biol* 2016; **92**: 405-426 [PMID: 27266588 DOI: 10.1080/09553002.2016.1186301]
- 20 **Huda W**, Nickoloff EL, Boone JM. Overview of patient dosimetry in diagnostic radiology in the USA for the past 50 years. *Med Phys* 2008; **35**: 5713-5728 [PMID: 19175129 DOI: 10.1118/1.3013604]
- 21 **Berrington de Gonzalez A**, Iulian Apostoaei A, Veiga LH, Rajaraman P, Thomas BA, Owen Hoffman F, Gilbert E, Land C. RadRAT: a radiation risk assessment tool for lifetime cancer risk projection. *J Radiol Prot* 2012; **32**: 205-222 [PMID: 22810503 DOI: 10.1088/0952-4746/32/3/205]
- 22 **Omori Y**, Hosoda M, Takahashi F, Sanada T, Hiraos S, Ono K, Furukawa M. Japanese population dose from natural radiation. *J Radiol Prot* 2020; **40**: R99-R140 [PMID: 32031989 DOI: 10.1088/1361-6498/ab73b1]

Prospective Study

Interobserver reliability of computed tomography angiography in the assessment of ruptured intracranial aneurysm and impact on patient management

Ali H Elmokadem, Basma Abdelmonaem Elged, Ahmed Abdel Razek, Lamiaa Galal El-Serougy, Mohamed Ali Kasem, Mohamed Ali EL-Adalany

Specialty type: Radiology, nuclear medicine and medical imaging

Provenance and peer review: Invited article; Externally peer reviewed.

Peer-review model: Single blind

Peer-review report's scientific quality classification

Grade A (Excellent): 0
Grade B (Very good): 0
Grade C (Good): C, C
Grade D (Fair): 0
Grade E (Poor): 0

P-Reviewer: Taheri M, Iran; uz Zaman M, Pakistan

Received: December 23, 2022

Peer-review started: December 23, 2022

First decision: March 28, 2023

Revised: April 17, 2023

Accepted: May 31, 2023

Article in press: May 31, 2023

Published online: June 28, 2023



Ali H Elmokadem, Basma Abdelmonaem Elged, Ahmed Abdel Razek, Lamiaa Galal El-Serougy, Mohamed Ali EL-Adalany, Department of Radiology, Mansoura University, Mansoura 35516, Egypt

Mohamed Ali Kasem, Department of Neurosurgery, Mansoura University, Mansoura 35516, Egypt

Corresponding author: Ali H Elmokadem, MD, PhD, Associate Professor, Department of Radiology, Mansoura University, Elgomhoria St, Mansoura 35516, Egypt.
mokademr83@gmail.com

Abstract

BACKGROUND

Aneurysmal subarachnoid hemorrhage is an emergency that can lead to a high mortality rate and many severe complications. It is critical to make a rapid radiological evaluation of ruptured intracranial aneurysms (RIAs) to determine the appropriate surgical treatment.

AIM

To assess the reliability of computed tomography angiography (CTA) in assessing different features of ruptured intracranial aneurysm and its impact on patient management.

METHODS

The final cohort of this study consisted of 146 patients with RIAs (75 male and 71 female) who underwent cerebral CTA. Their age ranged from 25 to 80, and the mean age \pm SD was 57 ± 8.95 years. Two readers were asked to assess different features related to the aneurysm and perianeurysmal environment. Inter-observer agreement was measured using kappa statistics. Imaging data extracted from non-contrast computed tomography and CTA were considered to categorize the study population into two groups according to the recommended therapeutic approach.

RESULTS

The inter-observer agreement of both reviewers was excellent for the detection of

aneurysms ($K = 0.95$, $P = 0.001$), aneurysm location ($K = 0.98$, $P = 0.001$), and ($K = 0.98$, $P = 0.001$), morphology ($K = 0.92$, $P = 0.001$) and margins ($K = 0.95$, $P = 0.001$). There was an excellent interobserver agreement for the measurement of aneurysm size ($K = 0.89$, $P = 0.001$), neck ($K = 0.85$, $P = 0.001$), and dome-to-neck ratio ($K = 0.98$, $P = 0.001$). There was an excellent inter-observer agreement for the detection of other aneurysm-related features such as thrombosis ($K = 0.82$, $P = 0.001$), calcification ($K = 1.0$, $P = 0.001$), bony landmark ($K = 0.89$, $P = 0.001$) and branch incorporation ($K = 0.91$, $P = 0.001$) as well as perianeurysmal findings including vasospasm ($K = 0.91$, $P = 0.001$), perianeurysmal cyst ($K = 1.0$, $P = 0.001$) and associated vascular lesions ($K = 0.83$, $P = 0.001$). Based on imaging features, 87 patients were recommended to have endovascular treatment, while surgery was recommended in 59 patients. 71.2% of the study population underwent the recommended therapy.

CONCLUSION

CTA is a reproducible promising diagnostic imaging modality for detecting and characterizing cerebral aneurysms.

Key Words: Computed tomography angiography; Intracranial aneurysm; Subarachnoid hemorrhage; Intracranial hemorrhage; Observer variation

©The Author(s) 2023. Published by Baishideng Publishing Group Inc. All rights reserved.

Core Tip: This study evaluated the interobserver reliability of computed tomography angiography (CTA) in the assessment of ruptured intracranial aneurysm features among 146 patients. Our results showed good to an excellent inter-observer agreement in imaging features related to the aneurysm, aneurysm characters, measurements, and perianeurysmal information. Imaging data extracted from non-contrast computed tomography and CTA guided the multidisciplinary neurovascular team to better treatment approach selection.

Citation: Elmokadem AH, Elged BA, Abdel Razek A, El-Serougy LG, Kasem MA, EL-Adalany MA. Interobserver reliability of computed tomography angiography in the assessment of ruptured intracranial aneurysm and impact on patient management. *World J Radiol* 2023; 15(6): 201-215

URL: <https://www.wjgnet.com/1949-8470/full/v15/i6/201.htm>

DOI: <https://dx.doi.org/10.4329/wjr.v15.i6.201>

INTRODUCTION

Acute subarachnoid hemorrhage (SAH) is a medical emergency that can lead to a high mortality rate and many severe complications. The most frequent cause of non-traumatic SAH is a ruptured aneurysm. Ruptured aneurysms not only cause subarachnoid bleeding but can also cause subdural or intracerebral hematomas. It is critical to make a rapid radiological evaluation of ruptured intracranial aneurysms (RIAs) to determine the appropriate surgical treatment of SAH[1]. Different imaging modalities are used or have been used to assess intracranial vascular lesions. Digital subtraction angiography (DSA) has been considered the “gold standard” for detecting intracranial aneurysms and therapeutic decision-making. Additionally, intra-arterial cone beam computed tomography angiography (CTA) using a flat panel detector incorporates the high spatial vascular resolution of three-dimensional (3D) rotational angiography with computed tomography (CT) postprocessing techniques to increase the contrast resolution[2]. Nevertheless, it is an invasive and time-consuming technique with a reported 0.5% risk of neurological complications[3]. Magnetic resonance (MR) angiography enables visualization of intra-cranial arteries without ionizing radiation or intravenous contrast material. The performance of MR angiography in evaluating acute SAH also has been compared favorably with that of DSA. However, MR angiography can be technically challenging for acutely ill patients. Additionally, aneurysms less than 5 mm in diameter might be missed in MR angiography studies[4].

Compared to DSA, CTA is a safe, relatively inexpensive, and noninvasive imaging. CT angiography is not associated with significant patient risks other than those related to administering iodinated contrast media. Images can be relatively safely obtained without the need for arterial puncture or catheter manipulation that carries the possibility of acquiring a permanent neurologic deficit[5]. For these reasons, helical cerebral CT angiography has been widely used in detecting intracranial aneurysms, with a reported sensitivity of 70%-96%[6]. Currently, multidetector CT angiography has the ability to detect most intracranial aneurysms of 5 mm or larger. Multidetector row CT scanners provide

increased spatial resolution and decreased scanning time, which should increase the sensitivity of the technique in depicting aneurysms of less than 5 mm in diameter. Currently, CT angiography is accepted as a first-line diagnostic imaging modality for evaluating intracranial aneurysms. Nevertheless, using CT angiography to depict intracranial aneurysms showed variable sensitivity. The reported sensitivity of CTA in detections of small intracranial aneurysms (< 3 mm) varied from 28%–43% in a study that included 99 small aneurysms[7] to 83%–92% in another study had 579 small aneurysms[8].

Deciding whether to perform surgical clipping or endovascular therapy for an intracranial aneurysm is vital. Treatment of intracranial aneurysms depends on clinical features, including age, Hunt and Hess grade, neurological or medical comorbidity, and characters of the aneurysm itself. Advances in imaging technologies have improved our comprehension of the 3D geometry of cerebral aneurysms, which has further affected treatment procedures, and helps neurosurgeons in the diagnosis, planning, and assessment of the therapeutic modalities. Exact information must be obtained preoperatively regarding the location, size, and morphology of the aneurysm and the property of the aneurysmal wall, its relationship with the parent vessel and adjacent branches, vessel incorporation, presence of calcification or thrombus[9]. Perianeurysmal information such as associated vasospasm, vascular variants, presence of vascular malformations, and the relationship of the aneurysm to the bony skull base is also crucial for proper treatment method selection.

This work aims to assess the inter-observer reliability of CTA in assessing different features of RIAs and their impact on patient management.

MATERIALS AND METHODS

Study population

The Institutional review board approved this single-center prospective study. One hundred sixty-one consecutive patients with clinically suspected intracranial aneurysms were recruited. Inclusion criteria were adult patients with imaging signs of SAH by non-enhanced CT. The exclusion criteria were patients with renal insufficiency ($n = 6$), pregnant or lactating females ($n = 2$), and non-diagnostic examinations ($n = 7$). The final cohort of our study included 146 patients (75 male and 71 female). Their age ranged from 25 to 80 years, with a mean age was 57 ± 8.9 years. Once enrolled, all patients were submitted to a contrast-enhanced CTA scan for diagnosis of intracranial aneurysm. The commonest clinical presentation was a headache, neck pain, and depressed consciousness in 130 patients, hemiparesis in 12 patients, cranial nerve palsies, and blurring of vision being less common presenting symptoms in 3 patients. One patient presented in an accident. The flow chart of our study is illustrated in (Figure 1).

CTA Technique

All examinations were carried out with 160-slice computed tomography (Toshiba Aquilion Prime 160, Tochigi, Japan). Examinations were performed in a supine position with the arms of the patients beside the body. We first performed a non-contrast CT (NCCT) scan of the whole brain in an axial plane tilted along the orbitomeatal line using the following parameters: tube voltage 100 kVp, field of view (FOV) 220 mm, collimation 0.75 mm, matrix size 512×512 , slice thickness 3.0 mm, and rotation time 1.0 s. CTA examinations were achieved using the bolus triggering technique for the timing of contrast medium injection. A region of interest (ROI) was centered at the upper end of the common carotid artery and sized to include only the lumen of the artery. The bolus triggering technique started automatically after contrast-medium injection when an attenuation value of 100 HU was reached in ROI. Non-ionic contrast medium Ultravist 370 (370 mgI/mL, Bayer Healthcare Ltd, Guangzhou, China) at a dose of 1 mL/Kg and rate of 4mL/s followed by a 50 mL saline flush administered *via* automatic injector (Medrad Stellant, Warrendale, PA) through a 20 G intravenous cannula in the antecubital fossa of either upper extremity. The following parameters were used: Tube voltage 120 kVp, automatic tube current modulation, FOV 250 mm, collimation 0.75 mm, matrix size 512×512 , slice thickness 1.5 mm, rotation time 0.3 s. Scanning was performed in the caudocranial direction and started at the level of the aortic arch up to the vertex. Axial images were stored and transferred into the workstation as source images after reconstruction at 0.625-mm intervals. Multiplanar reformats (MPR), maximum intensity projection (MIP), and 3D volume-rendered images were used for further analysis.

Image analysis

Image analysis was conducted on the PACS system (GE Healthcare, Waukesha, WI). All CTA examinations were revised and interpreted by two experienced neuroradiologists with 14 and 8 years of experience in neurovascular imaging (AHE, BE). They independently reviewed the images blinded to patient data and final diagnosis. The following features obtained at NCCT were individually evaluated for each patient: The degree of SAH using the Fisher scale, associated parenchymal hemorrhage, hydrocephalus, and ischemic changes. Both readers were asked to predict the location of the aneurysm based on the distribution of SAH and Intraparenchymal hematoma (IPH). At CTA, both readers were asked to evaluate the following aneurysm features': (1) Number; (2) Size; (3) Location (anterior *vs*

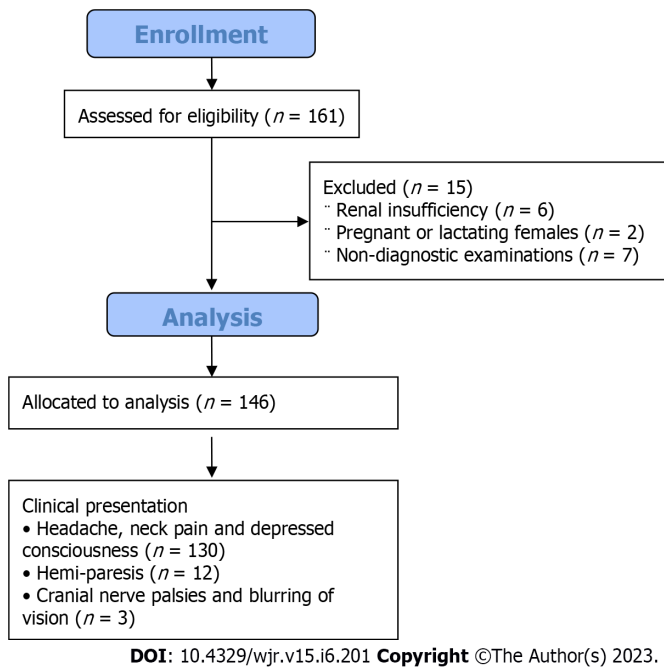


Figure 1 Flow chart of the study.

posterior circulation, parent artery, and affected segment); (4) Shape (saccular, fusiform, serpentine or blister); (5) Margin (sharp, irregular/daughter sacs); (6) Presence of calcification and/or thrombus; (7) The presence of branch incorporation; and (8) The orientation of the aneurysm in relation to the parent vessel (*e.g.*, pointing superior/inferior, medial/Lateral, anterior/posterior). Aneurysm size was defined by the maximum measurement of aneurysm width, neck width (the largest cross-sectional diameter of the aneurysm neck), depth (the longest diameter between the neck and dome), and aneurysm neck-to-dome length. According to size, aneurysms were classified into: (1) Small aneurysms are less than 5 mm; (2) Medium-sized aneurysms are 6–15 mm; (3) Large aneurysms are 16–25 mm; and (4) Giant aneurysms are > 25 mm. The following features related to the perianeurysmal environment were evaluated by both readers: (1) Associated vasospasm; (2) Perianeurysmal cysts; (3) Associated vascular malformations (type and classification based on relation to aneurysm); (4) Vascular variants; and (5) The relationship of the aneurysm to the bony landmarks or related osseous changes (remodeling or fractures).

Management selection

Imaging data extracted from NCCT and CTA were considered to categorize the study population into two groups according to the recommended therapeutic approach. The first group was recommended to proceed to endovascular therapy, and the second group was advised to undergo surgical management (clipping).

Features in favor of endovascular therapy (coiling) were: (1) Absence of parenchymal hematoma; (2) Posterior circulation aneurysm; (3) Small aneurysm neck < 4 mm; (4) Aneurysm diameter < 15 mm; (5) Unilobar shape; (6) Multiple aneurysms; (7) Calcification located at the aneurysm neck that might interfere with clipping; and (8) Presence of vasospasm. Coiling using balloon remodeling technique or stent-assisted coiling was recommended with wide-neck aneurysms.

Features favored surgical management (clipping) Were (1) Presence of intra-parenchymal hematoma; (2) Middle cerebral and pericallosal arteries aneurysm; (3) Wide neck of the aneurysm > 4 mm; (4) Aneurysm diameter > 15 mm; (5) Abnormal configuration unsuitable for endovascular therapy; (6) Aneurysmal sac incorporating arterial branches; (7) Presence of intraluminal thrombus; and (8) Vascular variant interferes with endovascular management. Features considered in managing RIAs are listed in Table 1.

Statistical analysis:

All statistical analyses were performed with software (SPSS, version 16.0; SPSS, Chicago, Ill). The Kolmogorov-Smirnov Z-test was used to test the normality of the continuous variable groups. The CTA image quality scores were ranked and listed as a mean and standard deviation. The kappa statistic (K), including a 95%CI with an intra-class correlation (r), was used to estimate the proportion of interobserver agreement beyond that expected by chance for the image quality grading and depiction of the aneurysm, its neck, parent artery, and associated anomalies. A P value less than 0.05 was considered to

Table 1 Imaging features considered in the management of ruptured intracranial aneurysms

	Endovascular therapy	Surgical management
Non-contrast computed tomography	Absence of parenchymal hematoma	Presence of intra-parenchymal hematoma
Aneurysm characters	Posterior circulation aneurysms	Middle cerebral and pericallosal arteries aneurysm
	Small aneurysm neck < 4 mm	Aneurysm diameter > 15 mm Wide neck aneurysm > 4 mm
	Aneurysm diameter < 15 mm	Abnormal configuration
	Unilobar configuration	Aneurysmal sac incorporating arterial branches
	Multiple aneurysms	Presence of intraluminal thrombus
	Calcification located at the aneurysm neck	
Perianeurysmal findings	Presence of vasospasm	Vascular variants interfere with endovascular management

indicate a statistically significant difference. The K values were interpreted as follows: K values between 0.61 and 0.80 represented good; K values between 0.81 and 1.00 represented excellent agreement.

RESULTS

NCCT findings

Both readers used the Fisher scale to assess SAH. The means scores were (3.47 ± 0.6 and 3.33 ± 0.4) with a good interobserver agreement ($K = 0.79$, $P = 0.001$). Excellent interobserver agreement between both readers in the detection of IPH ($K = 0.1$, $P = 0.001$) as well as in the detection of hydrocephalus ($K = 0.92$, $P = 0.001$). A statistically significant strong positive correlation was found between the location of SAH and IPH on NCCT scan and the eventual location of a ruptured cerebral aneurysm in single ones and as a differentiating point of culprit aneurysm in multiple aneurysms confirmed by CTA and surgical or endovascular intervention. The sensitivity of NCCT predicting aneurysms depends on blood distribution of more than 85% in our study. [Table 2](#) shows the inter-observer results of CT and CTA findings.

Aneurysm characters:

Detection: The first reader detected 166 aneurysms [126 single aneurysms (75.9%) and 40 multiple aneurysms (24.1%)], while 2nd reader detected 169 aneurysms [127 single aneurysms (75.1%) and 42 multiple aneurysms (24.9%)]. An excellent interobserver agreement was found between both readers in detecting an aneurysm [98.8% ($K = 0.95$, $P = 0.001$)]. Among multiple aneurysms, 14 were mirror image aneurysms (MA), and the remaining were non-mirror image (NMA). The commonest location of MA in our series was the M1 segment or at the middle cerebral artery (MCA) bifurcation ($n = 3$), followed by the cavernous portion of internal carotid artery (ICA) ($n = 2$) ([Figure 2](#)), the posterior communicating artery (PCOM) ($n = 1$), and ICA terminus ($n = 1$). The sensitivity of CTA compared to DSA in the detection of intracranial aneurysms was 98.8%. DSA identified 89 aneurysms in 80 patients. Among these aneurysms, CTA failed to detect one in a patient with three other aneurysms. The missed aneurysm was located in posterior cerebral artery (PCA) with diameters of 3 mm. In two cases, CTA depicted aneurysms, which DSA missed. An ICA blister and a distal MCA mycotic aneurysm were the two missed aneurysms.

Location: For most of the study, the population was harboring anterior circulation aneurysms (94%). Excellent interobserver agreement was found between both readers in the detection of aneurysms in the anterior and posterior circulation ($K = 0.95$, $P = 0.001$) as well as its site in parent artery and segment ($K = 0.98$, $P = 0.001$), and ($K = 0.98$, $P = 0.001$). In this study, Acom was the most affected artery, and Acom-left anterior cerebral artery (ACA) complex was the most affected segment. Both readers successfully detected intracranial aneurysms in relatively rare locations such as basilar perforators (2/L46), distal ACA (4/L46), pericallosal artery (2/L46), and azygous ACA (2/L46). Inter-observer results of the CTA location of the aneurysm are summarized in [Table 3](#).

Morphology: Among the assessed aneurysms, (96.4%) were saccular, (2.4%) were fusiform, and (1.1%) were serpentine ([Figure 3](#)). Excellent interobserver agreement was found between both readers in the detection of aneurysm shape ($K = 0.92$, $P = 0.001$) and for margins ($K = 0.95$, $P = 0.001$). Other features such as calcification or thrombus, branch incorporation, and aneurysm orientation also show excellent inter-observer agreement. Calcification and thrombosis were detected in large and giant aneurysms ([Figure 4](#)). Branch incorporation was found in association with 55 aneurysms, one of them showed 3rd A2 segment incorporated Acom aneurysm dome (ACA trifurcation), to the best of the author's knowledge this association is not reported before in the literature ([Figure 5](#)).

Table 2 Inter-observer agreement of computed tomography and computed tomography angiography features of aneurysm

Signs		Reader 1	Reader 2	K	95% CI	P value	Agreement, %
NCCT findings							
SAH Fisher scale		3.47 ± 0.6	3.33 ± 0.4	0.84	0.78-0.85	< 0.001	89.50
Hydrocephalus (HCP)	Negative (N)	93	95	0.91	0.85-0.97	< 0.001	95.90
	Positive (p)	53	51				
Intraparenchymal hematoma (IPH)	Negative (N)	105	105	1	1.0-1.0	< 0.001	100.00
	Positive (p)	41	41				
Aneurysm features							
Number	Total	166	169	0.95	0.89-1.0	< 0.001	98.80
	Single	126	127				
	Multiple	40	42				
Size	Small	55	57	0.89	0.83-0.96	< 0.001	94.70
	Medium	101	102				
	Large	5	5				
	Giant	5	5				
Site	Anterior	156	157	0.94	0.83-1.0	< 0.001	99.40
	Posterior	10	12				
Shape	Saccular	160	162	0.92	0.76-1.0	< 0.001	99.40
	Fusiform	4	4				
	Serpentine	2	2				
	Blister	0	1				
Margin	Sharp	71	75	0.95	0.90-0.99	< 0.001	97.60
	Lobulated	95	94				
Thrombus		6	9	0.82	0.65-0.99	< 0.001	97.60
Calcification		9	9	1	1.0-1.0	< 0.001	100.00
Branch incorporation		50	55	0.9	0.83-0.97	< 0.001	95.90
Orientation				0.95	0.91-0.97	< 0.001	96.50
Peri-aneurysmal findings							
Vasospasm		21	25	0.9	0.81-0.99	< 0.001	97.60
Peri-aneurysmal cyst		1	1	1	1.0-1.0	< 0.001	100.0
Other vascular lesions		2	4	0.82	0.59-1.0	< 0.001	98.80
Bony relations		23	26	0.88	0.78-0.98	< 0.001	97.00
Bone fracture		1	1				
Vascular variant		84	88	0.89	0.83-0.96	< 0.001	94.90
Overall agreement				0.95	0.94-0.96	< 0.001	97.80

NCCT: Non-contrast computed tomography; SAH: Subarachnoid hemorrhage; IPH: Intraparenchymal hematoma.

Measurements: Most cases were medium-sized aneurysms (60.8%), followed by small-sized (30.1%). Both readers measured aneurysm size, neck, and dome-to-neck ratio with an excellent interobserver agreement ($K = 0.89$, $P = 0.001$), ($K = 0.85$, $P = 0.001$), and ($K = 0.98$, $P = 0.001$). Inter-observer results of CTA measurements of an aneurysm are summarized in Table 4.

Peri-aneurysm findings: Excellent interobserver agreement was found between both readers in detecting vasospasm in the nearby arterial segment ($K = 0.91$, $P = 0.001$) and detection of the perian-

Table 3 Inter-observer agreement of computed tomography angiography locations of aneurysm

Parent artery	Reader 1	Reader 2
ACOM	73	73
ACA	5	6
RT ICA	20	20
LT ICA	16	16
RT MCA	21	22
LT MCA	20	20
Basilar	8	9
LT PCA	1	1
RT Vertebral	1	1
LT SCA	0	1
K	95%CI	P value
0.97	0.87-1.0	< 0.001
Arterial segment	Reader 1	Reader 2
ACOM- Lt ACA complex	36	36
ACOM- Rt ACA complex	34	34
ACOM proper	3	3
A1	1	1
RT A2	1	1
LT A2	0	1
Azygous A2	2	2
A3	1	1
RT MCA bifurcation	14	14
LT MCA bifurcation	15	15
RT M1	4	4
LT M1	3	3
RT M2	3	3
LT M2	2	2
M4	0	1
RT PCOM	12	12
LT PCOM	9	9
RT ICA Terminus	4	4
LT ICA Terminus	2	2
RT Cavernous ICA	4	4
LT Cavernous ICA	5	5
Basilar tip	4	4
Mid Basilar	2	3
Basilar Perforators	2	2
Rt V4	1	1
LT SCA	0	1
Lt P1	1	1
K	95%CI	P value

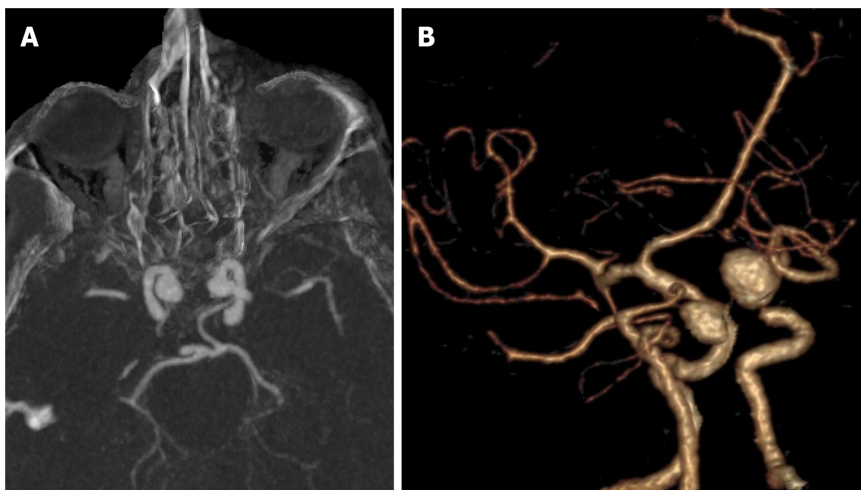
0.97	0.87-1.0	< 0.001
------	----------	---------

ACA: Anterior cerebral artery; RT: Right; ICA: Internal carotid artery; LT: Left; MCA: Middle cerebral artery; PCA: Posterior cerebral artery; SCA: Superior cerebellar artery; PCOM: Posterior communicating artery.

Table 4 Inter-observer agreement of computed tomography angiography measurements of aneurysm

	Size		Dome		Neck		Dome/neck ratio	
	Reader 1	Reader 2	Reader 1	Reader 2	Reader 1	Reader 2	Reader 1	Reader 2
Mean	7.4	7.4	3.7	3.6	2.7	2.7	1.3	1.3
Median	6	6	3	3	2.3	2.3	1.2	1.2
SD	5.44	5.47	3.2	3.1	2.1	2.1	0.8	0.8
Minimum	1.8	1.8	1	1	1	1	0.2	0.2
Maximum	40	42	22	22	20	20	4.7	5.6
ICC	0.97		0.97		0.96		0.98	
95%CI	(0.96-0.98)		(0.96-0.97)		(0.95-0.97)		(0.97-0.98)	

ICC: Interclass correlation.



DOI: 10.4329/wjr.v15.i6.201 Copyright ©The Author(s) 2023.

Figure 2 Mirror image intracranial aneurysms. A: Axial computed tomography angiography (CTA) in maximum intensity projection; B: Three-dimensional CTA for mirror image internal carotid artery aneurysm.

eurysmal cyst ($K = 1.0, P = 0.001$). Associated vascular lesions, including arterio-venous malformation (AVM) and developmental venous anomalies (DVA) (Figure 6), were detected by both readers with an excellent interobserver agreement ($K = 0.83, P = 0.001$). Vascular variations commonly affected the A1 segment, followed by PCA and MCA. Both readers detected an important bony variant in a case presented with a PCOM aneurysm in the form of a bridging sella turcica which was managed surgically by clitoridectomy (Figure 7).

Management: Based on imaging features, 87 patients were recommended to have endovascular treatment, while surgery was recommended in 59 patients. 71.2% of the study population underwent the recommended therapy, as 19 patients did not receive any therapy for the culprit, 66 underwent endovascular treatment, and 61 underwent surgical clipping. Only 15% of the study population needed external ventricular drain (EVD) to manage associated hydrocephalus.

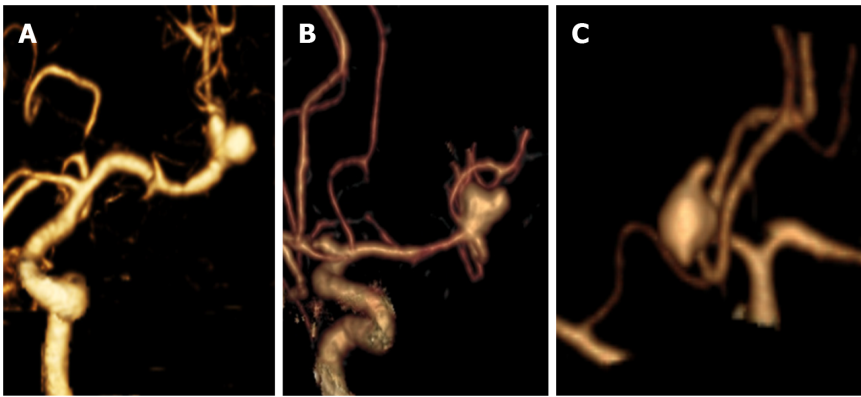
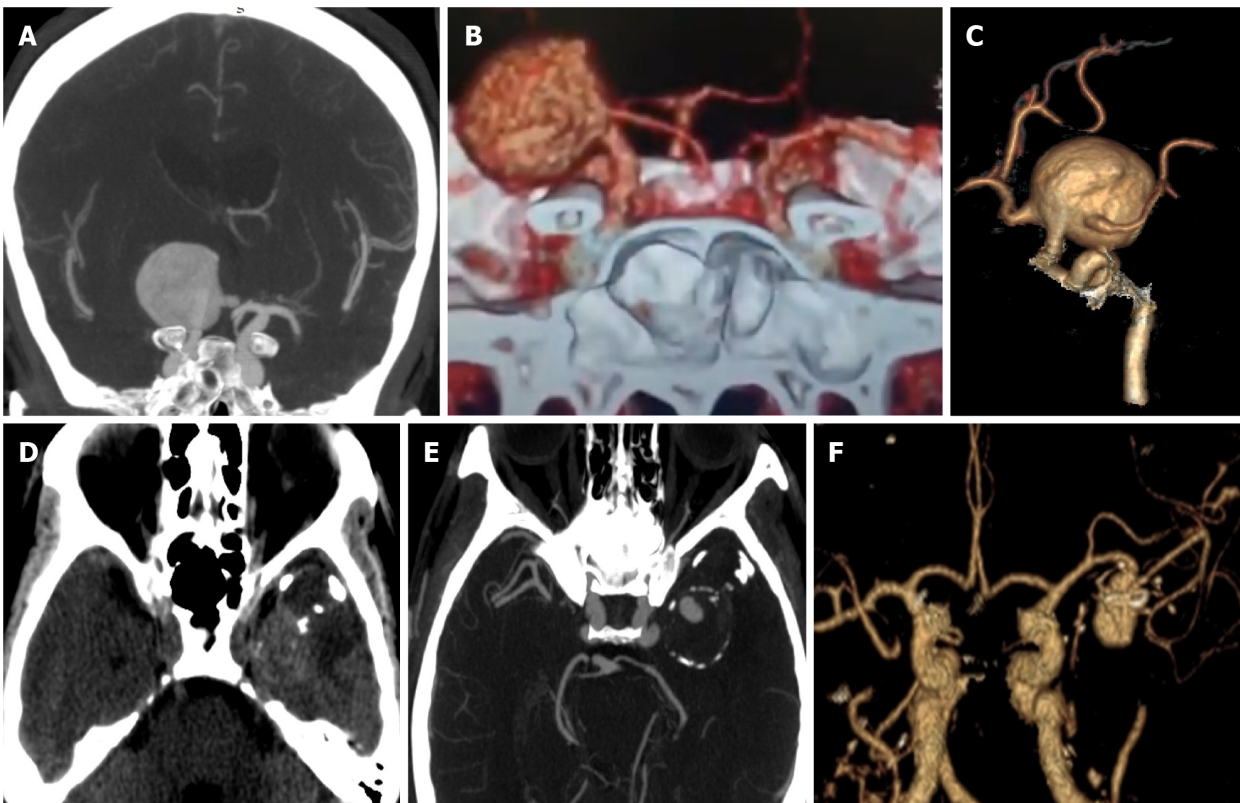


Figure 3 Morphology of intracranial aneurysms. A: Three-dimensional (3D)-computed tomography angiography (3D-CTA) for saccular aneurysm at middle cerebral artery (MCA) bifurcation with smooth margins; B: 3D-CTA for saccular aneurysm at MCA bifurcation with daughter sac; C: 3D-CTA for Acom saccular aneurysm with multiple blebs.



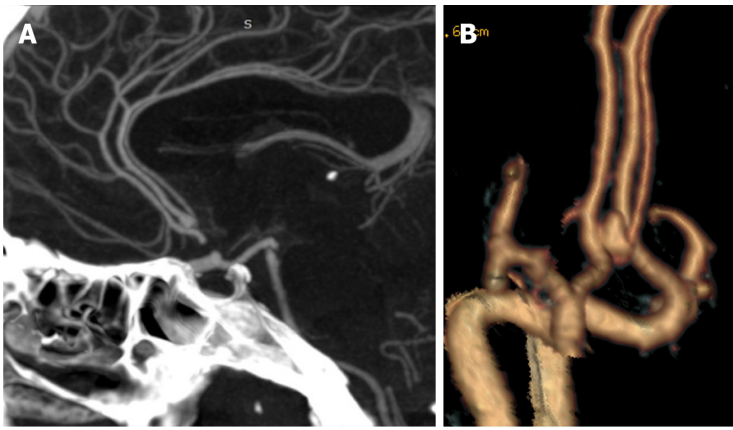
DOI: 10.4329/wjr.v15.i6.201 Copyright ©The Author(s) 2023.

Figure 4 Giant intracranial aneurysms. A: Axial computed tomography angiography (CTA) in maximum intensity projection (MIP); B and C: Three-dimensional (3D)-CTA for giant saccular aneurysm arising from right internal carotid artery and incorporating the origin of anterior cerebral artery and middle cerebral artery (MCA); D: non-contrast computed tomography for another patient shows a well defined lobulated lesion of mixed density in the left temporal lobe with foci of peripheral calcification; E: MIP-CTA axial image shows giant partially thrombosed saccular aneurysm of left MCA; F: 3D-CTA image shows a patent portion of left MCA aneurysm.

DISCUSSION

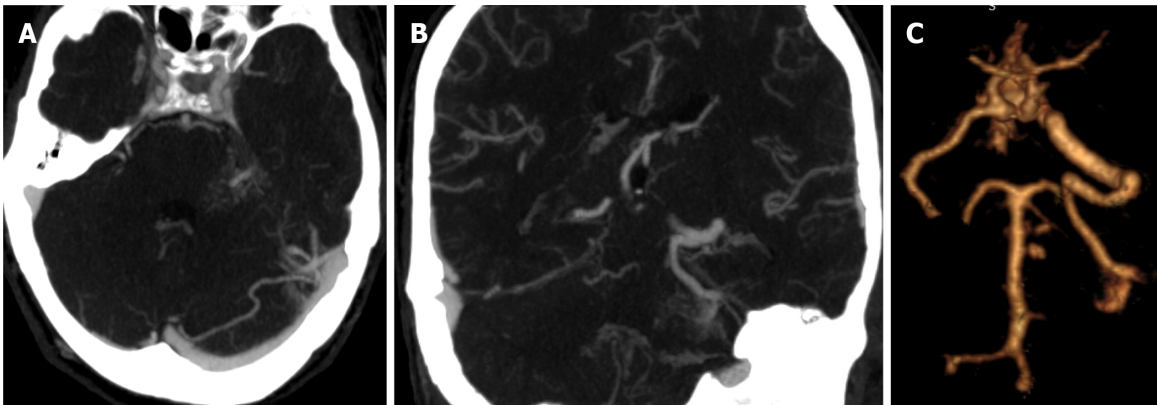
This study evaluated the interobserver reliability of CTA in the assessment of ruptured intracranial aneurysm features among 146 patients. Our results showed good to an excellent inter-observer agreement in imaging features related to the aneurysm, aneurysm characters, measurements, and perianeurysmal information. Imaging data extracted from NCCT and CTA guided the multidisciplinary neurovascular team to better treatment approach selection.

Our results showed high sensitivity of NCCT (85%) in predicting aneurysms' location depending on blood distribution with a good inter-observer agreement regarding the Fischer scale scores for SAH. The



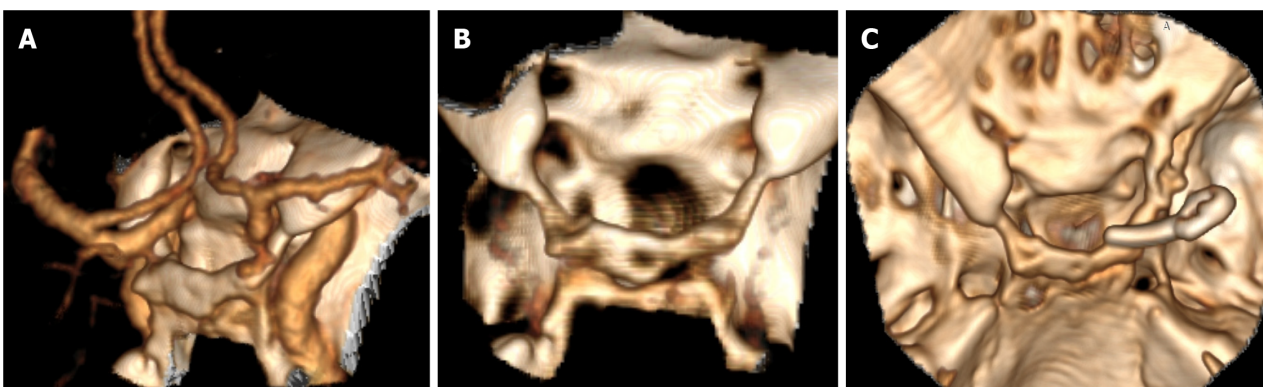
DOI: 10.4329/wjr.v15.i6.201 Copyright ©The Author(s) 2023.

Figure 5 Anatomical variants with intracranial aneurysms. A: Sagittal reformatted maximum intensity projection-computed tomography angiography (CTA); B: Three-dimensional-CTA for a saccular aneurysm at anterior cerebral artery trifurcation.



DOI: 10.4329/wjr.v15.i6.201 Copyright ©The Author(s) 2023.

Figure 6 Vascular malformation with intracranial aneurysms. A: Axial maximum intensity projection (MIP)-computed tomography angiography (CTA) shows a small saccular aneurysm that arises from the left basilar artery perforators; B: Coronal reformatted MIP-CTA shows left cerebellar developmental venous anomalies (DVA) drains into the left sigmoid sinus; C: Three-dimensional-CTA shows the basilar perforator aneurysms and the left cerebellar DVA.



DOI: 10.4329/wjr.v15.i6.201 Copyright ©The Author(s) 2023.

Figure 7 Bony landmarks related to the aneurysm. A: Three-dimensional (3D)-computed tomography angiography shows a posterior communicating artery aneurysm close to the anterior clinoid process; B: 3D-computed tomography (CT) for the skull base shows bridging sellae and bony fusion; C: Post-operative 3D-CT shows partial clinoidectomy and metallic clip.

combination of NCCT images and CTA is a valuable tool for detecting intracranial aneurysms and predicting outcomes. Aneurysm detection could be expected by assessing the distribution of SAH, the site of the largest clot, the difference in attenuation, and the presence of mural calcification. A recent study performed on patients with SAH and multiple cerebral aneurysms found that NCCT can identify

the source of bleeding with high accuracy for ACA, ACom, and MCA aneurysms, especially with the presence of intracranial hemorrhage (ICH)[10]. Our results showed excellent inter-observer agreement for detecting acute hydrocephalus with a variable degree of acute ventricular dilation, yet only 15% of our cases need management by EVD. Our results were close to those of the study performed on 389 patients with aneurysm-associated SAH[11].

We found that CTA has a high sensitivity for detecting intracranial aneurysms and avoids false-negative results. In a meta-analysis of extracted data from 8 studies, CTA had a pooled sensitivity of 99% and specificity of 94% for detecting and ruling out cerebral aneurysms[12]. Our study had an excellent interobserver agreement for detecting the aneurysms; the first reader detected 166 aneurysms, while the second reader detected 169 aneurysms. Yang *et al*[8] revealed a similar discrepancy in number detection by two observers, as one reviewer missed three aneurysms[8]. The inter-observer discrepancy usually occurs in a set of multiple small aneurysms in uncommon locations, such as the distal MCA. In this study, we detected mirror MA in 7 patients. Our results concord with the data obtained by a recent study by Rajagopal *et al*[13].

In our study, the anterior cerebral circulation aneurysms remained the predominant location of all aneurysms detected by CTA, constituting about 94% of the anterior and 6% of the posterior circulation. Acom aneurysm is the most common location of aneurysm in our results followed by ICA and MCA aneurysms, respectively. A similar distribution was reported by previous studies that assessed CTA *vs* DSA in the detection of intracranial aneurysms[14,15]. Imaging is vitally important to determine the location of the aneurysm and its relationship to the surrounding anatomy. Data from many studies suggest that surgical clipping may be superior in managing anterior circulation aneurysms with low recurrent rates. In contrast, posterior circulation aneurysms may be better treated through an endovascular approach[16]. Both readers successfully detected intracranial aneurysms in relatively rare locations, such as basilar perforators and azygous ACA. These findings aligned with prior studies stating that basilar perforator aneurysms are sporadic lesions often not recognized on initial imaging[17,18]. Similarly, azygos ACA aneurysm has a low incidence among intracranial aneurysms in literature ranging from 0.38 to 3.7%[19].

In this study, non-saccular intracranial aneurysms were less frequent. The margins were sharp (42.7%), and the rest were lobulated. These results partially agree with Rai *et al*[15], who reported 91% of saccular aneurysms, with only 22% having lobulated margins[15]. An irregular margin or lobulation along the margin of an aneurysm suggests rupture. It is an important observation in the setting of diffuse SAH and multiple intracranial aneurysms when treatment is directed at the culprit aneurysm [20]. Excellent inter-observer agreement was found in the assessment of branch incorporation and aneurysm orientation. The location of a branch to the aneurysm is a critical finding, as inadvertent occlusion of this branch during aneurysm treatment could have devastating consequences[21]. Therefore, it is essential to have a basic understanding of cerebral circulation and anatomical variants when interpreting CTA studies. Aneurysm orientation, especially Acom aneurysm, is a crucial element in selecting surgical *vs* endovascular management. Aneurysms with a more complex surgical approach are often assessed for endovascular therapy rather than surgical management[22].

Excellent agreement was found in this study between both readers regarding aneurysm measurements, including size, neck diameter, and dome-to-neck ratio. As the size of the aneurysm is the most significant predictor of SAH risk, accurate measurement of the aneurysm (s) is imperative for proper management. Aneurysms larger than 12 mm had a 2.6 relative risk of poor outcomes[23]. Kim *et al*[24] stated that intra-observer and interobserver variability in CTA were considerable in aneurysmal size measurements ranging from 12 to 18%. Therefore, follow-up size changes exceeding 20% in the aneurysm dimension should be considered a true change rather than a measurement error[24]. In contrast to these results, another study reported a poor ability of CTA to identify aneurysm enlargement accurately in assessing an in-vitro model. However, they recommended further human studies to confirm their findings[25]. CTA in this study detected the neck of all saccular aneurysms by both readers. Neck dimension and neck-to-dome ratio are crucial to deciding between surgical or endovascular treatment and simple coiling or adjunctive techniques to facilitate coil embolization through wide neck, such as neck remodeling using balloons or stent-assisted embolization[26].

The majority of our cases were medium-sized aneurysms (60.8%). This finding was in line with results reported by previous studies, which noted that medium-sized aneurysms were the majority of intracranial aneurysms[14,15]. We also observed that the presence of thrombosis and calcification was strongly tied to aneurysm size in large-sized and giant aneurysms compared to the corresponding intra-operative details of each case. Spontaneous thrombosis of intracranial aneurysms may occur in up to 40% of giant aneurysms, eventually becoming symptomatic due to mass effect or stroke. On the contrary, spontaneous thrombosis of a non-giant aneurysm (< 25 mm) is rarer[27]. Calcification appears to be an important pre-operative indicator of poor outcomes[28] and should be considered when deciding treatment options for a patient with a calcified aneurysm.

Perianeurysmal findings such as vasospasm, perianeurysmal cyst, associated vascular lesions or variants, and bony landmarks or pathologic changes are essential factors that might change the treatment decision. Cerebral vasospasm and resultant delayed cerebral ischemia consider a significant etiology of morbidity and mortality in patients with aneurysmal SAH (DCI)[29]. CTA is a fast and reliable tool for detecting decreases in vessel caliber, as demonstrated by excellent interobserver

agreement in this study.

The rarity of a perianeurysmal cyst may lead to a false diagnosis of cystic neoplasm and missing the possibility of a ruptured cerebral aneurysm. Interestingly, a perianeurysmal cyst was described in one out of 146 patients in our study. Pedro and Sih[30] reported a case of a sizeable pontine cyst associated with an enhancing mural nodule that was misdiagnosed as a cystic neoplasm. During surgery, an aneurysm of the left PCA was identified and clipped successfully[30].

Our work included four patients with associated vascular anomalies, including AVMs and DVA. The risk of intracranial hemorrhage in patients with coexisted AVM and aneurysm has been reported to be 7% annually, compared with 2%–4% annually for those with AVM alone or isolated intracranial aneurysm[31,32]. To our knowledge, the association between intracranial aneurysms and DVA is infrequent, and few case reports have been published[33].

In our study, both observers noted a sphenoid bone fracture and a nearby aneurysm of paraclinoid ICA secondary to head trauma. It is in agreement with results done on 5532 patients with cerebral aneurysms over 30 years by Jung *et al*[34], who state that traumatic intracranial aneurysm (TIA) after blunt brain trauma is rare and represents (0.23%)[34]. Osseous landmarks such as the optic strut and the tuberculum sellae are considered the anatomical boundary between the intradural and extradural segments of the ICA in the paraclinoid region, which is an important factor in determining treatment strategy[35].

We recommended surgical clipping or endovascular management for the culprit aneurysms based on data extracted from NCCT and CTA. 71.2% of the study population underwent the recommended therapy. The ideal therapeutic approach for RIAs is still controversial. In general, the decision on whether to clip or coil depends on several factors related to the patient, such as age and comorbidities, burden, and location of hemorrhage, aneurysm characteristics such as size, number, location, and morphology, or related procedure such as competence, technical skills and availability[36]. Endovascular treatment has been associated with shorter recovery but with higher retreatment rates and slightly higher rebleeding events[16]. An endovascular approach is indicated in a ruptured intracranial aneurysm with comorbidity, old age, narrow neck, and a posterior circulation aneurysm. Surgery is warranted if the patient is young with an MCA aneurysm and interested in durability.

There are a few limitations to this study. First, there is no correlation with conventional angiography in all cases. Second, the general drawbacks of CT include patient exposure to ionizing radiation and the risks of iodinated contrast medium. Further studies with applications of low-dose CTA, such as the use of automatic tube current modulation and a small amount of contrast medium, are recommended. Additionally, future studies using advanced CT techniques such as higher 320 slices CT scan[37], dual-energy[38] or source CTA, and time-resolved 4D CTA will improve temporal and spatial resolution and the image quality CTA. Also, applications of advanced vascular post-processing packages for analyzing CTA images will give comprehensive image interpretation in different planes and angles. We recommend further studies assessing the inter-observer agreement between neuroradiologists, neurologists, neurosurgeons, and neuro-interventionist.

CONCLUSION

We concluded that CTA is a promising diagnostic imaging modality for assessing intracranial aneurysm features that impact management and patient outcomes.

ARTICLE HIGHLIGHTS

Research background

Aneurysmal subarachnoid hemorrhage (SAH) is an emergency that can lead to a high mortality rate and many severe complications. It is critical to make a rapid radiological evaluation of ruptured intracranial aneurysms (RIAs) to determine the appropriate surgical treatment.

Research motivation

The high morbidity and mortality of RIAs necessitate rapid diagnosis and management decision. Compared to Digital subtraction angiography, computed tomography angiography (CTA) is a safe, relatively inexpensive, and noninvasive imaging. Computed tomography (CT) angiography is not associated with significant patient risks other than those related to administering iodinated contrast media. Images can be relatively safely obtained without the need for arterial puncture or catheter manipulation that carries the possibility of acquiring a permanent neurologic deficit. Our motivation is to assess the reliability of CTA in assessing different features of ruptured intracranial aneurysm and its impact on patient management.

Research objectives

To assess the reliability of CTA in assessing different features of ruptured intracranial aneurysm and its impact on patient management. We found out that CTA is a promising diagnostic imaging modality for assessing intracranial aneurysm features and help in management decision and patient outcomes. We recommend further studies assessing the inter-observer agreement between neuroradiologists, neurologists, neurosurgeons, and neuro-interventionist.

Research methods

Helical cerebral CT angiography has been widely used in detecting intracranial aneurysms, with a reported sensitivity of 70%–96%. Currently, multidetector CT angiography has the ability to detect most intracranial aneurysms of 5 mm or larger. Multidetector row CT scanners provide increased spatial resolution and decreased scanning time, which should increase the sensitivity of the technique in depicting aneurysms of less than 5 mm in diameter. Currently, CT angiography is accepted as a first-line diagnostic imaging modality for evaluating intracranial aneurysms. Nevertheless, using CT angiography to depict intracranial aneurysms showed variable sensitivity. The reported sensitivity of CTA in detections of small intracranial aneurysms (< 3 mm) varied from 28%–43% in a study that included 99 small aneurysms to 83%–92% in another study had 579 small aneurysms. CTA examinations for 146 patients in the current study were revised and interpreted by two experienced neuroradiologists to assess the inter-observer agreement of CTA findings related to intracranial aneurysms. Data extracted from CT was considered in patient management decision.

Research results

This study evaluated the interobserver reliability of CTA in the assessment of ruptured intracranial aneurysm features among 146 patients. Our results showed good to an excellent inter-observer agreement in imaging features related to the aneurysm, aneurysm characters, measurements, and perianeurysmal information. Imaging data extracted from NCCT and CTA guided the multidisciplinary neurovascular team to better treatment approach selection. There are a few limitations to this study. First, there is no correlation with conventional angiography in all cases. Second, the general drawbacks of CT include patient exposure to ionizing radiation and the risks of iodinated contrast medium.

Research conclusions

We concluded that CTA is a promising diagnostic imaging modality for assessing intracranial aneurysm features that impact management and patient outcomes. We recommend endovascular approach in a ruptured intracranial aneurysm with comorbidity, old age, narrow neck, and a posterior circulation aneurysm, and surgical clipping is warranted if the patient is young with an MCA aneurysm and interested in durability.

Research perspectives

Further studies with applications of low-dose CTA, such as the use of automatic tube current modulation and a small amount of contrast medium, are recommended. Additionally, future studies using advanced CT techniques such as higher 320 slices CT scan, dual-energy or source CTA, and time-resolved 4D CTA will improve temporal and spatial resolution and the image quality CTA. Also, applications of advanced vascular post-processing packages for analyzing CTA images will give comprehensive image interpretation in different planes and angles.

FOOTNOTES

Author contributions: Abdel Razek A and El-Serougy LG proposed the study concept and design; Elged BA searched Database; Kasem MA performed surgical procedures; Elmokadem AH performed DSA; Elged BA, EL-Adalany MA, and El-Serougy LG contributed to analysis and interpretation of data; Elged BA and Elmokadem AH contributed to drafting of the manuscript; Elmokadem AH and Abdel Razek A contributed to Revision of the manuscript; EL-Adalany MA and El-Serougy LG supported technical, or material.

Institutional review board statement: The study was approved by Mansoura university institutional review board (IRB).

Informed consent statement: Patients were not required to give a written consent for the study as the analysis used anonymous data.

Conflict-of-interest statement: All the authors report no relevant conflicts of interest for this article.

Data sharing statement: All data generated or analyzed during this study are included in this published article.

Open-Access: This article is an open-access article that was selected by an in-house editor and fully peer-reviewed by

external reviewers. It is distributed in accordance with the Creative Commons Attribution NonCommercial (CC BY-NC 4.0) license, which permits others to distribute, remix, adapt, build upon this work non-commercially, and license their derivative works on different terms, provided the original work is properly cited and the use is non-commercial. See: <https://creativecommons.org/licenses/by-nc/4.0/>

Country/Territory of origin: Egypt

ORCID number: Ali H Elmokadem 0000-0001-5119-9548; Basma Abdelmonaem Elged 0000-0002-7442-9673; Ahmed Abdel Razek 0000-0002-9613-5932; Mohamed Ali Kasem 0000-0002-2633-6472; Mohamed Ali EL-Adalany 0000-0001-8226-7814.

S-Editor: Li L

L-Editor: A

P-Editor: Zhao S

REFERENCES

- Turan N**, Heider RA, Roy AK, Miller BA, Mullins ME, Barrow DL, Grossberg J, Pradilla G. Current Perspectives in Imaging Modalities for the Assessment of Unruptured Intracranial Aneurysms: A Comparative Analysis and Review. *World Neurosurg* 2018; **113**: 280-292 [PMID: 29360591 DOI: 10.1016/j.wneu.2018.01.054]
- Al-Smadi AS**, Elmokadem A, Shaibani A, Hurley MC, Potts MB, Jahromi BS, Ansari SA. Adjunctive Efficacy of Intra-Arterial Conebeam CT Angiography Relative to DSA in the Diagnosis and Surgical Planning of Micro-Arteriovenous Malformations. *AJNR Am J Neuroradiol* 2018; **39**: 1689-1695 [PMID: 30093482 DOI: 10.3174/ajnr.A5745]
- Howard BM**, Hu R, Barrow JW, Barrow DL. Comprehensive review of imaging of intracranial aneurysms and angiographically negative subarachnoid hemorrhage. *Neurosurg Focus* 2019; **47**: E20 [PMID: 31786554 DOI: 10.3171/2019.9.FOCUS19653]
- Elsherbini MM**, Elmokadem AH, El-Morsy A, Sherif FM, Khalil AF. Inter-Observer Reliability of Fused Time-of-Flight MR Angiography and 3D Steady State Sequence vs 3D Contrast Enhanced Images in Evaluation of Neurovascular Compression. *Open Journal of Modern Neurosurgery* 2022; **12** [DOI: 10.4236/ojmn.2022.122009]
- Ares WJ**, Jankowitz BT, Tonetti DA, Gross BA, Grandhi R. A comparison of digital subtraction angiography and computed tomography angiography for the diagnosis of penetrating cerebrovascular injury. *Neurosurg Focus* 2019; **47**: E16 [PMID: 31675711 DOI: 10.3171/2019.8.FOCUS19495]
- Yoon NK**, McNally S, Taussky P, Park MS. Imaging of cerebral aneurysms: a clinical perspective. *Neurovascular Imaging* 2016; **2**: 1-7 [DOI: 10.1186/s40809-016-0016-3]
- Bechan RS**, van Rooij SB, Sprengers ME, Peluso JP, Sluzewski M, Majoie CB, van Rooij WJ. CT angiography versus 3D rotational angiography in patients with subarachnoid hemorrhage. *Neuroradiology* 2015; **57**: 1239-1246 [PMID: 26341107 DOI: 10.1007/s00234-015-1590-9]
- Yang ZL**, Ni QQ, Schoepf UJ, De Cecco CN, Lin H, Duguay TM, Zhou CS, Zhao YE, Lu GM, Zhang LJ. Small Intracranial Aneurysms: Diagnostic Accuracy of CT Angiography. *Radiology* 2017; **285**: 941-952 [PMID: 28654338 DOI: 10.1148/radiol.2017162290]
- Kizilkilic O**, Huseynov E, Kandemirli SG, Kocer N, Islak C. Detection of wall and neck calcification of unruptured intracranial aneurysms with flat-detector computed tomography. *Interv Neuroradiol* 2016; **22**: 293-298 [PMID: 26842608 DOI: 10.1177/1591019915626591]
- Sawicki M**, Kościukiewicz K, Jeżewski D, Chelstowski K, Gołofit P, Skoczylas MM, Gębka M, Grabizna K, Kołaczek K, Zwarzany Ł, Sagan L, Poncyłjusz W. Diagnostic value of non-enhanced computed tomography in identifying location of ruptured cerebral aneurysm in patients with aneurysmal subarachnoid haemorrhage. *Neurol Neurochir Pol* 2020; **54**: 47-53 [PMID: 31967317 DOI: 10.5603/PJNNS.a2020.0007]
- Woernle CM**, Winkler KM, Burkhardt JK, Haile SR, Bellut D, Neidert MC, Bozinov O, Krayenbühl N, Bernays RL. Hydrocephalus in 389 patients with aneurysm-associated subarachnoid hemorrhage. *J Clin Neurosci* 2013; **20**: 824-826 [PMID: 23562295 DOI: 10.1016/j.jocn.2012.07.015]
- Feng TY**, Han XF, Lang R, Wang F, Wu Q. Subtraction CT angiography for the detection of intracranial aneurysms: A meta-analysis. *Exp Ther Med* 2016; **11**: 1930-1936 [PMID: 27168830 DOI: 10.3892/etm.2016.3166]
- Rajagopal N**, Balaji A, Yamada Y, Kawase T, Kato Y. Etiopathogenesis, clinical presentation and management options of mirror aneurysms: A comparative analysis with non-mirror multiple aneurysms. *Interdisciplinary Neurosurgery* 2019; **18**: 100535 [DOI: 10.1016/j.inat.2019.100535]
- Maniharan S**, Athukorala ADP, Pullaperuma DLN, Pirasath S, Lekamge IN. Role of digital subtraction angiography in detection of intracranial aneurysms compared with computed tomographic angiography. *Sri Lanka Journal of Radiology* 2019; **5** [DOI: 10.4038/slj.v5i1.76]
- Rai SP**, Chandran P, Pai M, Kamath M, Bele K, Kumar A, Chakraborti S. Comparison of Morphology of Intracranial Aneurysms on Computed Tomography Angiography with Digital Subtraction Angiography and Intraoperative Findings-A Single Centre Experience. *J Clin Diagn Res* 2019; **13** [DOI: 10.7860/JCDR/2019/37967.12420]
- Abecassis IJ**, Zeeshan Q, Ghodke BV, Levitt MR, Ellenbogen RG, Sekhar LN. Surgical Versus Endovascular Management of Ruptured and Unruptured Intracranial Aneurysms: Emergent Issues and Future Directions. *World Neurosurg* 2020; **136**: 17-27 [PMID: 31899398 DOI: 10.1016/j.wneu.2019.12.127]
- Daruwalla VJ**, Syed FH, Elmokadem AH, Hurley MC, Shaibani A, Ansari SA. Large basilar perforator pseudoaneurysm: A case report. *Interv Neuroradiol* 2016; **22**: 662-665 [PMID: 27485048 DOI: 10.1177/1591019916659261]

- 18 **Enomoto N**, Shinno K, Tamura T, Shikata E, Shono K, Takase K. Ruptured Basilar Artery Perforator Aneurysm: A Case Report and Review of the Literature. *NMC Case Rep J* 2020; **7**: 93-100 [PMID: 32695555 DOI: 10.2176/nmccrj.cr.2019-0143]
- 19 **Meguins LC**, Hidalgo RC, Spotti AR, de Morais DF. Aneurysm of azygos anterior cerebral artery associated with falx meningioma: Case Report and review of the literature. *Surg Neurol Int* 2017; **8**: 25 [PMID: 28303205 DOI: 10.4103/2152-7806.200577]
- 20 **Wang GX**, Gong MF, Wen L, Liu LL, Yin JB, Duan CM, Zhang D. Computed Tomography Angiography Evaluation of Risk Factors for Unstable Intracranial Aneurysms. *World Neurosurg* 2018; **115**: e27-e32 [PMID: 29567291 DOI: 10.1016/j.wneu.2018.03.083]
- 21 **Kawabata Y**, Nakazawa T, Fukuda S, Kawarazaki S, Aoki T, Morita T, Tsukahara T. Endovascular embolization of branch-incorporated cerebral aneurysms. *Neuroradiol J* 2017; **30**: 600-606 [PMID: 29171364 DOI: 10.1177/1971400917698002]
- 22 **Chen J**, Li M, Zhu X, Chen Y, Zhang C, Shi W, Chen Q, Wang Y. Anterior Communicating Artery Aneurysms: Anatomical Considerations and Microsurgical Strategies. *Front Neurol* 2020; **11**: 1020 [PMID: 33013671 DOI: 10.3389/fneur.2020.01020]
- 23 **Ajiboye N**, Chalouhi N, Starke RM, Zanaty M, Bell R. Unruptured Cerebral Aneurysms: Evaluation and Management. *ScientificWorldJournal* 2015; **2015**: 954954 [PMID: 26146657 DOI: 10.1155/2015/954954]
- 24 **Kim HJ**, Yoon DY, Kim ES, Lee HJ, Jeon HJ, Lee JY, Cho BM. Intraobserver and interobserver variability in CT angiography and MR angiography measurements of the size of cerebral aneurysms. *Neuroradiology* 2017; **59**: 491-497 [PMID: 28343249 DOI: 10.1007/s00234-017-1826-y]
- 25 **Al Kasab S**, Nakagawa D, Zanaty M, Bathla G, Policeni B, Soni N, Allan L, Hudson J, Limaye K, Ortega-Gutierrez S, Samaniego EA, Hasan D. In vitro accuracy and inter-observer reliability of CT angiography in detecting intracranial aneurysm enlargement. *J Neurointerv Surg* 2019; **11**: 1015-1018 [PMID: 30842308 DOI: 10.1136/neurintsurg-2019-014737]
- 26 **Waqas M**, Chin F, Rajabzadeh-Oghaz H, Gong AD, Rai HH, Mokin M, Vakharia K, Dossani RH, Meng H, Snyder KV, Davies JM, Levy EI, Siddiqui AH. Size of ruptured intracranial aneurysms: a systematic review and meta-analysis. *Acta Neurochir (Wien)* 2020; **162**: 1353-1362 [PMID: 32215742 DOI: 10.1007/s00701-020-04291-z]
- 27 **Vandenbulcke A**, Messerer M, Starnoni D, Puccinelli F, Daniel RT, Cossu G. Complete spontaneous thrombosis in unruptured non-giant intracranial aneurysms: A case report and systematic review. *Clin Neurol Neurosurg* 2021; **200**: 106319 [PMID: 33268195 DOI: 10.1016/j.clineuro.2020.106319]
- 28 **Bhatia S**, Sekula RF, Quigley MR, Williams R, Ku A. Role of calcification in the outcomes of treated, unruptured, intracerebral aneurysms. *Acta Neurochir (Wien)* 2011; **153**: 905-911 [PMID: 21286763 DOI: 10.1007/s00701-010-0846-8]
- 29 **Kolias AG**, Sen J, Belli A. Pathogenesis of cerebral vasospasm following aneurysmal subarachnoid hemorrhage: putative mechanisms and novel approaches. *J Neurosci Res* 2009; **87**: 1-11 [PMID: 18709660 DOI: 10.1002/jnr.21823]
- 30 **Pedro KM**, Sih IM. Perianeurysmal Parenchymal Cyst of the Pons: A Case Report and Review of Literature. *Interdisciplinary Neurosurgery* 2020; **100731** [DOI: 10.1016/j.inat.2020.100731]
- 31 **Chen J**, Wang Y, Li P, Chen W, Zhou J, Hu X, Zhu J, Jiang B. Treatment of a giant arteriovenous malformation associated with intracranial aneurysm rupture during pregnancy: A case report. *Exp Ther Med* 2016; **12**: 1337-1340 [PMID: 27588055 DOI: 10.3892/etm.2016.3505]
- 32 **Flores BC**, Klinger DR, Rickert KL, Barnett SL, Welch BG, White JA, Batjer HH, Samson DS. Management of intracranial aneurysms associated with arteriovenous malformations. *Neurosurg Focus* 2014; **37**: E11 [PMID: 25175430 DOI: 10.3171/2014.6.FOCUS14165]
- 33 **Li J**, Du S, Sun L, Shang F, Zhang H, Li G. Hybrid Operation of a Ruptured Aneurysm Associated with a Developmental Venous Anomaly. *World Neurosurg* 2018; **120**: 63-65 [PMID: 30099185 DOI: 10.1016/j.wneu.2018.07.292]
- 34 **Jung SH**, Kim SH, Kim TS, Joo SP. Surgical Treatment of Traumatic Intracranial Aneurysms: Experiences at a Single Center over 30 Years. *World Neurosurg* 2017; **98**: 243-250 [PMID: 27836703 DOI: 10.1016/j.wneu.2016.11.005]
- 35 **Lefevre E**, Apra C, Chodraui-Filho SF, Chauvet D, Smajda S, Piotin M, Fahed R. Reliability of Bony Landmarks to Predict Intradural Location of Paraclinoid Aneurysms. *Clin Neuroradiol* 2020; **30**: 843-848 [PMID: 32170338 DOI: 10.1007/s00062-020-00896-0]
- 36 **Steiner T**, Juvela S, Unterberg A, Jung C, Forsting M, Rinkel G; European Stroke Organization. European Stroke Organization guidelines for the management of intracranial aneurysms and subarachnoid haemorrhage. *Cerebrovasc Dis* 2013; **35**: 93-112 [PMID: 23406828 DOI: 10.1159/000346087]
- 37 **Kim HJ**, Yoon DY, Kim ES, Yun EJ, Jeon HJ, Lee JY, Cho BM. 256-row multislice CT angiography in the postoperative evaluation of cerebral aneurysms treated with titanium clips: using three-dimensional rotational angiography as the standard of reference. *Eur Radiol* 2020; **30**: 2152-2160 [PMID: 31844961 DOI: 10.1007/s00330-019-06560-7]
- 38 **Yun SY**, Heo YJ, Jeong HW, Baek JW, Choo HJ, Shin GW, Kim ST, Jeong YG, Lee JY, Jung HS. Dual-energy CT angiography-derived virtual non-contrast images for follow-up of patients with surgically clipped aneurysms: a retrospective study. *Neuroradiology* 2019; **61**: 747-755 [PMID: 30684114 DOI: 10.1007/s00234-019-02170-8]



Published by **Baishideng Publishing Group Inc**
7041 Koll Center Parkway, Suite 160, Pleasanton, CA 94566, USA
Telephone: +1-925-3991568
E-mail: bpgoffice@wjgnet.com
Help Desk: <https://www.f6publishing.com/helpdesk>
<https://www.wjgnet.com>

